Fast Sample Injection for Dissolution Dynamic Nuclear Polarisation NMR Spectroscopy

by

Sotirios Katsikis

A thesis submitted to the

University of Birmingham

for the degree of

DOCTOR OF PHILOSOPHY

Supervisors: Ulrich Günther & Christian Ludwig

HWB-NMR
Institute of Cancer and Genomic Sciences
College of Medical and Dental Sciences
The University of Birmingham
October 2015

Abstract

Introduction:

One of the most critical problems of NMR is the intrinsic lack of sensitivity owing to the small energy difference between nuclear energy levels. This issue can be addressed in different ways. One possibility is to reduce the spectral noise, which to a large extent is created by the console electronics. Another approach is to actually increase the signal strength of the NMR signal. An experimental approach to achieve this is *ex situ* dissolution Dynamic Nuclear Polarisation. It increases the population difference of the spin states by transferring the high electron polarization to the NMR detectable nuclei. A theoretical introduction into NMR, quantum mechanical basics of spin physics and DNP are presented in Chapters 1 and 2.

Methods:

One of the main drawbacks of D-DNP is the necessity for a post-polarisation sample transfer to an NMR spectrometer. One of the major aims of the work presented in this thesis was to build an autonomous robotic device to transfer the sample under pressure controlled by Arduino microelectronics to overcome problems associated with the sample transfer. Chapter 3 presents how this device was constructed and. In addition applications performed using this device are presented.

Results:

The benefits of the application of this device for fast-relaxing nuclei are discussed in chapter 4 with the application on 2-D DNP-NMR acquisition of U-^{13}C Glucose. Novel experiments using Dissolution DNP were also performed as part of the work for this thesis. A method for analysing aminoacids of biological fluids using DNP is presented in the Chapter 5 by

acetylating which creates long lived tags. An approach for extracting the maximum of information out of a single polarisation experiment is what Chapter 6 covers with an approach to perform Parallel Receiver DNP and the application on ATP and 1-13C TetraMethylPhosphonium. Finally, the future applications of the DNP and the authors' personal ideas for further development are presented in Chapter 7, the discussion. Briefly, DNP-NMR using a fast sample transfer system can be a capable system for performing different types of analysis, but the maximum outcome is always when the system is combined with *in-vivo* MRI scanners.

Acknowledgments

Contents

List of Figures

List of Tables

Abbreviations

CE – Cross Effect

DNP – Dynamic Nuclear Polarisation

EPR – Electron Paramagnetic Resonance

FID – Free Induction Decay

FT – Fourier Transform

HMQC – Heteronuclear Multiple Quantum Coherence Spectroscopy

HSQC – Heteronuclear Single Quantum Coherence Spectroscopy

MAS – Magic Angle Spinning

MRI – Magnetic Resonance Imaging

NMR – Nuclear Magnetic Resonance

OE – Overhauser Effect

PHIP – Para Hydrogen Induced Polarisation

SABRE – Signal Amplification By Reversible Exchange

SE – Solid Effect

TM – Thermal Mixing

Theoretical Part

Introduction

In Ancient Greece, Democritus suggested that matter can break down to particles that cannot be further split. Thus the name atom, from the Greek word άτομο, coming from α+τομή, no+split. Although back then science was a philosophical approach well before experiments were able to prove or neglect theories, this theory still stands true when we refer to subatomic particles. Leptons, like the electron, cannot be split, same stands for quarks that build the hadrons (like proton and neutron – which are baryons) –at present-.

Nowadays it is well known that matter consists of molecules, and molecules break down to atoms. Inside atoms we find the nucleus, consisting of protons and neutrons. All but some of these spin 0 particles have an intrinsic property called spin. Spin was introduced in 1925 by Uhlenbeck and Goudsmith [1] (intrinsic angular momentum). Although the term indicates spinning this is not true from a quantum mechanical perspective. Particles can either have integer or half-integer spins. This fundamental separation for sub atomic particles divides matter in two main groups, fermions and bosons. Fermions are the semi-integer spins (described by Fermi-Dirac statistical model) and bosons are the integer spins (described by Bose-Einstein statistical model). All nuclei except the hydrogen nucleus consist of both protons and neutrons, thus the total nuclear spin can vary [1].

Electronic spin is the reason that electrons occupy different energy levels in atomic and molecular orbitals. According to the Pauli principle [2], which suggests that the wave functions describing half-integer spins are anti-symmetric [3], electrons with the same set of quantum numbers cannot occupy the same state, thus differentiating into different states with different energy levels in the various atomic orbitals (s, p, d, f etc.). These atomic orbitals then form molecular orbitals (σ, π, etc.) and the chemical bond. This is in contrast with integer spin particles like the photons, in which multiple particles can occupy the same quantum mechanical state. A demonstration of this is the Light Amplification by Stimulated

Emission of Radiation (laser). The possibility of building a laser was predicted theoretically by Einstein and nowadays it has many usages in everyday life (optical discs, medical lasers, laser pointers etc.). A laser can only emit bosons, as they have to occupy the same state. In conclusion, this differentiation and the antisymmetric character of the wave function is the main interest of chemistry as a science, being the cause of all type of bonds.

Although the nuclei are the reason for having the specific amount of electrons, chemistry is mainly the science of the electron. During the end of World War II when science in the US states was at a peak an observation was made independently by Bloch, Hansen and Packard at Stanford, California [4] and by Purcell in Massachusetts [5, 6]. They observed that atomic nuclei in a magnetic field can resonate at radiowave frequencies. From this originated Nuclear Magnetic Resonance (NMR). Small frequency differentiation comes from chemical environment, thus giving scientists, in particular chemists, a strong spectroscopic tool. The NMR technique was soon identified as a leading spectroscopic technique for validating chemical structures (*"The Nobel Prize in Physics 1952 was awarded jointly to Felix Bloch and Edward Mills Purcell "for their development of new methods for nuclear magnetic precision measurements and discoveries in connection therewith""*). Organic and inorganic chemistry benefit from this technique, as the NMR active nuclei of ^1H and ^{13}C are present in the majority of organic compounds and many inorganic compounds consist of NMR active nuclei. Other NMR active nuclei include ^{14}N, ^{19}F, and ^{31}P. Pulse Fourier Transform NMR [7, 8] pioneered by R.R. Ernst (FT-NMR) replaced the slow and insensitive sweeping mode and brought the break-through for NMR as an analytical technique (*"The Nobel Prize in Chemistry 1991 was awarded to Richard R. Ernst" for his contributions to the development of the methodology of high resolution nuclear magnetic resonance (NMR) spectroscopy"*). The realisation that imaging on substances can be carried out using NMR by Paul Lauterbur and Sir Peter Mansfield created the Nuclear Magnetic Resonance Imaging, or Magnetic

Resonance Imaging (MRI) awarded by a Nobel prize ("*The Nobel Prize in Physiology or Medicine 2003 was awarded jointly to Paul C. Lauterbur and Sir Peter Mansfield "for their discoveries concerning magnetic resonance imaging""*"). These applications greatly broaden the applicability of NMR in a variety of diverse scientific fields. The evolution of the magnet design also played a key role in these developments and in the possibility of performing structural analysis of proteins and Kurt Wuthrich was awarded the Nobel Prize of Chemistry in 2002 for "*development of methods for identification and structure analyses of biological macromolecules [...]. The other half [is awarded] to Kurt Wüthrich for his development of nuclear magnetic resonance spectroscopy for determining the three-dimensional structure of biological macromolecules in solution"*.

NMR is a spectroscopic technique utilising the Zeeman Effect of atomic nuclei. When matter enters a strong magnetic field, degeneration of spin states cancels and they split into two states, depending on Spin operator sign. The difference of population of these two groups is given by the Boltzmann distribution. For two different states, the difference of the energy state populations is given by the equation:

$$\frac{S_2}{S_1} = e^{\frac{E_1 - E_2}{kT}} \tag{0.1}$$

These two states in a half integer spin system are the Up and Down states, so this equation is converted as:

$$\frac{N_{up}}{N_{down}} = e^{\frac{E_1 - E_2}{kT}} \Leftrightarrow N_{up} = N_{down} * e^{\frac{E_1 - E_2}{kT}} \tag{0.2}$$

In this equation, N_{up} and N_{down} represent the population of nuclei in up and down energy states, E_1-E_2 is the energy difference between the spin states, k is the Boltzmann constant (1.3805×10^{-23} J/Kelvin) and T is the temperature in Kelvin. Calculating the percentage of polarisation is given by the following calculation:

$$\frac{N_{up}-N_{down}}{N_{up}+N_{down}} = \frac{N_{down}*e^{\frac{E_1-E_2}{kT}}-N_{down}}{N_{down}*e^{\frac{E_1-E_2}{kT}}+N_{down}} = \frac{e^{\frac{E_1-E_2}{kT}}-1}{e^{\frac{E_1-E_2}{kT}}+1} = \frac{e^{\frac{\gamma\hbar B_0}{kT}}-1}{e^{\frac{\gamma\hbar B_0}{kT}}+1} = \tanh(\frac{\gamma\hbar B_0}{kT}) \qquad (0.3)$$

The last part is in accordance with Jeffries expression for polarisation [9].

This difference is 1 for every 10^5 spins at room temperature for a proton in a 11.7T magnet [10]. The importance of this number is that with NMR only this single spin can give a detectable signal, as the main population cancels out. NMR therefore has an inherent disadvantage in terms of sensitivity compared to other spectroscopic techniques such as molecular spectroscopy or mass spectrometry.

There are ways to circumvent this inherently low sensitivity. One way is to engage an Overhauser effect [11]. This term is used to describe a variation of signals in dual resonance experiments. Overhauser predicted theoretically that it is possible to polarise nuclei by saturating the resonance frequencies of the electrons. As it was explained earlier, electrons also have a spin. The electron spin benefits from a much larger population difference owing to a larger energy difference between the spin states (Equation 0.2). Carver and Slichter[12] proved experimentally the Overhauser effect by saturating electron frequency in [7]Li and thus transferring polarisation to the [7]Li nuclei. This is called Dynamic Nuclear Polarisation (DNP) and enables spin polarisations of larger magnitude than the ones allowed thermodynamically by Boltzmann's distribution.
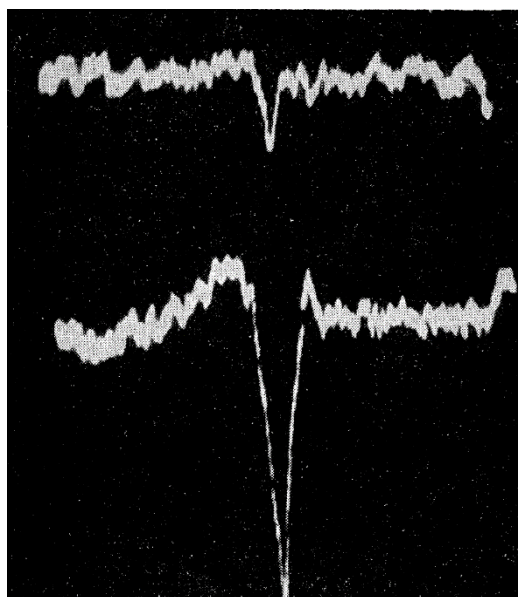
Figure 0.1: The First DNP Experiment by Carver and Slichter, showing a signal of polarised of ^{7}Li (lower spectrum) versus a glycerol sample (upper spectrum). Taken from [12]

This PhD Thesis is based on DNP using an implementation pioneered by Ardenkjaer-Larsen et.al. where samples are polarised in the solid at very low temperature and subsequently dissolved to be measured at higher field as a liquid [13]. This implementation of DNP has been termed Dissolution DNP or *ex-situ* Dissolution Dynamic Nuclear Polarisation (DNP), [14] because the polarisation is carried out outside the magnet where the NMR measurement is acquired. A second, usually lower field, polarisation magnet is used to polarise in a glassy state at very low temperature, followed by fast dissolution and melting of the polarised substance to be transferred into another magnet to acquire the NMR spectrum.

Chapter 1 – Principles of NMR

1.1 - Nuclear Magnetism

1.1.1 - Spin

As mentioned in the introduction, spin is an intrinsic property of matter. Spin is a form of angular momentum. It is known from classical physics that a rotating and charged body has a magnetic moment $\vec{\mu}$. In classical mechanics it is known that:

$$\vec{\mu} = \sum_i \frac{q_i}{2M_i c} \vec{J}_i \tag{1.1}$$

where i is an ensemble of particles of a macroscopic system, q_i and M_i the charge and the mass of the particle i respectively, c is the speed of light and $\vec{J}_i$ the vector of the angular momentum of particle i. If all of the moving particles have the same factor of charge to mass $(q_i/M_i = q/M)$ the magnetic moment can be expressed as:

$$\vec{\mu} = \frac{q}{2Mc} \sum_i \vec{J}_i = \frac{q}{2Mc} \vec{J} = \gamma \vec{J} \tag{1.2}$$

where $\vec{J}$ is the total angular momentum and γ is the gyromagnetic ratio, equal $q/2Mc$. For this classical physics approach i is assumed that the macroscopic system consists of a defined number of particles, meaning it has a structure, and that the magnetic moment $\vec{\mu}$ is proportional to angular momentum. Transferring the classical model into quantum mechanics it can be assumed that if $\vec{J} = \vec{\mathcal{L}}$, where $\vec{\mathcal{L}}$ is the angular momentum of the electron, the magnetic moment of the angular momentum, $\vec{\mu_{\mathcal{L}}}$ equals:

$$\widehat{\vec{\mu_{\mathcal{L}}}} = -\frac{e\hbar}{2mc} \widehat{\vec{\mathcal{L}}} \tag{1.3}$$

In order to extend this equation to the spin angular momentum, the dipolar moment must be calculated. But this assumes an internal structure of the electron, which is not existent, as an

electron is a lepton. It has been proven that the dipolar moment of the electron arising from spin, $\overrightarrow{\mu_S}$, equals:

$$\widehat{\overrightarrow{\mu_S}} = -g_e \frac{e\hbar}{2mc} \widehat{\overrightarrow{S}} \qquad (1.4)$$

This equation illustrate that classical physics fails to describe spin adequately. A correction term, the electronic g-factor is introduced. From quantum electrodynamics is it possible to calculate the g-factor, although only for the electron. The theoretical value is in accordance with the experimental results and g-factor equals approximately 2.0023. For all the other particles, this value has to be measured experimentally. The g-factor can be measured with an ion-trap, the same that is commonly used as a Mass Spectrometry detector *("The Nobel Prize in Physics 1989 was divided, one half awarded to Norman F. Ramsey "for the invention of the separated oscillatory fields method and its use in the hydrogen maser and other atomic clocks", the other half jointly to Hans G. Dehmelt and Wolfgang Paul "for the development of the ion trap technique""").*

The g-factor is a dimensionless value. Gyromagnetic ratio γ is commonly used to replace the constants, so equation 1.4 is usually transcribed as:

$$\widehat{\overrightarrow{\mu_S}} = \gamma \widehat{\overrightarrow{S}} \qquad (1.5)$$

With the general term spin two different quantum mechanical properties are described, the spin quantum number *S* and the actual spin state m_s. For a given S, m_s can adopt values from –S to S in steps of 1. For example for a spin 1 nucleus (S=1), m_s can adopt the values 1,0 or 1. For a nucleus with S= ½, m_s can be either -½ or +½, referring to the nuclear spin being in α state (parallel to the external magnetic field, m_s= +½) or β state (anti-parallel to the external magnetic field, m_s=-½).

The energy in quantum mechanics is given by applying the Hamiltonian operator in the wave function in a time-independent Schrödinger equation:

$$\widehat{\mathcal{H}}\vec{\Psi} = E\vec{\Psi} \tag{1.6}$$

Using the Dirac notation (bra-ket) this can be expressed as:

$$E = \langle\widehat{H}\rangle = \langle\vec{\Psi}|\widehat{H}|\vec{\Psi}\rangle \tag{1.7}$$

The energy of a magnetic dipole in a magnetic field is given by equation:

$$\widehat{H} = -\mu B_0 \hbar \widehat{S_z} = \omega_0 \hbar \widehat{S_z} \tag{1.8}$$

Eigenstates of $\widehat{S_z}$ are $|\alpha\rangle$ and $|\beta\rangle$ with eigenvalues of +½ and -½ respectively.

Matrix representation of $\widehat{I_z}$ can be written as

$$S_z = \begin{bmatrix} 1/2 & 0 \\ 0 & -1/2 \end{bmatrix} \tag{1.9}$$

Spin angular momentum can be calculated by using the equation

$$S = \hbar\sqrt{m_s(m_s + 1)} \tag{1.10}$$

where $\hbar$ is Planck's constant in rads and S is the spin quantum number.

It should be noted that nuclear spin is usually denoted as I and electronic spin as S. Due to the similarity between I and l in Latin alphabet, the character S has been used for describing spin in order to avoid mixing spin angular momentum with magnetic angular momentum m_l. The equations presented so far can describe both electronic and nuclear spin systems.

The precession frequency, which the magnetic moment of the nucleus rotates around the main axis of the external magnetic field (also known as the Larmor frequency) can be derived from this property. In Figure 1.1 a graphical representation of the sign of the gyromagnetic ratio in relation with magnetic moment and spin angular momentum is presented.
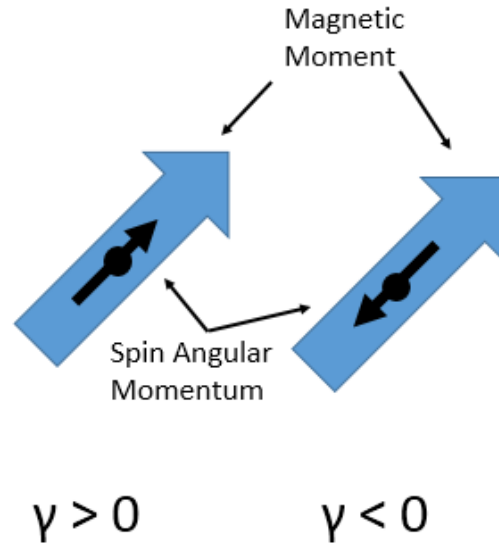
Figure 1.1 - The sign of gyromagnetic ratio in relation to magnetic moment and spin angular momentum (adapted from [10])

So, for a particle with spin S = ½, such as a proton, the magnetic moment is:

$$\hat{\mu} = \gamma\hat{S} = \hbar\gamma\sqrt{S(S+1)} \qquad (1.11)$$

1.1.2 - Larmor Frequency and Spin Precession

In the absence of a magnetic field, spins tend to be random in space. In the presence of a field they polarise by orienting in the magnetic field, and in a classic picture they start to precess around the z axis. This precession has a specific Larmor frequency that is unique for each nucleus. It is given by equation 1.12.

$$\omega_0 = -\gamma B_0 \qquad (1.12)$$

where gamma is the gyromagnetic ratio.

This effect is graphically represented in Figure 1.2.

B_0

B_0

$\gamma < 0$

$\gamma > 0$
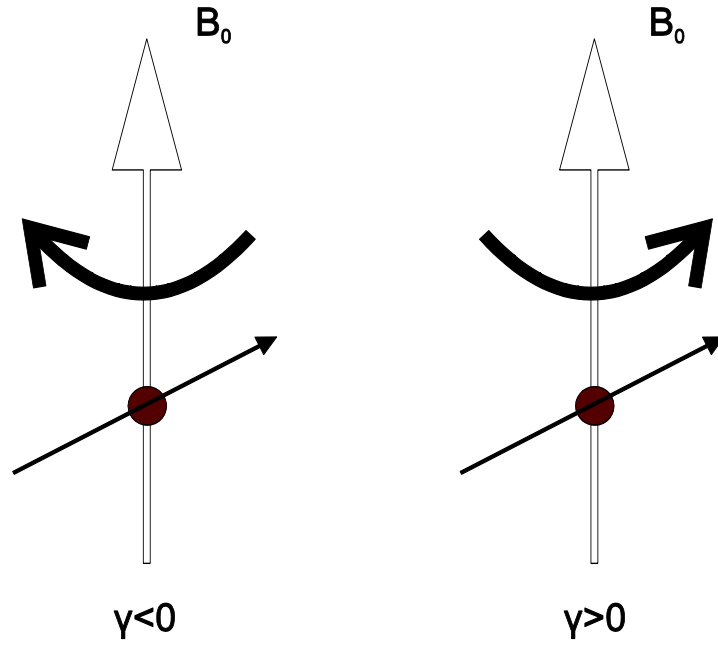
Figure 1.2 – Spin precession on the effect of the external magnetic field B_0

Within a known magnetic field, resonance frequencies of the electron and the nucleus can be calculated using the equations 1.14 and 1.16, derived from 1.13 and 1.15 respectively.

$$\omega_{electron\ spin} = \frac{2\mu_e B}{\hbar} = 1.7608 \ x \ 10^{11} s^{-1} \qquad (1.13)$$

$$\nu = \frac{\omega}{2\pi} = 28.025 \ GHz \ T^{-1} \qquad (1.14)$$

$$\omega_{proton\ spin} = \frac{2\mu_p B}{\hbar} = 2.6752 \ x \ 10^8 s^{-1} \qquad (1.15)$$

$$(1.16)$$

$$\nu = \frac{\omega}{2\pi} = 42.5781 \ MHz \ T^{-1}$$

A list of a common gyromagnetic ratios and associated frequencies calculated with equations 1.14 and 1.16 is presented in Table 1.1 displaying frequencies in both the high-resolution NMR system (11.7T) and the polariser (3.34T).

TABLE 1.1 – FREQUENCIES, GYROMAGNETIC RATIOS AND NATURAL ABUNDANCE AT 500 MHz (NMR MAGNET) AND 143 MHz (POLARISER'S MAGNET)

Particle	Ground State Spin	Natural Abundance	Gyromagnetic ratio γ/rad s^{-1} T^{-1}	NMR frequency at 11.7 T	NMR frequency at 3.34 T
e^-	½	-	1.7608×10^{11}	327.8925 GHz	93.6035 GHz
^1H	½	~0.015	26.7522×10^7	500 MHz	143 MHz
^2H	1	0.01150	4.10663×10^7	76.753 MHz	21.951 MHz
^{13}C	½	1.07	6.72828×10^7	125.725 MHz	35.957 MHz
^{14}N	1	99.63200	1.93378×10^7	36.132 MHz	10.334 MHz
^{15}N	½	0.36800	-2.71262×10^7	50.684 MHz	14.496 MHz
^{31}P	½	100	10.83940×10^7	202.404 MHz	57.887 MHz

1.1.3 - Longitudinal Magnetisation and Relaxation

In the absence of an external magnetic field spins are not oriented, in fact there may not be a spin without a magnetic field. By applying an external magnetic field, spins orient and start to precess at the Larmor frequency. This does not happen immediately. There is build-up period forthe orientation and thus the magnetisation in z-axis. This build-up period is a thermodynamic effect and is also the same when inverting the process; by removing the field, the orientation is not becoming random spontaneously, but time has to pass. The cause of this effect is that the molecular environment of the nuclei can bring small fluctuations in the magnetic field that is sensed by the nucleus. The system is not isotropic any more, and the small anisotropic distribution parallel to the external field is the thermal equilibrium, or

polarisation. This small net magnetisation that the thermal equilibrium brings about is known as longitudinal magnetisation. The build-up of the small net magnetisation across the z-axis is given by the equation:

$$M_z{}^{nuc}(t) = M_{eq}{}^{nuc}(1 - e^{-\frac{t-t_0}{T_1}}) \tag{1.17}$$

where t_0 is the time when the external field is applied and T_1 is the spin-lattice relaxation time constant. This time is called spin-lattice or longitudinal relaxation. It can have values between microseconds and many hours, depending on the temperature, the nucleus and the nuclear environment. Relevant longitudinal relaxation times for this work of ^{13}C nuclei in aqueous solvents are typically in the range of milliseconds to several seconds. In special cases like benzene T_1 can be several minutes.

1.1.4 - Transverse Magnetisation

After applying a pulse, magnetisation is found in the xy plane instead of the z –axis. This magnetisation is perpendicular to the external magnetic field and this is the one producing signal. When the RF pulse is a frequency matching the energy difference between the spin states Is applied to the spin system, transitions are induced between the spin states and the resulting state will be temporarily phase coherent. The effect of this is that when RF is turned off the net spin magnetisation is transferred from the z-axis to the y-axis. This magnetisation is called transverse magnetisation. The transverse components of the magnetisation consisting of x and y elements can be expressed with the Bloch equations as:

$$M_x{}^{nuc}(t) = M_{eq}{}^{nuc} sin(\omega_0 t)e^{-\frac{t}{T_2}}) \tag{1.18}$$

$$M_y{}^{nuc}(t) = M_{eq}{}^{nuc} cos(\omega_0 t)e^{-\frac{t}{T_2}}) \tag{1.19}$$

After time evolution, spins start to be phase incoherent due to variations in effective field (for each spin). The result is that the magnetization decays, and this decay is called homogenous relaxation. The time constant T_2 is the term describing this spin-spin relaxation effect, which can last for several seconds in liquids. It varies with nuclei and it is different for ^{1}H and ^{13}C.

1.2 - Nuclear Magnetic Resonance Spectroscopy

1.2.1 - Introduction

When NMR was discovered by Bloch in 1945 a continuous wave was applied and the nuclei were found in resonance sequentially. This was done by changing the magnetic field instead of the irradiation frequency, thus shifts could be upfield or downfield. Nowadays, FT-NMR has replaced CW-NMR because it is possible to excite and detect the radiofrequency field of interest simultaneously. Advantages of FT-NMR include much faster acquisition, the ability to average scans, sensitivity enhancement and the ability to perform more complicated experiments including two dimensional spectroscopy.

Figure 1.3 – A classical analogue for Continuous Wave (A) and Pulsed NMR (B) approaches. (adapted from [15])

Figure 1.3 shows this in a classical mechanics vague – analogue. In order to get the resonance frequencies of a bell, one can either scan the acoustic spectrum using a speakerphone and a microphone or hit the bell and record the frequencies. (Adapted from[15]).

The largest application of NMR today is in Magnetic Resonance Imaging (MRI), which has become an important diagnostic method alongside X-ray Computed Axial Tomography (CAT). The main advantage of MRI is that magnetic field is not interacting with biomolecules in the way X-rays do and is therefore not harmful. In chemistry and biology, NMR spectroscopy is a useful tool to identify molecular structure of inorganic and organic compounds, and in Biochemistry to determine structures of proteins and other biopolymers such as DNA and RNA [10, 16]. The structural information obtained by NMR is based on frequency, splitting, couplings and homo and heteronuclear correlations. [17]. The main drawback of NMR is the relatively low sensitivity, and this is a direct consequence of the small energy difference between the Zeeman split spin states. The relation showing this energy difference -for half spin systems such as ^{1}H, ^{13}C, ^{15}N, ^{31}P, ^{19}F etc.- is $\Delta E = \gamma \hbar B_0$, with γ being the gyromagnetic ratio and B_0 being the magnetic field. The population of the spin states is determined by this energy difference. Polarisation is derived in the Introduction, equation 0.3, and is defined as [18]:

$$P = \tanh \frac{\gamma \hbar B_0}{2kT} \qquad 1.20$$

Equation (1.20) clearly shows the implications of the NMR spectroscopy regarding sensitivity. Using the maximum available magnetic field of 23.5 T, the polarisation of the proton is only 0.008%. Lowering the temperature to 1 K the polarisation can be increased to 2.4%, and when lowering it down to 0.1 K, polarisation can be increased to 24%. But such

low temperatures mean that the sample is in a solid state. The temperature dependent polarisation is shown graphically for protons and electrons in Figure 1.4.
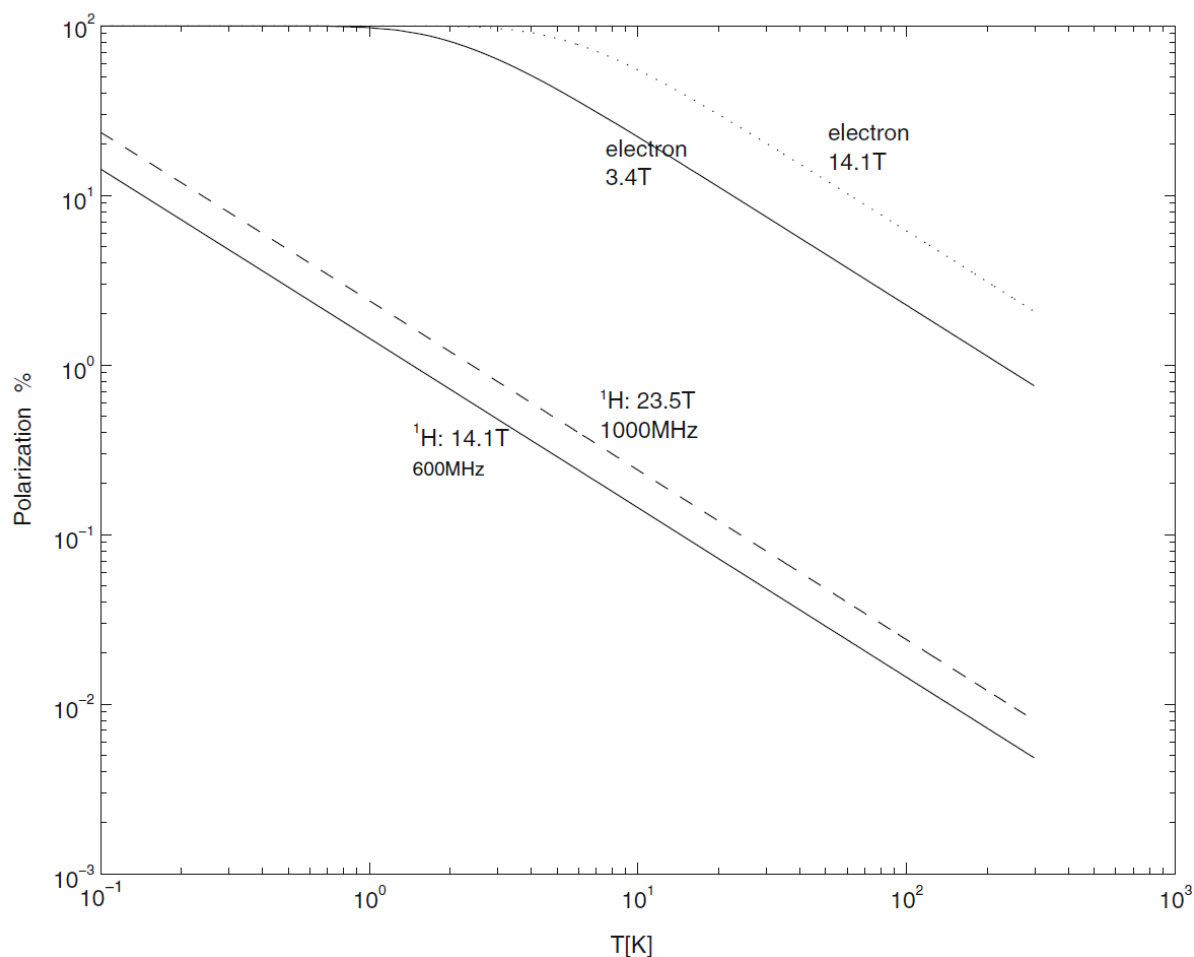
Figure 1.4 – Polarisation levels of protons and electrons in relation with the temperature and the field strength. Taken from [18]

1.2.2 - Chemical Shift

In many spectroscopic techniques, two signal parameters are distinguished: peak position and peak intensities [19]. In NMR the physical property responsible for signal dispersion is the chemical shift. Chemical shift arises from the nuclear shielding effect. Each nucleus is exposed to an effective field, because of differences in the density of surrounding electrons. According to quantum mechanics, electrons in molecules occupy molecular orbitals. The orbitals derive the type of the bond and the strength of the interaction. Each molecule has specific molecular orbitals and these affect the effective magnetic field. A theory that can

successfully calculate chemical shifts is the orbital density theory. Shielding by electrons alters that magnetic field observed by a nucleus. Therefore the chemical environment causes a difference in the frequency for a particular nucleus. Traditionally a downfield shift refers to a higher ppm value because a nucleus whose chemical shift is increased experiences a stronger magnetic field arising from reduced electron density.

One could use the frequency difference in Hz, but the advantage of the ppm scale is its independence of the field strength B_0. The ppm scale is defined by the following equation:

$$\delta = \frac{B_0 - B_1}{B_0} \, x \, 10^6 ppm \qquad\qquad 1.21$$

where δ is the chemical shift, B_0 is the reference magnetic field and B_1 is the induced field. A reference compound is usually present in each NMR sample as an internal standard in order to be able to calculate 0 ppm. By convention, the resonance frequency of TetraMethylSilanium is used as a zero ppm standard.

1.2.3 - Interactions – J couplings

In NMR, spectra of molecules with multiple nuclei interactions between different atoms connected through a chemical bond give rise to so-called scalar couplings, also called spin-spin coupling or –most commonly- J-coupling. The effect is very useful to establish which nuclei are close to others in a molecule. The effect of the J coupling in spectra is the splitting of peaks. Spins are dipoles, therefore there will be a dipole-dipole interaction. However in liquids because of fast tumbling, they are averaged out. But there are still couplings available, mediated through chemical bonds, which are called scalar couplings. The strength of these couplings is measured by the scalar coupling constant $^nJ_{AB}$. In this constant, A and B are the two nuclei species and n is the number of covalent bonds by which these two nuclei are separated. The multiplet structure for a two spin system AX is four peaks and multiplet structure can be calculated utilising the Pascal triangle. In order to avoid complicated spectra

arising from *J* splittings, decoupling is often utilised for heteronuclear couplings, in which the non-observed nucleus is irradiated during acquisition.

1.3 - NMR Instrumentation

An NMR system is composed of the subsystems shown in Figure 1.5 that enable the acquisition of NMR spectra [20]. Although NMR technology has developed over many years the basic components are the same in all NMR systems. These include a magnet, a radiofrequency transmitter, a radiofrequency receiver, the NMR probe and a signal recording device.
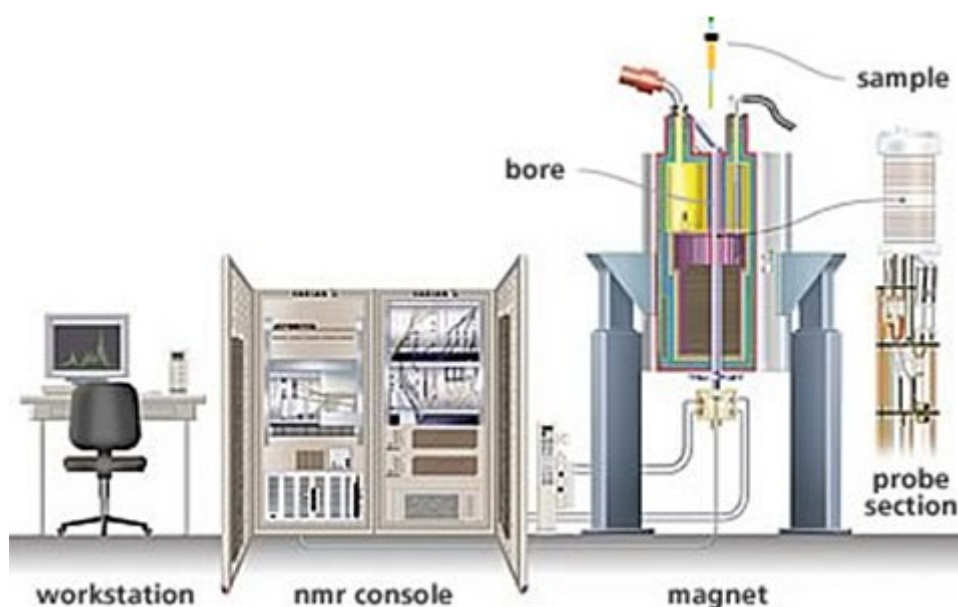
Figure 1.5 - A complete NMR system (image courtesy of Agilent)

1.3.1 - Magnets

The first NMR systems used conventional electromagnets requiring a constant power supply to maintain the magnetic field. Usually these magnets can produce magnetic field strengths up to 1 Tesla. The major advancement in magnet design came when superconductive magnets with much higher fields became available. The electromagnet in superconductive magnets has almost zero resistance and does therefore not suffer from energy losses through heating.

18

In modern times, a range from 3.34 to 21.7 Tesla is available, which in terms of proton frequency means 143 MHz to 1 GHz (a 900 MHz magnet, which is the highest available magnetic field at HWB-NMR, is shown in Figure 1.6). Superconductive magnets are cooled at liquid helium temperature and below by pumping off helium. The coils are made of alloys like niobium-titanium that can be superconductive at temperatures close to absolute zero. Typically, these temperatures are in the range of 2 to 4 Kelvin.

The field strength is important because it correlates with the chemical shift dispersion and signal intensity. There are also disadvantages for some nuclei as chemical shift anisotropy also increases with field strength. This causes increased line widths for ^{31}P may at higher field strengths.

Figure 1.6 - The 900MHz magnet found in HWB-NMR in Birmingham

1.3.2 - NMR Probes

NMR probes are inserted into the magnet and hold the sample, surrounded by one or multiple radiofrequency coils. Probes must be chosen according to the intended experiment. The first differentiation is the probe diameter. Usual dimension of NMR probes are 10, 5, 3 and 1.7 mm, and this classification arises from the NMR tube diameter. The coil arrangement is particularly important for the choice of experiment, as proton observed experiments have the proton coil inside and coils for other nuclei outside and vice versa. Probes used in this thesis also had magnetic field gradients; enabling gradient enhances pulse sequences for coherence selection.

A big technological advancement on the NMR probes was the introduction of the cryogenically cooled probes. In RF electronics, a quality factor is the signal to noise ratio (SNR). When electronics are cooled, electrical noise is low so the SNR increases. This greatly affects sensitivity compared to room temperature probes. A significant part of the noise is generated by the electronic components in the console. By cooling certain parts of the electronics down to 20-25K the electronic part of the noise can be minimised and on average 4-6 fold enhancements in SNR can be achieved. This approach (to minimise the spectral noise) is the opposite of what DNP is about, which is to enhance the NMR signal. Probes include parallel and serial capacitors to the RF coil in order to tune the probe frequency depending on the load of the coil, which depends on the sample. It is essential that each sample is tuned and matched in order to obtain the maximum signal intensity. Poor tuning and matching affects sensitivity and pulse length and the result can be poor pulse sequence performance and even complete absence of a signal. Tuning and matching is achieved by altering capacitances of serial and parallel capacitors relative to the coil of an NMR probe.

Figure 1.7 - A cryoprobe from Bruker. Image courtesy of Bruker

1.3.3 - NMR Console

The two main aspects of a console are the radiofrequency transmitter and the radiofrequency receiver. The transmitter consists of a pulse generator and a gated amplifier in order to apply a pulse to the NMR sample. The detector records the signal, in high-resolution experiments typically in a form of Free Induction Decay (FID). The console has also the necessary electronics to perform series of pulses, record and digitise FIDs. A gradient controller and amplifier allows for the application of gradient pulses during experiments.

In order to compensate for magnets field drifts in long experiments a lock signal is used. For this a deuterium signal is constantly acquired and the frequency of this signal is used ot adjust a room temperature B_0 coil on top of the cryogenic coil. For this lock signal a deuterated compound is added to the sample. In acqueous solutions, this is typically achieved by using 90% H_2O / 10% D_2O. In Dissolution DNP experiments the lock signal is not required as the experiments are basically a one scan experiment or with really short acquisition times (1-2 minutes maximum), in which magnet drift can be neglected.

With the term shimming an NMR spectroscopist refers to the settings of the 'shim' coils surrounding the probe in order to optimise the B_0 homogeneity over the NMR sample. To obtain high-resolution spectra, the magnetic field needs to be homogenous to a very high degree. This can be achieved by generating small extra magnetic fields through applying currents in room temperature coils around the sample. This process is called shimming. It originated from the word shim, which is a small piece of material to fill gaps. In dissolution

DNP experiments, it is essential that a similar sample has been pre-shimmed. A blank deuterated sample of a similar composition as the dissolution sample is used for tuning and shimming before the actual sample is acquired because there is no time to shim the actual sample as the polarisation build up by DNP will relax fairly quickly after the dissolution process. The sample filling height is also a parameter affecting shimming so if the reproducibility of the dissolution volume is not sufficiently high, the resulting shim for the dissolution DNP-NMR experiment will be bad. As the sample is transferred using pressurised gas, pressure gradients and degassing effects can occur, which will lead to liquid/air interfaces in the NMR sample, which destroys the homogeneity of the sample [21].

1.3.4 - FT-NMR

Originally NMR experiments were carried out by either sweeping the magnetic field with a fixed microwave frequency of by sweeping the microwave frequency for a fixed field. In 1966 Richard Ernst developed the first pulsed Fourier Transform NMR spectrometer [7]. The decisive step in the development was the Cooley–Tukey Fast FT algorithm, which reduced the number of operations from N*N to N*log(N). For the computers used at the time this brought the decisive break through for numerical Fourier transformations.

In FT-NMR a pulse excites the spin system and an FID is recorded. The FID is then transformed using the FFT routine to transfer the time domain into frequency domain. Pulses can vary in length and power and the excitation bandwidth of a pulse increases with shorter pulses. The time domain and the frequency domain signal are both complex functions.

Chapter 2 - Principles of DNP

2.1 Dynamic nuclear polarisation – Introduction

Dynamic Nuclear Polarisation (DNP) is a technique used in conjunction with NMR to enhance the signal intensity by transferring polarisation from unpaired electrons to atomic nuclei. DNP can be performed either in solids or in liquids. It was first predicted by Albert Overhauser [11] in 1953 and was proven experimentally by Carver and Slichter slightly afterwards [12, 22].

The mechanism of polarisation transfer is via the saturation of specific transition frequencies. There is a theoretical maximum for the enhancement that can be achieved through DNP and for each nucleus this is given by the gyromagnetic ratio γ_e/γ_n, where γ_e is the gyromagnetic ratio of the electron and γ_n the gyromagnetic ratio of the nucleus. For a proton, this theoretical value is approximately 660. The theory that lies beneath the experiments will be presented in the first part of this chapter. It includes a description of the possible polarisation experiments and an overview of the polarisation mechanisms.

Although DNP was known since the 50s, only recent developments made this technique applicable to a large variety of NMR experiments. These developments are presented in the second part of this chapter, the DNP Developments.

2.2 Polarisation Experiments: Theory and Mechanisms

Thermal equilibrium polarisation is derived in equation 0.3 and given by [9]:

$$P = tanh \frac{\gamma \hbar B_0}{2kT} \qquad\qquad 2.1$$

where γ is the gyromagnetic ratio, $\hbar$ Plancks constant divided by 2π, B_0 the external magnetic field strength, k the Boltzmann constant and T the temperature in Kelvin. Using this equation the polarisation levels of protons and electrons in different field strengths and at different

temperatures can be calculated. Owing to the higher gyromagnetic ratio γ, electrons achieve higher polarisations than e.g. protons. Temperature also contributes to the overall polarisation. Being the denominator, polarisation is lower for higher temperatures. Lowering the temperature down to 0.1 K would result in a 20% polarisation of protons at 11.74 T, although such low temperatures are difficult to achieve. All the techniques that induce a large population difference are part of the so-called hyperpolarisation methods. An overview of hyperpolarization methods is presented in 2.2.1.

2.2.1 The Experiments

The hyperpolarisation techniques fall in two main subgroups; experiments performed using microwave irradiation to induce the polarisation (DNP) and experiments inducing polarisation without microwave irradiation.

In the first subgroup, solid-state DNP can be found, mainly pioneered by Griffin [23] in the early 90's. Overhauser DNP also falls in this group, and with this term usually liquid state DNP is described. Pulsed DNP can also be considered a new field, as the polarisation mechanisms differ from the traditional approaches of continuous wave. After pioneering work of Larsen and Golman, it is possible to polarise in solid state and record a liquid NMR spectrum using ex-situ dissolution DNP.

In the second subgroup there are many ways proposed to enhance polarisation. The first and the most obvious is lowering the temperature of the system. This may not be possible in liquid state NMR, but in solid state NMR a big effort is made to lower the temperature of the experiment. A second technique is para-hydrogen induced polarisation (PHIP), in which the para-orientation of hydrogen molecule is utilised and the high polarisation is obtained through chemical reactions to an unsaturated organic molecule [24]. Polarisation transfer via a metal centre is also possible and this was pioneered by Duckett [25]. The main advantage of

PHIP is the high lifetime of the para orientation of hydrogen (can stay in para form for days) and the theoretical possibility to obtain a polarisation of 100%. Using SABRE technique (Signal Amplification By Reversible Exchange) the signal can be enhanced 1000 fold. The third approach is to use a process known as chemically induced dynamic nuclear polarisation (CIDNP) [26, 27]. With this approach reactions that are driven through radicals produce long-lived singlet states. Kaptein proposed to study protein structure as a specific probe for histidine, tryptophan and tyrosine [26]. The fourth approach is to use quantum rotor induced polarisation, in which the polarisation difference is driven through the Haupt Effect [28]. The proposed theory explains the effect as a quantum tunneling effect of rotational states of methyl groups in conjunction with temperature jumps from approximately 300K to 4 K [29]. A fifth method of polarisation is by optical pumping with circularly polarised laser light [30-32]. The advantage of this method is that optical polarised noble gases such as ^{129}Xe and ^{3}He can be used with Magnetic Resonance Imaging as they can be inhaled by patients. ^{83}Kr can also be employed.

This work is based on ex-situ dissolution DNP and a microwave source was used for every polarisation experiment.

2.2.2 The Theory of DNP

With a DNP experiment there is a maximum polarisation that can be achieved, and this is given by the ratio of the relative gyromagnetic rate ratio of the electron compared to the nucleus of interest. In table 2.1 maximum polarisations are shown for common nuclei by dividing the gyromagnetic ratios of the nuclei with the gyromagnetic ratio of the electron .[14].

Table 2.1 – The maximum polarisation enhancements for various nuclei

Particle	Gyromagnetic ratio γ/rad s^{-1} T^{-1}	Maximum Polarisation
e^-	1.7608 x 10^{11}	-
^1H	26.7522 x 10^7	658.18
^2H	4.10663 x 10^7	4287.70
^{13}C	6.72828 x 10^7	2617.12
^{14}N	1.93378 x10^7	9105.48
^{15}N	-2.71262 x 10^7	-6491.14
^{31}P	10.83940 x 10^7	1624.44

Although the theoretical maximum for polarisation is high, in practice less polarisation is achieved through DNP, owning to incomplete polarisation transfer, loss of polarisation after the transfer and various partially understood relaxation effects.

DNP is the transfer of polarisation from unpaired electrons to the nucleus. The way this transfer occurs varies and there are several mechanisms proposed for different conditions. The overall Hamiltonian of an electron-nuclear spin system with Zeeman split engaged is given by the equation [33]:

$$\hat{\mathcal{H}} = \omega_e S_Z - \omega_n I_Z + \mathcal{H}_{ee} + \mathcal{H}_{en} + \mathcal{H}_{nn} \qquad 2.2$$

The first two terms describe the Zeeman interactions for the electrons and for the nuclei respectively. The ω is proportional to the γB_0 ,with γ as the gyromagnetic ratio of electrons or nuclei. The three Hamiltonian terms describe the interactions between electrons, between electrons and nuclei and between nuclei respectively. The energy Hamiltonians have a different significance for different experimental conditions. In liquid state DNP the most important term is $\mathcal{H}_{en}$, describing electron nuclear interactions arise from dipolar coupling

and the scalar Fermi interaction. In solid state the $\mathcal{H}_{ee}$ is an important factor as in cross effect there is an electron-electron interaction. [18]

2.2.3 The mechanisms

2.2.1 - Overhauser DNP

If the sample is in liquid state, the mechanism that takes place is called the Overhauser DNP. It is discussed in the introduction that Overhauser was the first to propose theoretically the possibility to perform DNP and Carver and Slichter the first to prove this theory. This first application was carried out using the ^{7}Li alkali metal where polarisation was transferred from the endogenous electrons of the metal lattice to its NMR active nucleus.

The way it is performed is by irradiating at Larmor frequency of the electron. The thereby altered polarisation of electrons causes flip-flop (W_2) or flip-flip (W_0) transitions, which transfer polarisation to the nuclei. For a two spin system, these transitions are shown in figure 2.1[18].
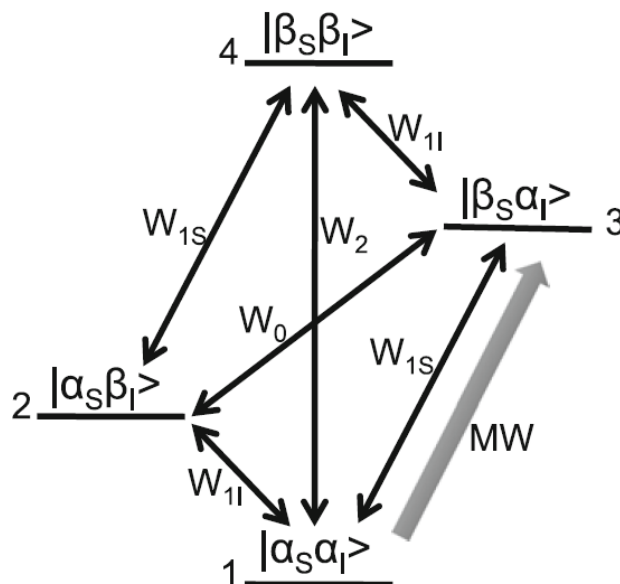
Figure 2.1 – The energy level diagram of a two-spin system IS showing the transition probabilities. In overhauser DNP the W_{1S} transition is irradiated. Taken from [18]

The following equation was proposed by Hausser and Stehlik and utilise the Solomon equations to describe the effect using rate equations[34]:

$$\frac{d\langle I_z \rangle}{dt} = -p(\langle I_z \rangle - I_0) - \sigma(\langle S_z \rangle - S_0)$$

2.3

where I_0 and S_0 are the thermal equilibrium values of the relevant expectation values.

With Hausser's introduction of a coupling factor (ξ), leakage factor (f) and saturation factor (s) a basic theory has been developed that describes the most relevant contribution towards polarisation in liquid. The coupling factor describes the contribution of molecular motions towards the transition probabilities W_2 and W_0. The leakage factor accounts for the loss of polarisation due to electrons, and the saturation factor simply accounts for the saturation achieved for the electrons.

2.2.2 The solid effect

The solid effect is observed when a sample is polarised frozen in the solid state. This mechanism usually engages in temperatures lower than 1.5 K. The main characteristic is the irradiation frequency. Instead of irradiating the Larmor frequency of the electrons the solid effect demands irradiation of the W_0 or W_2 transitions. Therefore the irradiation frequency is the electronic Larmor frequency with the nuclear Larmor frequency substracted or added.

For a solid effect the EPR linewidth of the radical has to be narrow and the nuclear Larmor frequency large. If this is not the case, the solid effect is not well resolved. In experiments performed within this thesis, the solid effect was not very well resolved in most cases, therefore a contribution of thermal mixing is assumed. A simulated ideal separation is shown in figure 2.3[35].
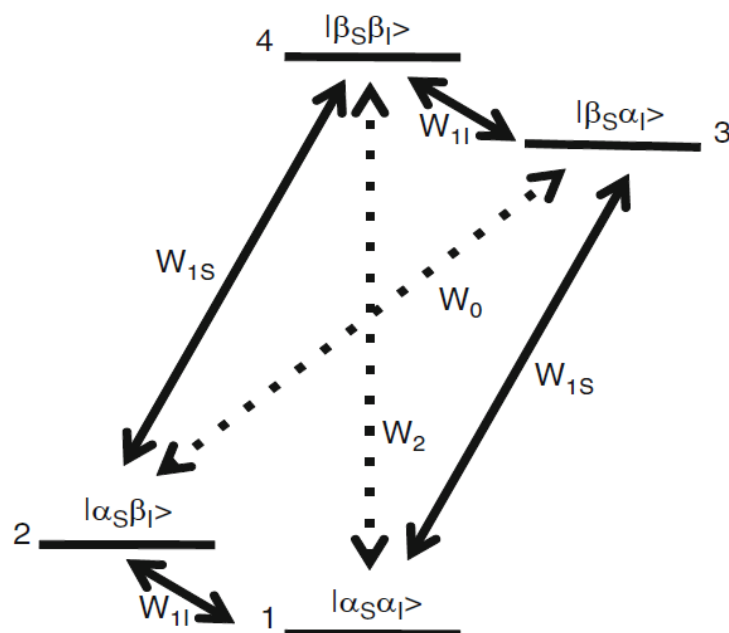
Figure 2.2 – The solid effect. Irradiation of the double or zero quantum transition lead to a mutual flip-flop or flip-flip and subsequent polarisation transfer from the electrons to the nuclei. Taken from [18]
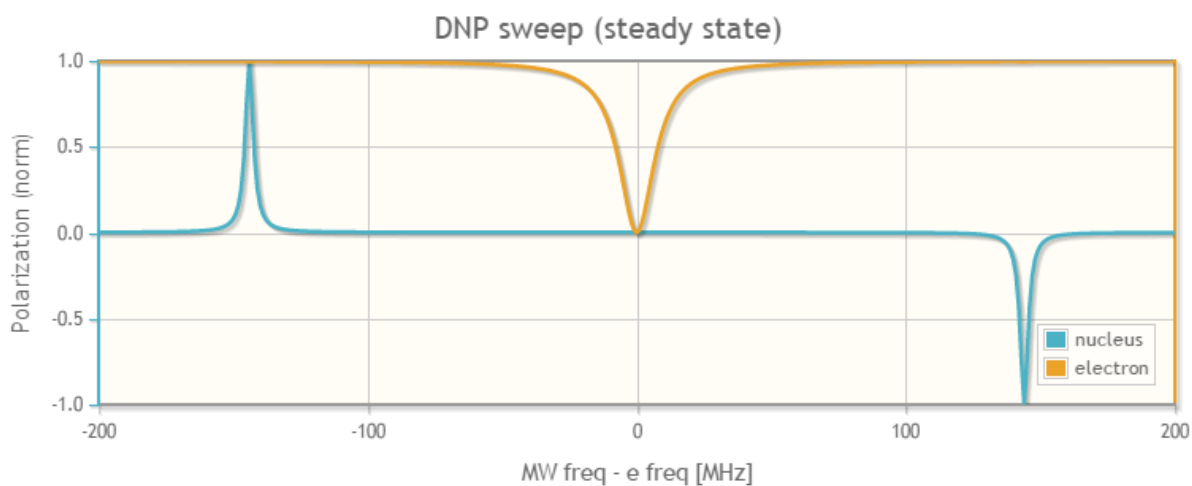
Figure 2.3 – A simulation of a microwave sweep demonstrating the solid effect [35]

2.2.3 - *The Cross Effect and the Thermal Mixing*

Cross effect and thermal mixing both require 2 or more electrons to be in close proximity. The necessary condition is that the inhomogeneous linewidth Δ is greater than the nuclear Larmor frequency ($\Delta > \omega_n$) while the homogenous width has to be smaller. If the EPR lines are

homogenously broadened, the TM is the dominant mechanism. If the EPR lines are inhomogeneously broadened cross effect mechanism is encountered.
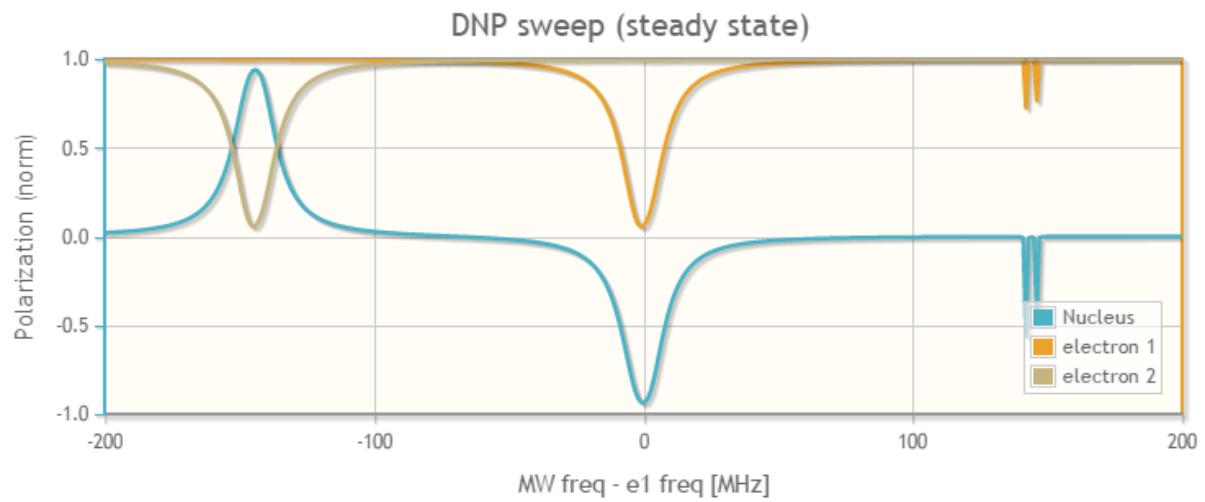
Figure 2.4– A simulation of a microwave sweep demonstrating the cross effect [36]

2.2.4 – Overview over the Polarisation Mechanisms

Table 2.2 provides an overview of the polarisation mechanisms showing the sample type, the conditions and the irradiation frequency.

Table 2.2 – An overview of the hyperpolarisation mechanisms in the different sample states and chemical environments[18].

Mechanism	OE	SE	CE	TM
Application	O-DNP	D-DNP	SS-DNP	D-|DNP
Sample	Liquids	Glassy state	Glassy state	Glassy state
Conditions	H_{en} time-dependent; polarisation transfer via relaxation	H_{en}^{Se} causes mixing of states; forbidden transisiton, slow build-up. Low concentration of radicals, no dipolar coupling between radicals.	Inhomogeneous broadening of ESR signal, large g-anisotropy, dipolar coupling between radicals.	Homogeneous broadening of the ESR signal. High concentration of radicals.
Frequency dependence	$\omega_c \tau_c < 1$	B_0^{-2}	B_0^{-1}	$\omega_{e1/2}$
MW irradiation frequency	$\omega = \omega_e$	$\omega = \omega_e + \omega_n$ Maxima in MW sweep separated by $2\omega_n$	ω_{max} at polarisation maximum, depends on EPR lineshape	ω_{max} at polarisation maximum, depends on EPR lineshape

2.2.5 – Pulsed DNP

As the DNP microwave instrumentation advances and moves to higher frequencies, other experiments are becoming possible. For example, pulsed DNP methods are now applied in order to study and overcome the inherent problems of CW polarisation methods and mechanisms.

2.3 DNP Instrumentation and Implementations

2.3.1 - Introduction

Several spectrometer configurations and experimental designs have been proposed for performing DNP experiments. The renaissance of DNP started after the possibility to make microwave sources that can work at high frequencies. The synthesis of stable radicals is also crucial for each experiment. Whether they have narrow or broad EPR linewidths determines the polarisation mechanism. The development of new radicals is ongoing and important to better understand polarisation mechanisms (see 2.3.3). The four most commonly used implementations of DNP are High Frequency-liquid DNP, Shuttle DNP, MAS DNP and Dissolution DNP and are presented in 2.3.4 – DNP instrumentation.

2.3.2 - Microwave sources

The development of microwave sources was a major milestone for performing high-field DNP. Before the 90's the highest possible microwave frequency suitable for DNP applications was 40GHz, or equivalent to 60 MHz proton frequency. The development of gyrotrons of 140GHz[23] and later 250GHz[37] allowed polarisation experiments in much higher fields. Nowadays the technology allows for terahertz gyrotrons, operating at 980GHz[38].

2.3.3 - Stable free Radicals used in DNP

In every DNP experiment the presence of a paramagnetic source is essential. For the first years of DNP experiments, metals or organic radicals such as DPPH, BDPA and TEMPO were used as paramagnetic agents.

A stable free radical is an inorganic or organic molecule that has an unpaired electron. When two unpaired electrons are in the same molecule the compound is called a biradical. There are three basic methods of synthesising free radicals in organic chemistry. The first is homolytic

cleavage, in which the electron pair is split, the second is redox reactions with electron tranfer and the third is using a radical as a reagent to act on an organic compound [39].

In general, free radicals are very unstable compounds with average half time of 10^{-3} s. However, there are stable radicals with life times of years. In DNP applications there is a need of stable radicals that can be added to the polarisation matrix as source of free electron [40-48]. One of the most stable radicals is DPPH (Diphenylpicrylhydrazyl radical) forming dark red crystals and is stable for years (at 4°, in the absence of air, humidity and light sources). Another stable radical used for DNP is the OX63 trityl radical (that has a triphenyl structure). Trityl radicals have narrow EPR linewidths and allow for the direct polarisation of ^{13}C.

The stability of these radicals arises from a delocalization of electron density owing to multiple resonance-mesomerism forms forming a protected environment around the radical. Mulliken suggested that the basic factor that describes the stability of a radical is the hyperconjugation, and in case of alkyl radicals the 2p orbital having the unpaired electron interacts with the π and π^* molecular orbitals of the alkyl group.

Recently radicals have been optimised for DNP applications to produce larger enhancements at lower concentration. For DNP radicals have to be stable at room temperature and need to be soluble in the matrix that has to be polarised (typically a mixture that can form a glassy state solid). Common radicals that are used include the trityl radicals (OX63, Finland), TEMPOL and biradicals composed of TEMPOL or trityl subunits.

2.3.4 - DNP Instrumentation

The four most commonly used implementations are High Frequency-liquid DNP, Shuttle DNP, MAS DNP and Dissolution DNP. The first two are configured to polarise samples in liquid state in contrast with the latter two, which are polarising solid-state samples [49-59].
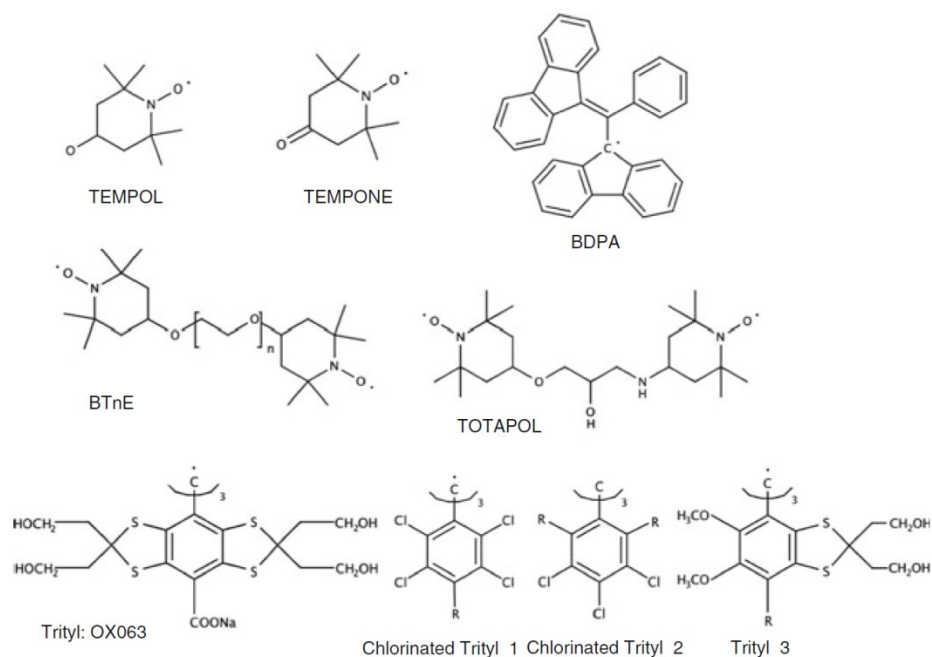
Figure 2.5 – Radicals used in DNP. For Trityl, A concentration of 15mM of OX63 is sufficient for DNP applications. Taken from [40].
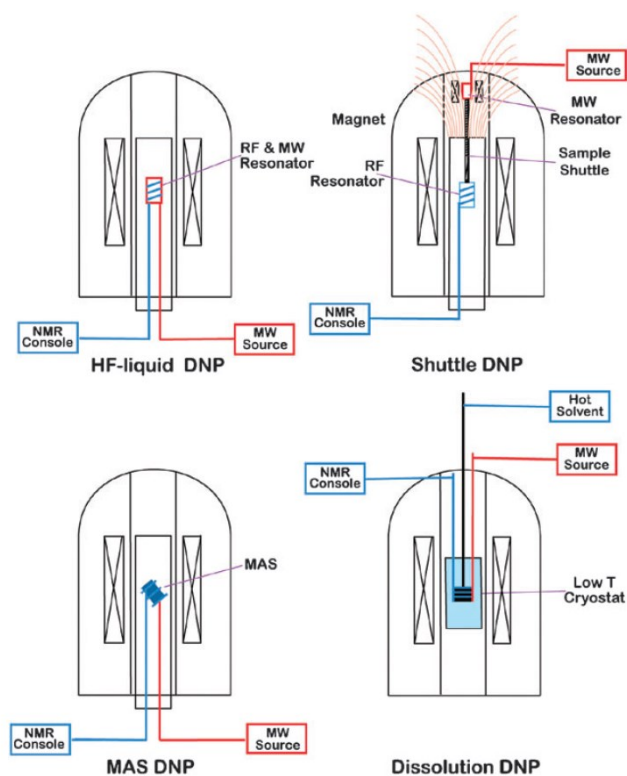
Figure 2.6 - Typical experimental designs / instrumentation for performing DNP experiments.

The HF-liquid DNP is a system designed for in-situ polarisation as the microwave irradiation is performed where the NMR measurement is been taken. With this setup, both the polarisation and the detection are performed at a relatively high field. This setup is has been used for Overhauser effect polarisations of liquids at room temperature [60-62]. Other implementations were designed for low temperature polarisations [63] with the main goal to study polarisation mechanisms.

The Shuttle DNP is a system where the polarisation is performed in a lower magnetic field. This lower field is separated from the place in the magnet where the spectrum is acquired. Therefore the sample has to be transferred to the high field after polarisation. This setup has been implemented with a two centre magnet. Dorn [49] combined HPLC with NMR performing DNP in liquid state within flowing liquids.

MAS DNP has been developed by Griffin [23, 64] and it is a system, in which the polarisation step is performed with the sample cooled in the solid state. It's also an in-situ device like the HF-liquid DNP, as the polarisation and the detection occur at the same place. The temperature that it was selected for cooling was the one of liquid N_2.

There is no doubt that instrumentation plays a major role in the interchangeable knowledge between experiment and theory. The devices presented in this chapter are recent developments, which greatly benefit from all the developments in the field of electrical engineering, in particular regarding the design of stable and high-powered microwave sources.

2.4 – Dissolution DNP

2.4.1 - Introduction

Dissolution DNP (D-DNP) is the implementation of DNP used in this thesis and will therefore been described in more detail in this separate subsection. It's also called *ex situ*

DNP[14] and represents the implementation of DNP with the largest enhancements. The large enhancement arises from the multiplication of the polarisation enhancement with the temperature jump enhancement. It is based on polarising in a low field magnet (typically 3.34 T field, 94 GHz microwave frequency, other implementations will be discussed in 2.4.3) at very low temperatures (1.4 K) and after polarisation the hyperpolarised sample is rapidly melted and dissolved in a hot solvent. Immediate transfer of the sample in to a conventional NMR magnet follows to acquire the enhanced NMR spectrum, which is recorded at room temperature. With this approach, two types of enhancements are combined, the Boltzmann temperature enhancement and the DNP enhancement. Therefore the final equation that will give the theoretical polarisation enhancement (ε) is[14]:

$$\boldsymbol{\varepsilon = \frac{\gamma_e}{\gamma_n} * \frac{B_{DNP}\, T_{NMR}}{B_{NMR}\, T_{DNP}}} \qquad 2.4$$

where B_{DNP}, B_{NMR} the field of the DNP and the NMR magnets, T_{DNP}, T_{NMR} the temperatures and γ_e, γ_n the gyromagnetic ratios of electron and nucleus. This leads to much larger enhancements than experiments without a temperature jump. For the system configuration used in this thesis, with B_{DNP} = 3.34 T, B_{NMR} = 11.74T, T_{DNP} = 1.4 K and T_{NMR} = 303 K the enhancement factor contributed by the temperature jump minor the losses of the lower magnetic field is 61.57. Table 2.3 shows the maximum theoretical enhancements using the system of this thesis. Achieving a 10000 fold polarisation means that the actual DNP enhancement is lower than the theoretical value given by the gyromagnetic ratios, usually in the range of 50.

Table 2.3 – Maximum polarisation with Temperature Jump contribution

Particle	Gyromagnetic ratio γ/rad s^{-1} T^{-1}	γ_e/γ_n	Maximum enhancement (ε)
e^-	1.7608 x 10^{11}	-	-
^1H	26.7522 x 10^7	658.18	40526
^2H	4.10663 x 10^7	4287.70	244359
^{13}C	6.72828 x 10^7	2617.12	149169
^{14}N	1.93378 x10^7	9105.48	518985
^{15}N	-2.71262 x 10^7	-6491.14	-369987
^{31}P	10.83940 x 10^7	1624.44	92568

2.4.2 - Polarisation mechanisms in D-DNP

Polarisation mechanism in D-DNP seems to be mainly the solid effect and thermal mixing [18]. This hypothesis is supported by the work of Ardenkjaer − Larsen with experiments examining the polarisation of ^{13}C-urea in glycerol with trityl radical OX63 at 1.4 K. The build-up constant τ observed for ^{13}C was 4,900 s and the T_{1n} of the ^{13}C signal was 28,200 s. Maximum polarisation was achieved with 15mM concentration of radical (42% for urea), with this number falling to 26% for 20mM concentration. Although thermal mixing seems to be the main mechanism, contribution of the solid effect is possible, especially when the polarisation process is relatively long.

Ardenkjaer-Larsen also examined the polarisation process of ^{13}C(1)-pyruvic acid at a 1.4 K polarisation temperature with 15 mM concentration of OX63Me and showed that T_{1e} is quite long with a value of 0.91 s, and T_{1n} is about 12,000 s at this temperature.[65]

The effect of the presence of Gd^{3+} in [40] the polarisation matrix was examined. Gd^{3+} drastically shortens T_{1n} and it is commonly used as a contrast agent in MRI.

2.4.3 – Implementations of D-DNP

This implementation is used more broadly because a commercial available instrument is available, which has also been used in this thesis (Oxford Instruments, by the name Hypersense[TM]) [66].

Using this polariser, ^{13}C can be polarised with trityl radicals and ^{1}H with TEMPO. A klystron is responsible for producing the microwave frequency and this is at a range of 94GHz and 100 mW power. This procedure is driven by direct SE to ^{13}C.
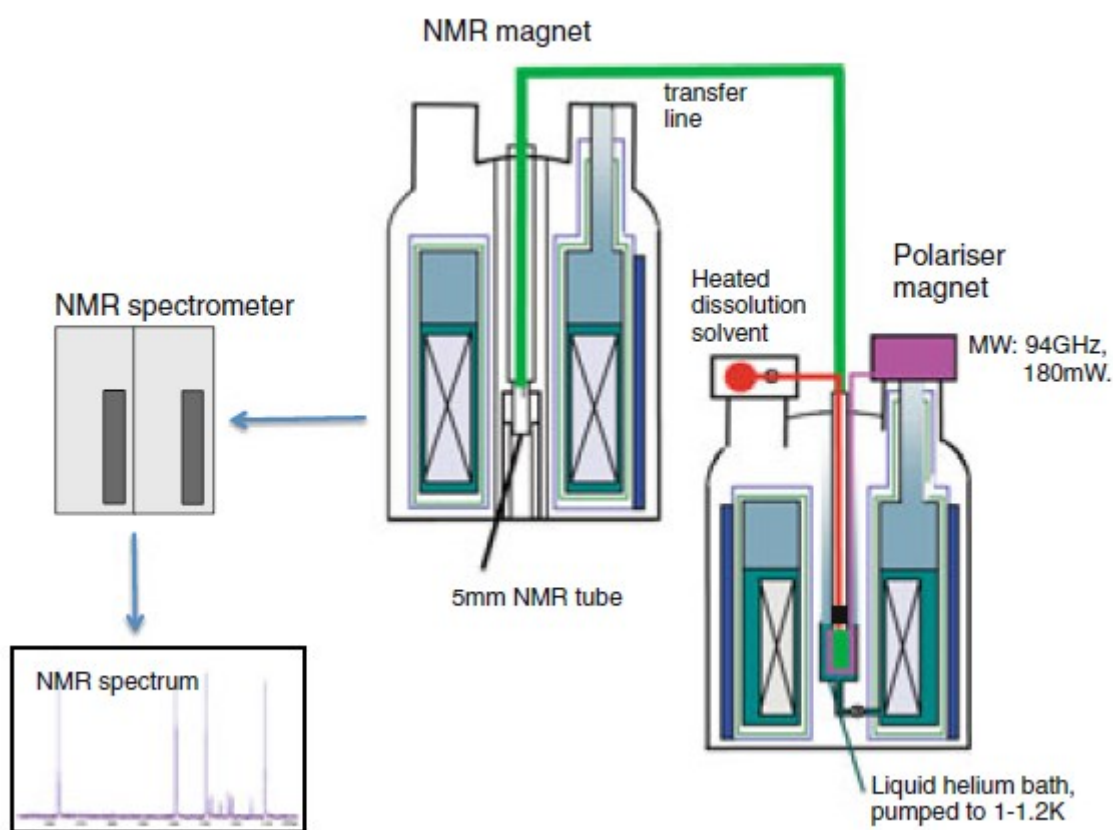
Figure 2.7 - The Hypersense polariser from Oxford Instruments. Taken by [18]

The main disadvantage of this DNP technique is that the melting and dissolution of the sample are irreversible and that means that only one scan can be acquired. The acquisition time of the NMR experiment is therefore limited by the life-time of nuclear spin polarisation, i.e. by the longitudinal relaxation times of the polarised nuclei.

On the other hand, with enhancements of 10^4 and the progress of the fast multidimensional techniques, the 'one scan' limitation can possibly be surpassed. One way to perform fast 2D experiments is by utilising small flip angle excitation with a small number of increments in the indirect dimension [67]. With this method the polarisation can be used in multiple steps. The limiting factor is relaxation, as if the increments delay the acquisition relaxation will take place. In this thesis this method was used in a fast HMQC pulse sequence. Another approach is the single scan ultrafast 2D that Lucio Frydman has developed[14]. Instead of having the increment in the indirect dimension, a gradient profile is selected to perform different excitation for each part of the sample. The advantage of this method is that is much quicker than the small flip angle excitation, but the disadvantage is the low sensitivity, as the sample is not be treated as a whole but is separated by gradients in 'smaller' samples.

2.4.3 - Experimental conditions for D-DNP

Sample preparation for D-DNP includes the following requirements and procedures:

The samples must be prepared in a glassy state matrix. These glassy state matrices can be prepared using mixtures of glycerol, DMSO, methanol and water. The maximum volume of the sample cup is 250 μL, so the amount that is usually been used is 100 to 200 μL. In order to achieve the optimum polarisation enhancement, the temperature of the He bath has to be approx. 1.4 K. The subsequent dissolution step is performed using hot solvents under pressure, like methanol and water. Methanol is used with nine bars of pressure and water with ten bars, where the solvent temperature reaches 180-200°C. After dissolution, the samples are transferred to the NMR tube using high gas pressure (2-3 bar) and 4 mL of solvent.

2.4.4 - Glassy state matrix

A glassy state matrix [48] is a necessary requirement for a successful DNP experiment. The term glassy state matrix describes a non-crystalline mixture, in this case at temperatures close to 1.4 K. The glassy state is commonly formed by shock-freezing certain mixtures of solvents

and can be readily identified as the sample remains transparent when it is frozen. The role of the glassy state matrix is to minimise homogeneous broadening. There are a numbers of substances that can be added in order to avoid crystallisation of the sample. Addition of glycerol and DMSO are the two reagents most commonly used in dissolution DNP. In Table 2.4 a selection of mixtures and the relative state is presented. In some cases substances can also be self-glassing. This is the case with pure pyruvic acid and this enhances the concentration of the dissolved solution, as addition of reagents that keep the sample in glass state usually dilute the polarised sample.

Table 2.4 – Mixtures of the sample matrix used in hyperpolarisation experiments

Compound of mixture at -196	Glassy state	Crystalline state
Water		x
Water/Glycerol	x	
Water/Glycerol/Any	X (>20% Glycerol)	
DMSO		x
DMSO/Water	x	
DMSO/Acetone		x
Acetone		x
Acetonitrile		x
Acetone/Water		x
DMSO/Water/Acetone	x	
Methanol		x
DMSO/Methanol	x	
Methanol/Glycerol	x	
Water/Methanol/Glycerol	x	
Water/DMSO/Methanol	x	
Isopropanole	x	

2.4.5 - Improvements of the Dissolution system of the Hypersense

Many attempts have been made to improve the dissolution procedure of the polariser. It is a critical step and usually acts as a limiting factor to the experiments than can be performed. The main limitation is the slow transfer time when compared to the fast relaxation times of many nuclei. The other limiting factor is the sample delivery instabilities that arise from poor transfer. In a conventional system, transfer is usually performed with a 3 bar carrier gas.

Hilty [68] developed a system that can perform the dissolution step faster than the standard dissolution approach by keeping the sample constantly under pressure. The Hilty dissolution system reduces the formation of bubbles in the NMR tube and shortens the dissolution time. The absence of bubbles is important for the homogeneity of the sample, which is required to obtain NMR signals with a minimal line width. A short dissolution time is important for measuring compounds with shorter relaxation times. Commonly, the dissolution process takes about 2-3 seconds. With Hilty's implementation, this time can be lowered down to 600 ms, enabling the acquisition of spectra from molecules with relaxation times of a few hundred ms.

Another addition is a device that can remove the radical at the dissolution step [18]. This is important for two main reasons: First with radical present the longitudinal relaxation times are shorter, and secondly, the radical is potentially toxic for *in vivo* applications. Recent applications indicate the possibility to have a conjugated flow cell/bioreactor in to a DNP system, so the hyperpolarised solvent can be driven into cell cultures.

2.4.6 - In vivo applications of tandem ex-situ D-DNP - MRI

Dissolution DNP has been used *in vivo* since the beginning of the development of the polariser [13]. Several clinical applications in combination with MRI are feasible. DNP-MRI has great potential as a non-invasive diagnostic technique detecting metabolic changes in tumours. It has been used in prostate and pancreatic cancer. Pancreatic cancer has the disadvantage that the diagnosis with MRI is hard as the bladder location is not allowing easy screening of the pancreas [69].

The main limitation of D-DNP arises from the need to carry out NMR experiments within the longitudinal relaxation time of the polarised substances. In general quaternary carbons have the longest longitudinal polarisation times. ^{13}C-1-pyruvic acid has become the most applied

substance in in vivo applications because the C_1 has a longitudinal relaxation time of 30 sec. There have been various attempts to broaden the spectrum of molecules that can be studied. Recent work involves the isolation of singlet states with longer relaxation times, and the use of deuterated compounds in order to lengthen relaxation times. [70]

In vivo applications of D-DNP represent a fast growing field holding promise for clinical applications. The main application targeted by current clinical trials is in detecting the fate of the ^{13}C-1-pyruvate in tumours, which reflects its metabolic state, by measuring of the ratio of alanine and lactate. Another application showed that the *in vivo* pH can be measured in tissue using hyperpolarised ^{13}C-labelled-bicarbonate, which can potentially be used to diagnose pathological processes that alter a tissue pH, including cancer, ischemia and inflammation.
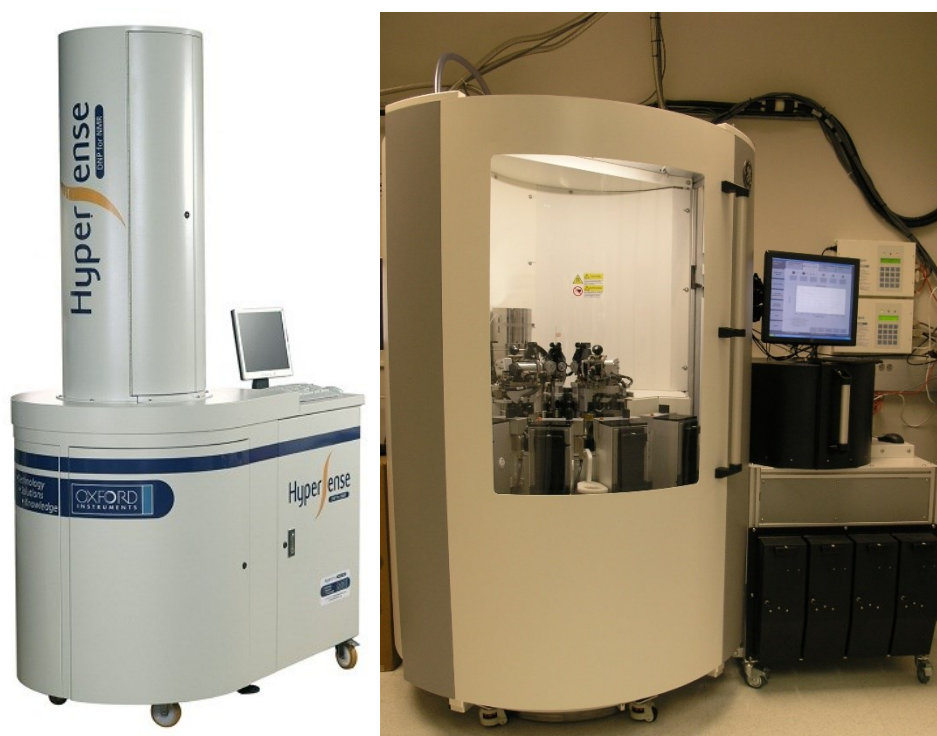
Figure 2.8 - A: The Hypersense Polariser B: Evolution of the polariser for clinical use

Experimental Part

Introduction to Experimental Part

In this PhD thesis the experimental part consists of four chapters, 3 to 6. Chapter 3 describes the development of a post-dissolution sample transfer device, chapter 4 shows applications using this device, chapter 5 shows DNP applications with acetylated compounds and chapter 6 is concerned with parallel receiver experiments in tandem with DNP. For this work a DNP and an NMR system were used and the principle of operation follows.

The DNP system

The Hypersense polariser from Oxford Instruments was used to prepare the polarised samples.
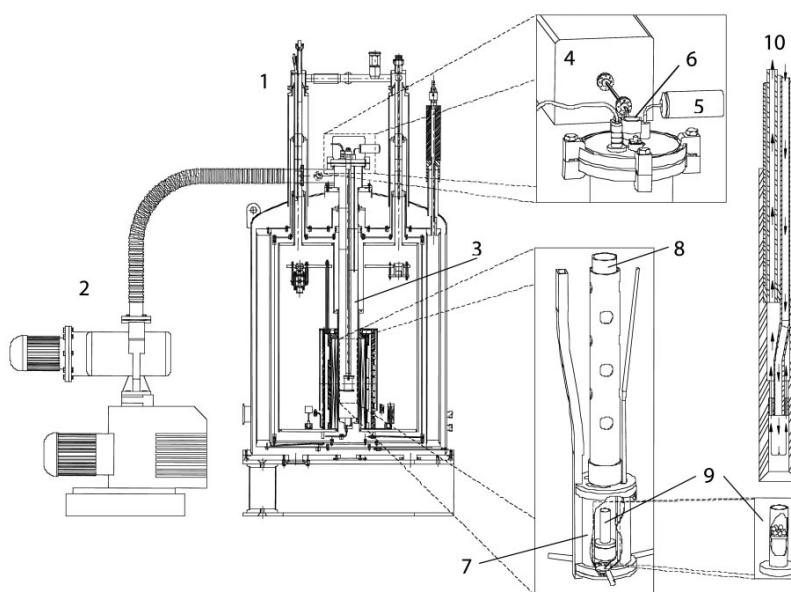
Figure Exp.1 - The Original Polariser Design Built By Jan Henrik Ardenkjaer-Larsen (Taken From [65]). 1, Dnp Polarizer; 2, Vacuum Pump; 3, Vti; 4, Microwave Source; 5, Pressure Transducer; 6, Sample Port;7, Microwave Container; 8, Sample Holder; 9, Sample Container; 10, Dissolution Wand.

The Hypersense is built based on the original design by Goldman et al [13]. A wide bore superconductive magnet with a field-strength of 3.34T (equivalent to 143 MHz proton frequency) has been used to house the polariser. At this field, the electronic Larmor

frequency is 94.100 GHz. The microwave source is an analogue source made by ELVA-1 (St. Petersburg) and has maximum output of 200 mW at 94 GHz. It can be tuned over a 500 MHz range.

The temperature control of the Helium bath is controlled by constant adiabatic expansion of helium gas. By reducing the vapour pressure using a vacuum pump, the helium bath can reach a temperature of 1.2K, even with the microwave source turned to on. The pressure above the liquid helium equals 0.8 mbar at 1.2 K is used to calculate the temperature. The level of Helium in the bath is determined by readout of three 100Ω carbon resistors, placed at three different height levels. In practice the instrument used for this thesis reached 1.3-1.4K.

There are several procedures required to operate this polariser. The first is the sample insertion. The sample is placed in a sample cup with volume of 100 μl to 200 μl. The system then raises the sample holder and opens the sample port so the sample can be inserted with a sample insertion wand (approximately 1 meter long). After the sample has been deposited below the sample holder, the sample holder moves into its lower position and the sample enters the helium bath, placed inside the microwave cavity.

The second procedure is usually the actual polarization during which the microwave source is turned on while the helium pressure is constantly regulated to maintain the intended temperature. During a polarization approximately 10l of liquid helium are needed per hour to keep a temperature of 1.4 K.

The third procedure is the dissolution process after the polarisation. The way it is performed is by adding 4 ml of solvent into a pressurisable container where it is heated to 180-200°C at 9-10 bar pressure, depending on the solvent (usually methanol at 180°C and 9 bars and H_2O at 200°C and 10 bars). A dissolution wand consists of a carbon fibre insert and two teflon tubes, one to direct the hot solvent to the sample cup and another to drive it out to the NMR

tube. The dissolution wand grips the sample cup and raises it out of the helium bath. The hot solvent enters the sample cup and melts the sample; the dissolved solution is then driven into a hose using helium gas pressure (chase gas). During this process the sample experiences a field gradient, a temperature gradient and a pressure gradient. The field gradient is 3.34 T in the core of the magnet and 3 T in the position when the sample holder has been raised. When it leaves the polarizer it is kept at a low magnetic field by a permanent magnet located on top of the superconductive magnet. Subsequently, during the transfer to the NMR magnet the field varies between the polariser magnet and the high-resolution magnet and at the end it enters the high resolution magnet (11.74 T in our case). Considering that the distance between the polarizer and the NMR magnet was only 1m and the NMR magnet is an older shielded design with a 5 Gauss line outside the cryostat there was no need to install magnets along the transfer line. As Figure 2 shows the magnetic field is never below 10G during the transfer. The Figure shown does not show the magnetic field in the current configuration as it was taken before a permanent magnet was installed on top of the polarizer.
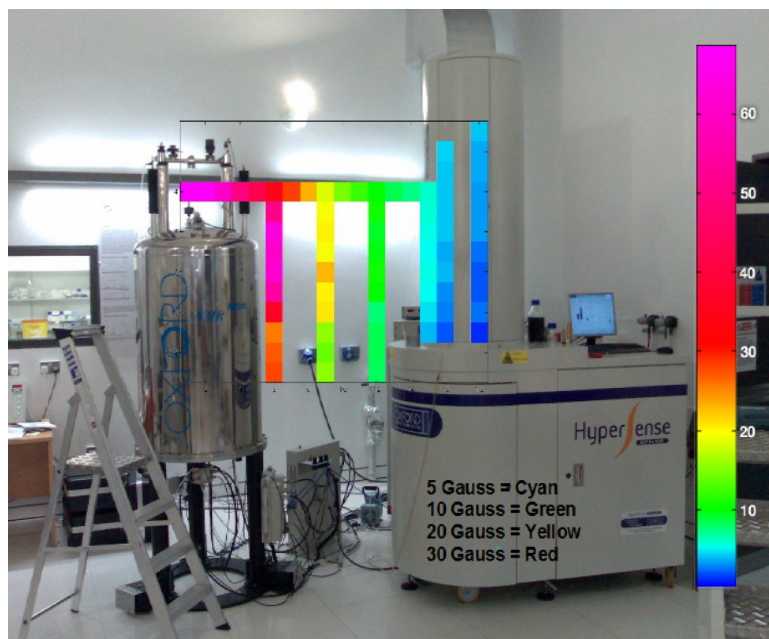
Figure Exp.2 - Field Gradient between DNP and NMR magnet in HWB-NMR. Taken form [28]

The temperature gradient ranges from 1.4K to 303K, although parts of the sample can - momentarily- reach higher temperatures from the hot solvents. Finally, there is a pressure gradient, from 9-10 bars (dissolution pressure) to 3 bars (carrier gas pressure) and then to atmospheric pressure (NMR tube). This pressure gradient can cause artifacts and this is one aspects covered by the dissolution sample transfer device that is presented has been developed in this thesis.

Chapter 3 - Development of a Post Dissolution Sample Transfer System

The DNP experimental setup used for this work consists of an Oxford Instruments Hypersense polariser operating at 3.34 T in conjunction with a 500 MHz (11.74 T) NMR magnet equipped with a 5mm broadband direct observe (Bruker TBO) probe and a Bruker Avance III console. *Ex situ* DNP using the Hypersense is carried out by cooling the sample down to 1.4 K in the presence of a stable radical, followed by polarising by microwave irradiation. After polarisation the sample is transferred through the dissolution process to the NMR magnet. This is one of the most crucial steps of the experiment.

3.1 The post-dissolution sample device - Principle of Operation

In order to improve the sample transfer process we built a device that transfers the sample using a larger pressure gradient. When dissolution is started the Hypersense performs a row of events that was described earlier.

In the original design of the Hypersense instrument, this sample is transferred into the NMR tube and the solvent experiences a change of pressure of 10 bar (in the dissolution pressurised chamber) – 3 bar (after release of the dissolution solvent and during the transfer procedure with Helium gas carrier) and 1 bar (after sample is rest in atmospheric pressure). This has a variety of disadvantages. The most severe disadvantage is that it is dependent on solvent surface tension. When water is used, sample transfer often fails. This is the reason for using methanol, which has better flow characteristics and is less prone to form bubbles. The second disadvantage is the long time needed for the process to complete, as transferring with 3 bars results in a slow transfer. Finally, the pressure difference that the sample is experiencing results in degassing effects when it finally enters in the NMR tube thus producing a sample with gas bubbles that greatly affects the line shape of the NMR signals.

In our design we changed the pressure gradient for the sample. We collect it from the polariser in a sample loop and then transfer it with a 7 bar pressure difference, by applying 10 bar forward / 3 bar backward pressure. This greatly enhances sample transfer speed and sample settling times and therefore changes the timing of the transfer from seconds to milliseconds. Also the selection of solvents is wider as higher viscosity solvents can be used. Figure 3.1 shows a sketch of the device built as part of this thesis.
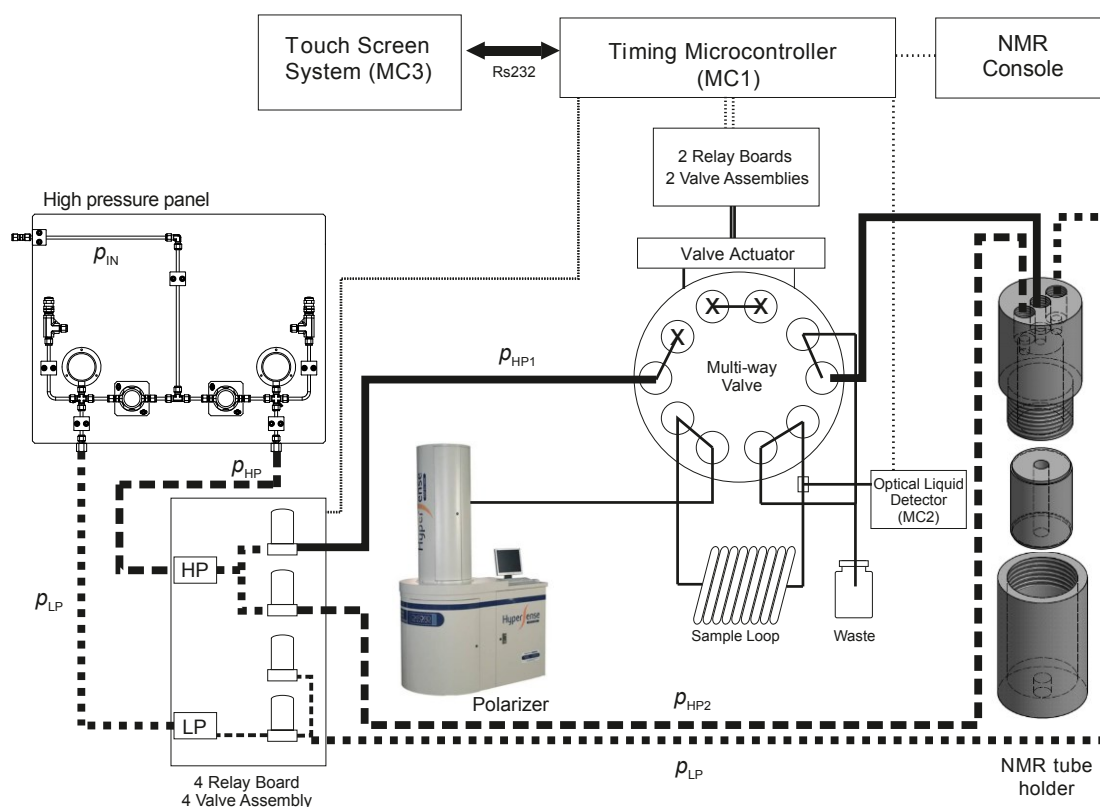
Figure 3.1 – An overview of the dissolution device, showing all the individual components.

3.2 The post-dissolution sample transfer device - Components

Our dissolution device consists of several components that can be split in two major groups, electronic and pneumatic. All the electronic components are either sensors or accurate time switches. The pneumatic components are graded for high pressure gas transfer and the purpose is to guide the sample into the NMR magnet.

3.2.1 Pneumatic Parts

The main building blocks of the pneumatic part of the design are the pressure regulating panel, the multi-position valve and the NMR Tube Holding System.

The pressure regulating panel is a high pressure manual valve system that can split a high pressure input in two different pressures. The input pressure (P_I) is a 12 bar output from a Nitrogen cylinder and the resulting output is set to 10 bars for the high pressure (P_{HP}) and 3 bars for the low pressure (P_{LP}). This design is presented in Figure 3.1. This panel was outsourced to Swagelok London. The main component is the KPR Pressure regulator, capable of delivering 0-34.4 bar output. This design meets the Health and Safety regulations for Gas Safety in the UK.

The two position valve is a VICI C22 6180 valve with a pneumatic actuator (Vici, Switzerland). The pneumatic actuator is connected to the air supply of the HWB-NMR facility and controlled by two relays by an Arduino controller [71]. The valve has 10 input/output positions that can be connected sequentially. So the connections are either 1-2, 3-4 etc. or 1-10, 2-3 etc. These two positions are named load position, for the sample loading and inject position, for the sample injection. The valve is connected as shown in Figure 3.1. In detail, the P_{HP} is connected to position 1, the sample loop is connected in position 2 and 5, the Hypersense output is connected in position 3, position 4 is connected to the waste and position 6 is connected to the NMR Tube Holding System. Position 7 is connected to the

waste and positions 8, 9, 10 are closed with a cap, so pressure is not leaking from the valve. In Figure 3.1, the load position is presented.

The NMR Tube Holding System was designed to hold the tube with a high reproducibly injection pattern avoiding glass breakage at high pressure. The design underwent several advancements during the course of this PhD thesis. The main idea of this holder is to have a gas tight grip of the NMR Tube that can stand high pressures in the range of 10-15 bar and a pressure jump of 7-10 bar. The design is gas proof up to 15 bar, but for everyday use it was found that using safer settings of a maximum of 10 bar is sufficient for having a stable and quick transfer.
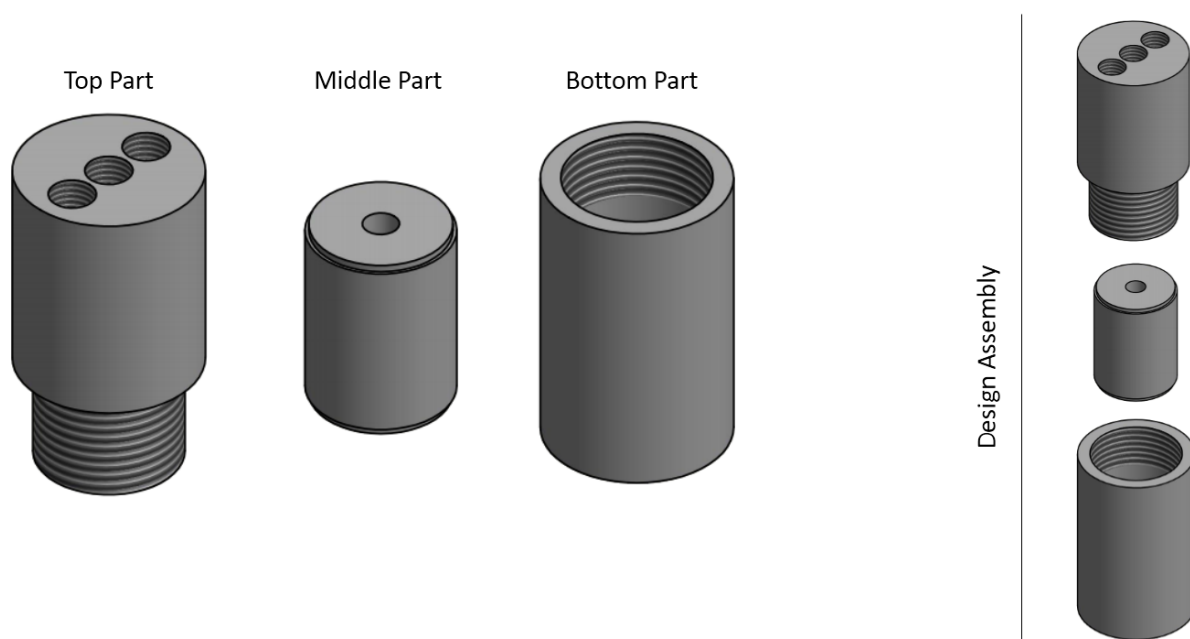
Figure 3.2 – Top, Middle and Bottom parts of the NMR Tube Pressure holder

This part was designed in Autodesk Inventor and consists of three major parts, named as the Top, the Middle and the Bottom part for convenience (Figure 3.2). The material used had to be chemically inert, sufficiently strong to hold high pressure and magnetically neutral, so PEEK was the material of choice. The Top Part is where all the inputs are connected and it is

the most challenging part to design and build. The Middle part is composed of a cylinder that has a 5mm hole in the middle to grip the NMR tube and the necessary chamfer at both sides to place sealing o-rings. Although the production of this part was outsourced to an external supplier the finished product needed subsequent optimisation. Two different approaches were explored, first one to heat the PEEK part close to the glass transition point and slide in the NMR tube, and second to widen the hole to 5.1 mm and fix the NMR tube with silicon. The first approach caused frequent glass breaks because of the abrupt pressure gradient on the glass at the end of the holder. In the second approach the thin silicon layer provides some elasticity, thus eliminating broken NMR tubes, and was therefore used. It has the disadvantage that pressures are limited as the NMR tube slips out of the silicon lined holder at higher pressures. Maximum pressure used with the silicon approach was 12 bars. The bottom part was designed to fit with the top part and provide a tight seal, so the holder was able to keep the pressure stable.
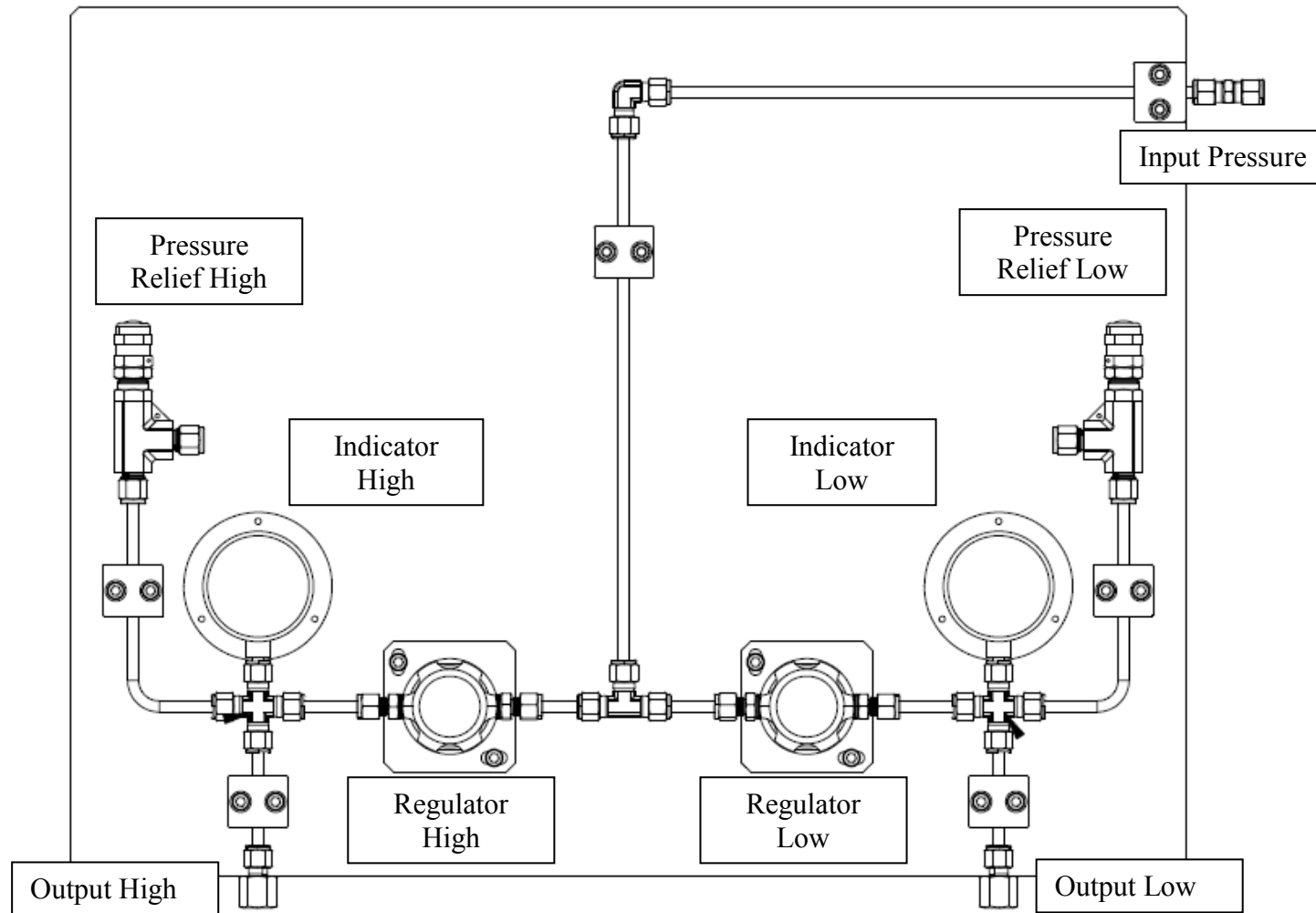
Figure 3.3 – Detailed Sketch of the Pressure Panel Assembly showing input/output

Several designs were tested over the course of the thesis to improve sample transfer. Initially the design was driven by a need to minimise weight (as the design is placed on the NMR tube) and maximise sturdiness of the parts suggested that the Top part and Bottom part are approximately the same length (4.5 cm for the Top Part, 4 cm for the Bottom Part). This design has proven successful for the whole range of experiments we conducted. This Top Part was matched with the necessary Bottom and Middle parts respectively (Figures 3.4 and 3.5).
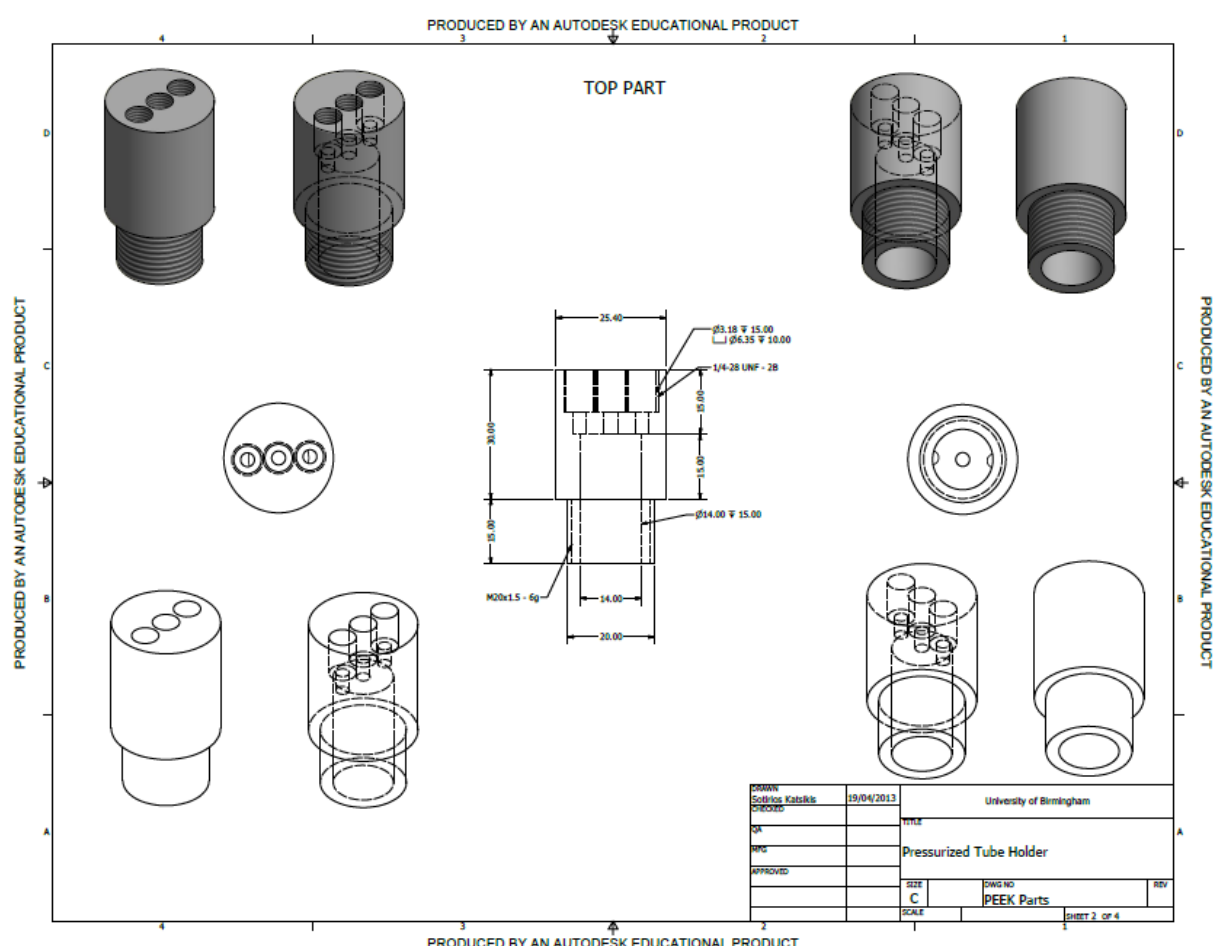
Figure 3.4 - Version 1 of the Top Part of the NMR Tube Pressure Holder

BOTTOM PART

DRAWN		
Sotirios Katsikis	19/04/2013	University of Birmingham
CHECKED		
QA		TITLE
MFG		Pressurized Tube Holder
APPROVED		
		SIZE C	DWG NO PEEK Parts	REV
		SCALE		SHEET 3 OF 4
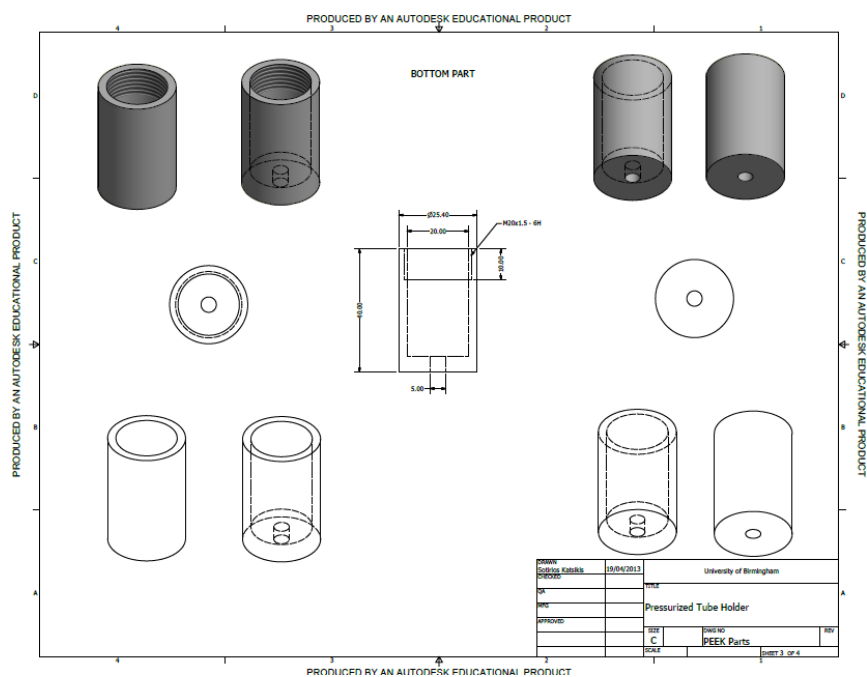
Figure 3.5 – Version 1 of the Bottom Part of the NMR Tube Pressure Holder

MIDDLE PART

DRAWN		
Sotirios Katsikis	19/04/2013	University of Birmingham
CHECKED		
QA		TITLE
MFG		Pressurized Tube Holder
APPROVED		
		SIZE C	DWG NO PEEK Parts	REV
		SCALE		SHEET 4 OF 4
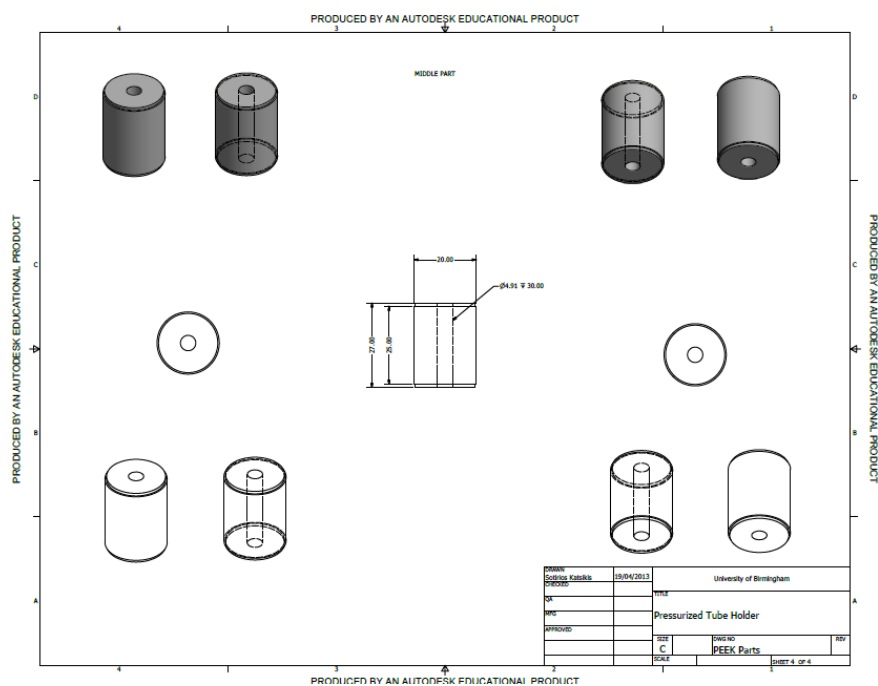
Figure 3.6 - Version 1 of the Middle Part of the NMR Tube Pressure Holder

55
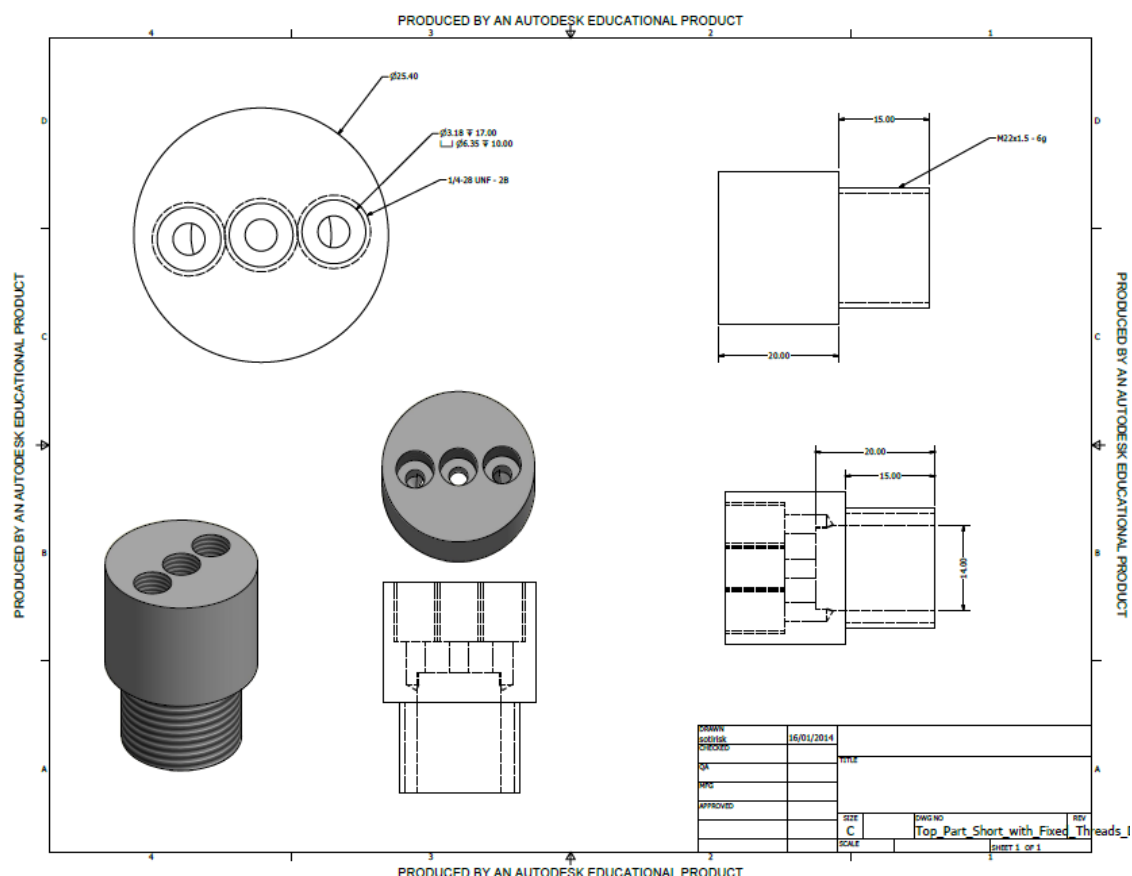
Figure 3.7 – Version 2 of the Top Part of the NMR Tube Pressure Holder
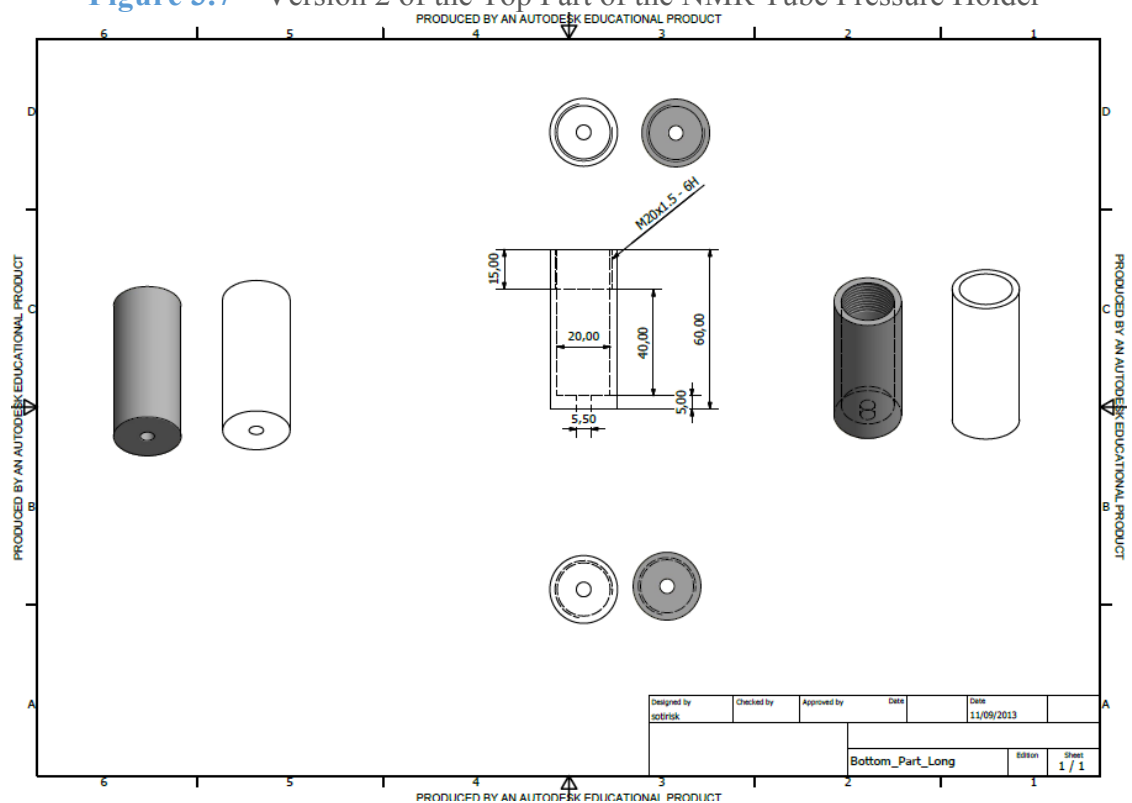
FIGURE 3.8 – VERSION 2 OF THE BOTTOM PART OF THE NMR TUBE PRESSURE HOLDER
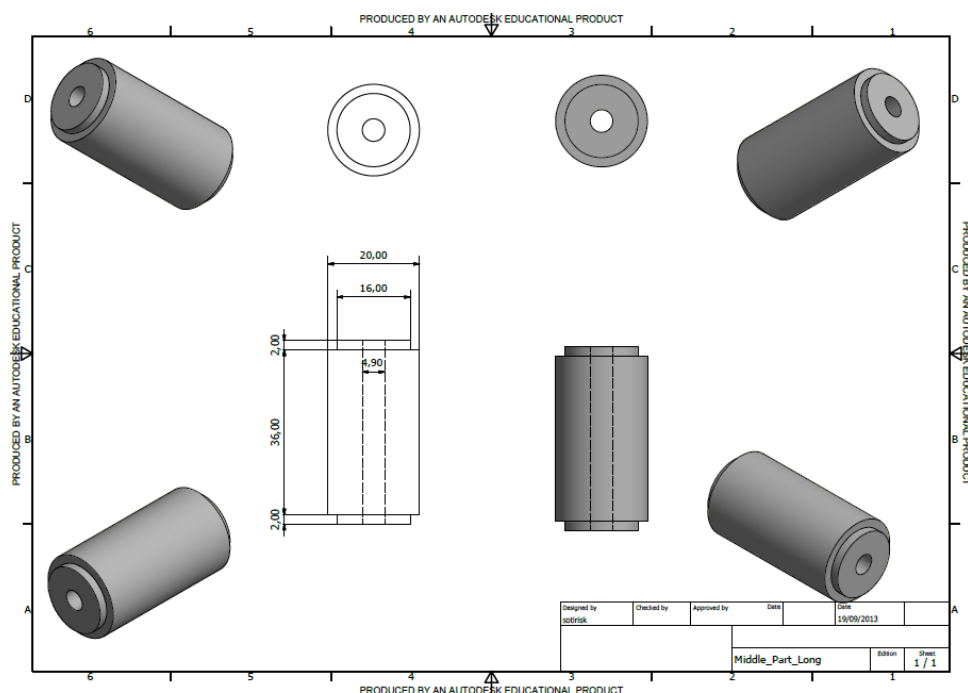
Figure 3.9 – Version 2 of the Middle Part of the NMR Tube Pressure Holder

The initial prototype designed following a previous implementation shared with us by Prof Walter Köckenberger had some significant disadvantages. The most important improvements were the following. First, the Top part was designed to have less dead volume so the pressure gradient (between 3 bar and 10 bar) is achieved faster and acquisition can be started faster. For this reason we designed a shortened part with 50% lower dead volume. Secondly, fixing the NMR tube tightly proved rather difficult, in particular to find a design that works without glass breaks. Therefore the idea of a longer Middle part giving the NMR tube a larger support surface was explored with longer versions of the Middle and matching Bottom parts. The longer version can allow for higher pressures for low viscosity dissolution solvents like water with glycerol. The third improvement was to change the depth and the type of the threaded connection holes of the Top part in order to allow the whole of the tubing inside bore to be in contact with the mixing chamber.
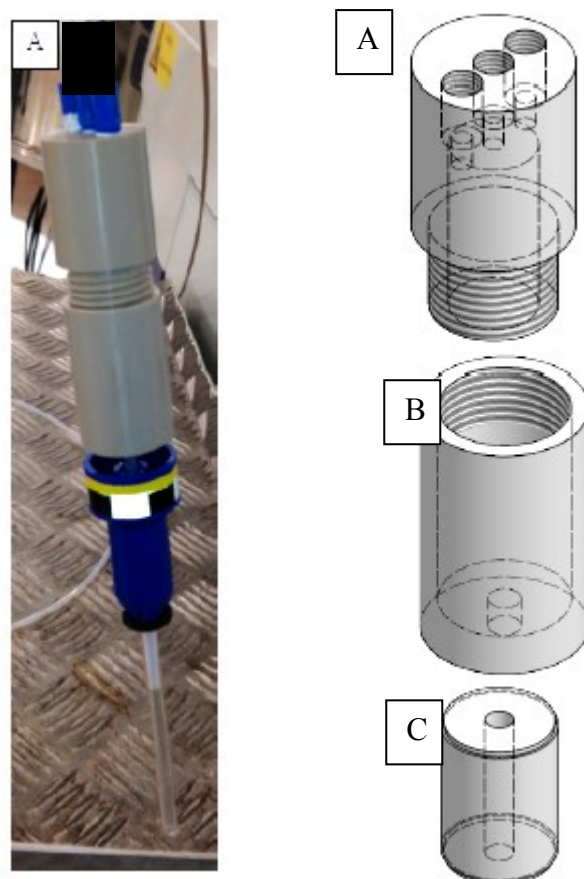
Figure 3.10 – Photograph of the actual NMR tube holder (left) along with a schematic sketch (right) showing the top (A), middle (B) and bottom part (C).

In addition to the overall scheme shown in Figure 3.1, the following minor pneumatic parts were used in order to achieve a reliable and easy to use prototype. A commercial valve manifold to switch the position of the pneumatic valve (VICI MSVA2) and several manual pressure switches to isolate lines for cleaning and depressurisation purposes after sample injection. The overall design schematic is shown in Figure 3.1.

3.2.2 Electronic Design

For the electronic parts, initial work started using a LabVIEW system, following Hilty's original design. The main disadvantage of this setup was the slow response to external commands, when millisecond accuracy was required. As an alternative an ensemble of microcontrollers was chosen to replace this system. The Arduino

platform was selected, mainly for the availability of expansion cards and the community support for a variety of projects. Low cost was also a big advantage so that multiple controllers could be used for each sensitive operation. We used two Arduino MEGA platforms and one Arduino Nano.

The Arduino platform is a development tool built around ATMEL microcontrollers and enables fast adaptation of microelectronics for a variety of applications. The principal idea was to have a system that is completely independent from the DNP and NMR hardware and can be easily adopted in a variety of laboratory environments. This overcomes the disadvantages of a personal computer controlled system running without a real-time module, which is prone to have significant variations in time sensitive switching options that can promote instability in the sample transfer process.

The new control unit was designed with an ensemble of microcontrollers consisting of three discrete systems, the main system, the touch screen interface and the liquid sensor. The main microcontroller system is based on an Arduino Mega 2560 platform and is the central point of interconnecting all the necessary electronic components. It is connected to 6 relay modules to enable operation of the 4 high-pressure electropneumatic valves (SMC VDW31) and the 2 low pressure valves for the VICI valve control module. It is also connected with the liquid sensor, the NMR console and the touch screen (Figure 3.1). This controller is programmed using a switch style loop that accepts RS232 commands from the touch screen. When dissolution is performed, the controller executes all the necessary operations [APPENDIX 2] to pre-pressurise the NMR tube and select the 'LOAD' position. After the dissolution is performed, the liquid sensor detects the presence of the liquid sample and switches the valve in the 'INJECT' position, so the sample enters the NMR tube.

The touch screen interface was built using an Arduino MEGA 2560 [71] controller and a 3.2 TFT touch screen LCD add-on, with native resolution of 320x240. It is necessary to be able to initialise the controller each time a sample is injected and to successfully clean and depressurise the system after each injection. All the components can be manually controlled through the screen. The touch screen interface is also capable of uploading the value of the delay of engagement of the stabilisation pressure to the main controller. The touch screen interface was designed to be as easy to use as possible. Another benefit of the design is that all the commands are sent through RS-232, so a different interface can be developed easily for controlling the device, like a newer version of Arduino with ARM microprocessor or different kinds of embedded and normal computer systems.

Figure 3.11 – Photograph of the Touch Interface splash and operation screen

The liquid sensor completes the trio of microcontrollers used. It was built using the Arduino Nano platform, mainly for the small package size. The purpose of the liquid sensor is vital for this design as it senses the moment of injecting the sample. Failure to detect the presence of liquid can result in a failed long hour polarisation experiments. The principle of operation for this detector is optical. At the beginning the sensor was built using a Light Emitting Diode (LED) and a Light Dependent Resistor (LDR) with the liquid passing through a Plexiglas cell. After comparing different options of available hardware, a commercial optical circuit (OPB350) was used that is bound along the tubing and senses the presence of liquid by altering the amount of IR irradiation sensed by a phototransistor. The great advantage of this design is that it can be easily programmed as a variable resistor circuit connected in an analogue input of the microcontroller. The change of voltage in the presence of a clear liquid is sufficient for a fast response time of 10 µs.
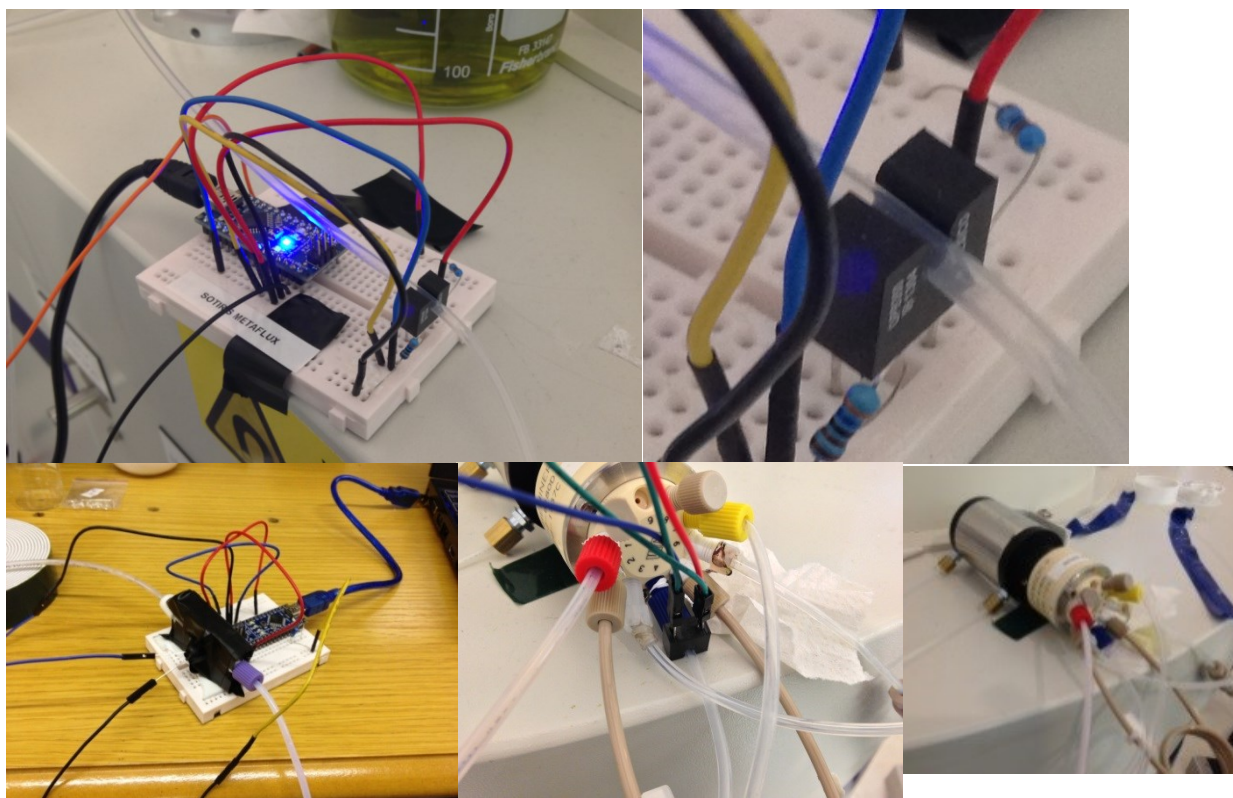
Figure 3.12 - Photograph of the Optical Sensor
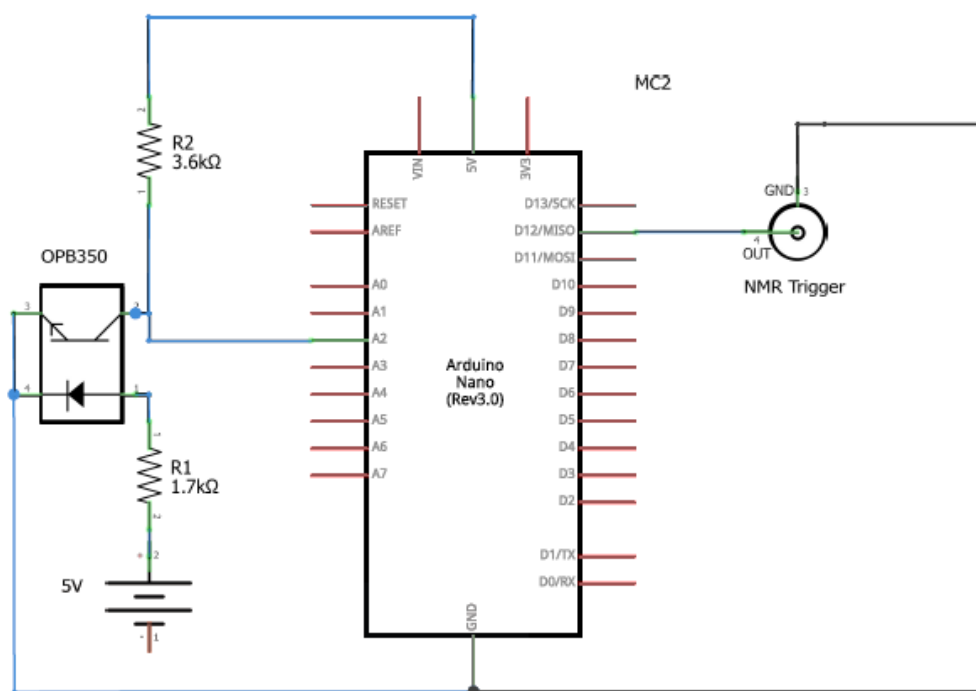
Figure 3.13 – The Optical Sensor electronic circuit

3.3 Design Aspects

To build a robustly working pressure dissolution device the design was carefully changed from what had previously been published by Hilty [72]. The optimisation included the thickness and length of tubing, the NMR tube and its sealing, the timing of the entire circuit, which was rebuilt using Arduino microcontrollers.

Almost all the pneumatic connections where made using 1/8" diameter PTFE tube. PEEK tube was also tested but it was difficult to successfully terminate the connection with PEEK flanges (flange material needs to be harder than the tube). PTFE tubing was terminated with VICI Flangeless fittings, having a specialised PEEK ring at the end.

The NMR tube that we used was a middle walled (0.8 mm wall thickness) NMR tube. The quality of the glass can be relatively low for a DNP 1 scan experiment, 100 or 200MHz certified tubes gave satisfactory performance. The one that served the majority of the experiments was a tube that was shortened from 7 to 6 inches. The tubing entering the NMR tube is a 1/16" tube and goes down to the very bottom of the tube to avoid bubble formation and to ensure smooth sample delivery.

The design of the PEEK fitting that holds the NMR tube is critical to avoid glass tube breakage. An initial design derived from Köckenberger's work heated the PEEK in order to seal against the NMR tube. As this design caused regular glass breakage just below the bottom part, we redesigned this with a larger diameter and tried different sealing options. Sealing with silicone with a slightly larger whole turned out to offer optimal sealing up to a pressure of 15 bar. At larger pressures the tube would slip through the hole even after long drying periods of the silicone.

The initial Bottom PEEK part also had to be broader in the tube diameter, as there was massive pressure change on the outside tube wall, which leads to glass tube rupture. This changed with the silicon layer as it was more elastic. A 5.5 mm drill was used to widen the bore diameter. The initial middle part was designed to accommodate the sealing o-rings and with smooth surface facing the Top Part to avoid leakage.

High Pressure connections were made using 1/4" copper tubing and Swagelok fittings. One of the disadvantages is that in case of dismantling the device, the copper tubes should be renewed as the flanges can only be sealed once.

Overall a design of a pressure dissolution device was implemented that overcomes major limitations of *ex situ* dissolution polarisers. This design was optimised for high

reproducibility, high stability and high transfer speed to successfully eliminate the

problem of bubble formation by degassing during the NMR experiment.
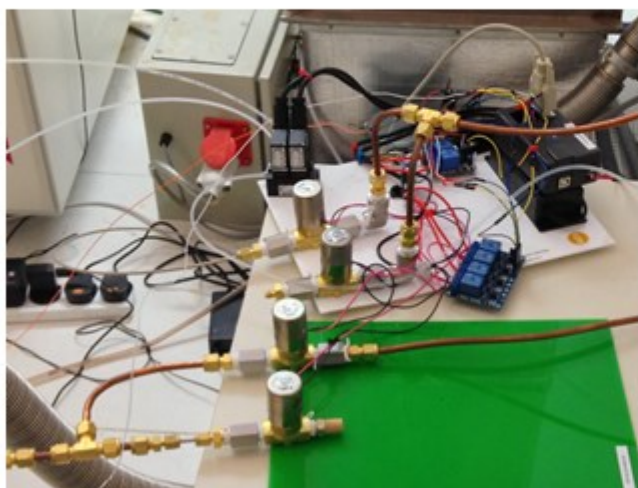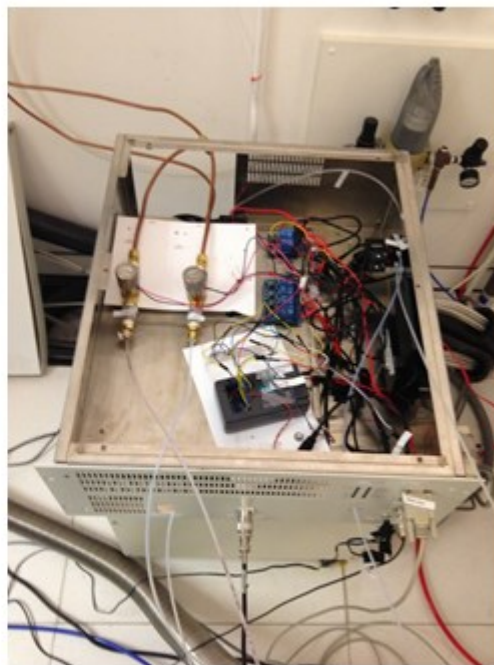
September 2013   November 2013

Figure 3.14 – Encapsulation of the device in a 2.5 Rack box

Chapter 4 - Applications of the Post-Dissolution Sample Transfer Device

4.1 Introduction

In the previous Chapter a detailed description of the post-dissolution transfer device was presented. This chapter follows from utilising the aforementioned device in dissolution DNP experiments with the addition of some experiments required to demonstrate the performance improvements afforded by the new system. In order to evaluate the performance of the post-dissolution transfer device an ensemble of experiments was performed. The experiments had two main purposes: First to evaluate the operating stability of the device; second, to improve the NMR spectral quality of the fast sample transfer process, to broaden the applicability of dissolution DNP to substances with shorter longitudinal relaxation times.

In the literature there are a few implementations of using a pressure gradient to efficiently degas the sample being transferred. Hilty and co-workers [68, 73] developed a computer controlled LabVIEW based system with automatic pressure regulators. Although this system is one of the first that has been published, key elements of the design are missing from the publication and the supporting information. One of these is the particular design of the NMR Tube Pressure Holder that is one of the most critical parts of the design. Some other approaches are also more complex than needed, like a conductivity detector sensing the presence of a liquid. A much simpler optical detector can be used instead. Hilty's lab also built a sample transfer device using liquid as the transfer medium, instead of compressed gas, mimicking FIA (flow injection analysis) from analytical chemistry. With this approach the pressure and flow rate have less variation so the transfer can have the

same settings for different dissolution products. This can result in a more precise sample transfer, less prone to bubbling than having a gas transfer. [74]

4.1.1 The NMR system

The NMR system used consists of a 500MHz superconductive magnet made by Oxford Instruments, a Bruker Avance III console equipped with a dual receiver system and a selection of two probes, one with direct proton observe and indirect carbon observe and one with direct broadband observe (carbon, phosphorus etc.), a separate phosphorus channel and an outer proton coil. For the majority of the work, the broadband probe was used. To start the acquisition of an NMR experiment after the DNP dissolution the trigger input of the NMR console is used.

4.1.2 Sample Preparation

For the experiments for the applications of the post-dissolution transfer device we prepared a number of solutions. To calibrate the necessary timings for the injection procedure for the given tube length and to have approximately 600 μL of sample in the NMR tube we used diluted red food dye. To check the stability of the device we prepared 0.1 M pyruvate standards in a 1:1 mixture of D_2O/DMSO-d_6. This sample was split into multiple aliquots for repeated test polarisations to check the stability of the device by evaluation of the T_1 relaxation time of pyruvate. In order to test the speed of the sample transfer a sample with a shorter T_1 relaxation time was needed. For this we employed [U-^{13}C]glucose with ^{13}C T_1 relaxation times of around 2 seconds [70]. We were able to record a 1D spectrum with sharp lines and a good quality 2D fast HMQC with 16 scans, in which 8-10 were showing signal. The quality of the 2D data shows a clear advantage compared to previous 2D spectra without the pressure dissolution system.

4.1.3 Pulse Sequences

For these experiments two different pulse sequences were used as shown in Figure 4.1.
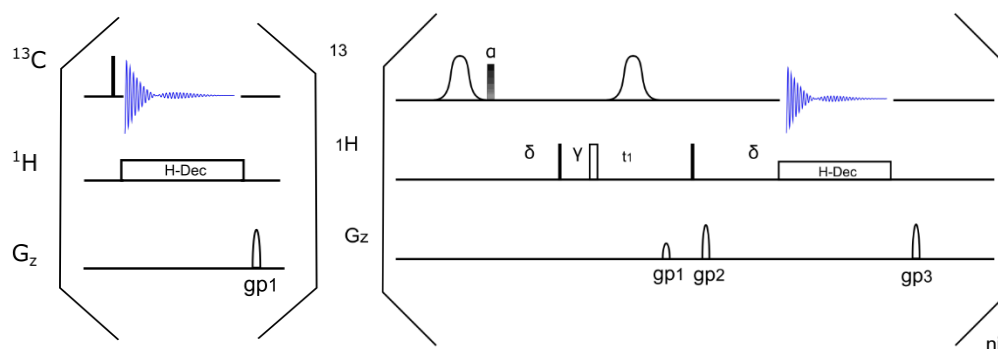
Figure 4.1 – A 1D and a 2D pulse sequence for DNP. The 1D was also applied for the T1 determination with altered parameters.

4.2 Stability

To evaluate the stability of the sample transfer system longitudinal relaxation measurements were carried out. Such measurements require a high degree of sample stability and show artefacts arising from air bubbles or turbulences in a sample. In order to measure T_1 in one scan using the single-scan FT (SSFT) method originally proposed by Kaptein and later adapted by Day et al. was used [75]. This method is ideal for nuclei with large T_1 relaxation times. Instead of using inversion recovery with long relaxation times of five times the T_1 SSFT uses a small flip angle pulse train. This method is compatible with polarised substances. In comparison with the normal inversion recovery experiment used to determine the spin-lattice relaxation times Day's method produces similar results when the pulse sequence does not require decoupling of attached ^{1}H nuclei. However when ^{1}H nuclei are decoupled during acquisition in the SSFT experiment, Day et al. observed an alteration in the apparent T_1 value. Because the experiment here was to establish the duration

stabilisation delay and the criterion for a sufficiently long stabilization delay was that the SSFT $T1$ corresponded to the thermal T_1 value obtained with an inversion-recovery sequence, the SSFT experiment was acquired without ^{1}H decoupling. The equation used to fit the data was:

$$M_{\underline{x}\atop y}(nT) = \left\{ M_{DNP}\alpha^n\beta^n e^{-nf\theta} + M_0(1-\beta)\frac{1-\alpha^n\beta^n e^{-nf\theta}}{1-\alpha\beta e^{-f\theta}} \right\} * sin\theta * e^{-f\theta}$$

where M_{DNP} is the polarisation intensity obtained; theta is the flip angle of the excitation pulse; alpha = cos(theta) and accounts for the repeated loss of longitudinal magnetisation through the application of the excitation pulse; beta=exp(-T/T_1), where T_1 is the longitudinal relaxation time and T is the repetition time (i.e. the time between RF pulses); n is the number of the current experiment; the parameter f accounts for B_1 field inhomogeneity; M_0 is the thermal equilibrium polarisation.

"A train of 30° pulses was employed, spaced 2s apart with data acquisition during the first 500ms of this period with a spectral width of 250ppm. In accordance with Day's publication, a pulsed field gradient of 2ms was employed to dephase remaining polarisation." [21]

The results are presented graphically in Figure 4.2. Figure 4.2.a *"shows the expected instability arising from sample stabilization"* without using the pressure device. *"For the simulation in Figure 4.2.e the first 4 data points (8 seconds) had to be omitted, as they show a build-up of signal arising from a slow sample stabilization over 8–10s. Figure 4.2b, c, f, g demonstrate the advantage obtained with the pressure dissolution kit. The T_1 obtained was the same for two consecutive polarizations within small error limits. Data points could be used from time zero, which is 600 ms after the sample transfer was started."*[21]
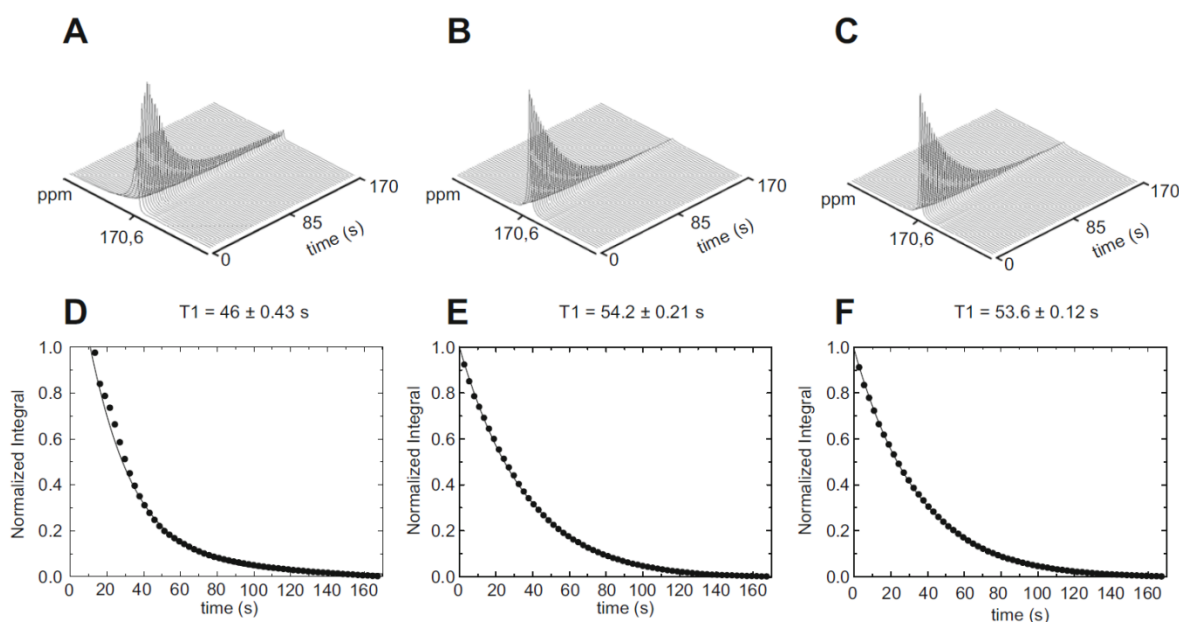
Figure 4.2 – "a) Repeated sequential small flip angle spectra of hyperpolarized 1-^{13}C-pyruvate collected every 2 s, acquired after a flip angle of 30° using the Hypersense transfer mechanism. b, c) Same train of spectra using the pressure dissolution kit. d–f) SSFT data from a–c fitted using Eq. 8 from [75] to calculate a T1 relaxation time" Taken from *[21]*

4.3 Performance in 1D ^{13}C Spectra

To evaluate the performance of the Post-Dissolution transfer device ^{13}C-labelled glucose was selected. Obtaining NMR spectra of polarised ^{13}C-labelled glucose is challenging due to the relatively fast relaxation of the glucose ^{13}C nucleus (<1s [70]). A comparison between the two available transfer systems was performed, first sample transfer using the standard Hypersense method and second with the post-dissolution pressure transfer device. For both acquisitions the system was prepared by repeated gradient shimming using a sample similar to that after the dissolution process. Shimming is impossible for dissolution DNP as it cannot be carried out on the actual sample.considering that the measurement needs to be completed within the longitudinal relaxation time of the sample. A reasonable solution to this problem is to shim a similar sample before the actual measurement.

The pulse sequence for ^{13}C-spectra used consisted of one scan without proton decoupling using a flip angle of 15° (8.12 μs for 90° pulse) and 16 k data points with 250 ppm spectral width. Polarisation time was 4 hours at 94.090 GHz and the sample was a mixture of 100 mM [U-^{13}C]glucose in 100 μl of a D$_2$O:d-6-DMSO mixture (1:1), frozen in 1.4 K and having 2 mM OX63 radical.
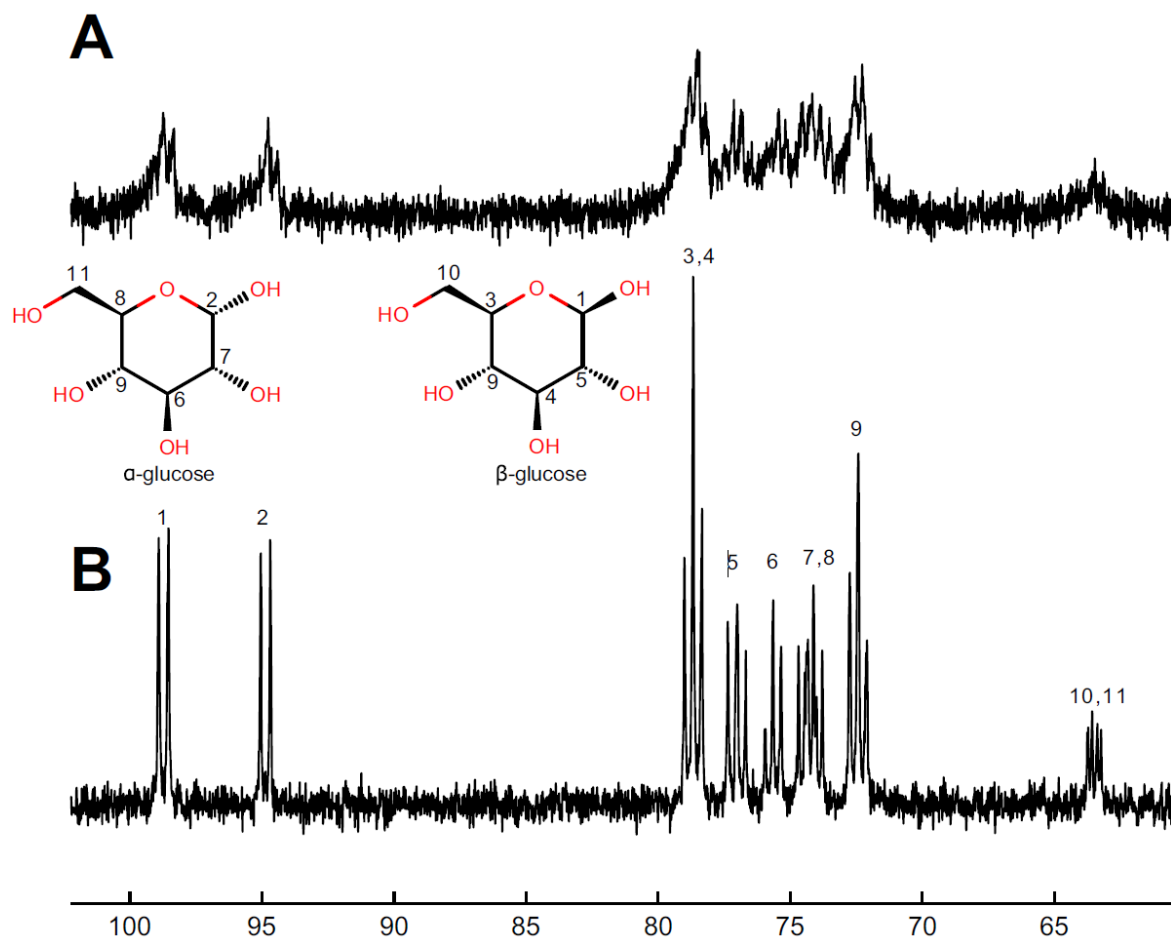
Figure 4.3 – *A. Dissolution using the conventional dissolution system B. Dissolution using the Post-dissolution transfer device. Taken from [21]* The peak assignment corresponds to a and b glucose

In Figure 4.3a, the conventional dissolution system was used and in 4.3b the post-dissolution sample transfer device. It can be clearly seen that the spectrum in Figure 4.3b has a narrower linewidth where the carbon-carbon multiplets (approx. 40Hz) can

be resolved. The line width in this spectrum is ca 7.7 Hz. This improvement arises from the pressure gradient during the sample transfer. Using the conventional dissolution system the pressure falls from 10 bar to atmospheric pressure during acquisition, in contrast to the new system where the pressure is increased to 12 bars for the acquisition. Depressurisation of the sample leads to formation of air bubbles, which affect the homogeneity of the sample. Inhomogeneous samples have broader lines because of susceptibility differences across the sample and thus varying resonance frequencies for spins at different locations in the sample tube.
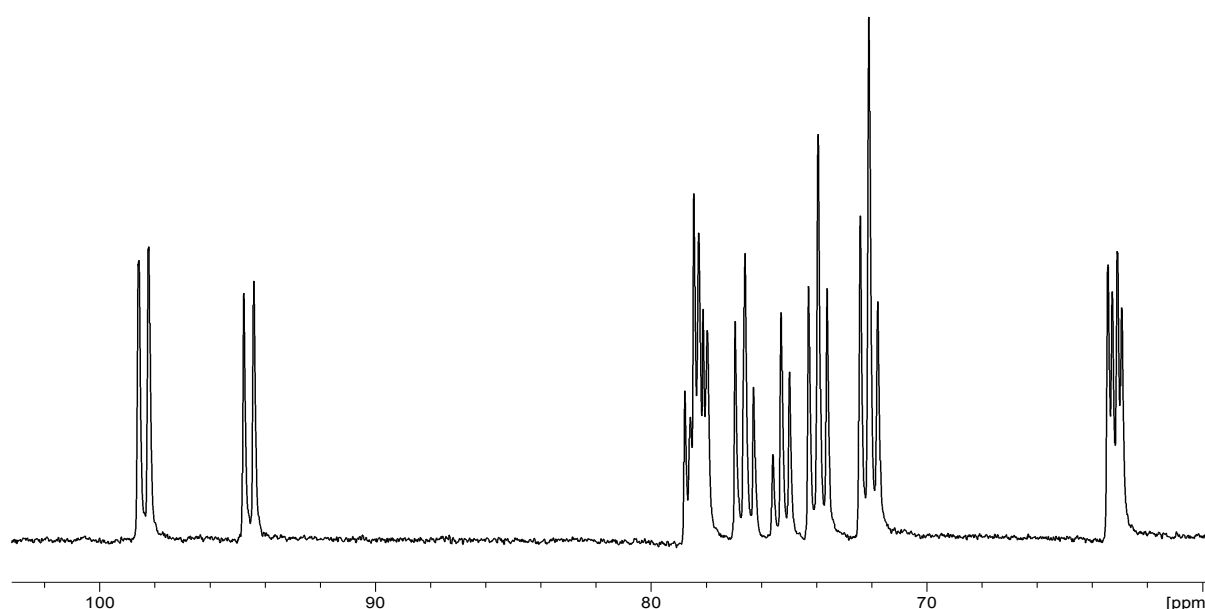
Figure 4.4 – A sample of [U-^{13}C]glucose acquired thermally with zg0ig pulse sequence, 32 scans, decoupling off. This sample is a concentrated 1M sample.

4.4 Performance in 2D ^{13}C Spectra

To further challenge the possible outcome of using an improved sample transfer device, a small flip angle ^{13}C-^{1}H-HMQC 2D spectrum of [U-^{13}C] glucose was acquired. [U-^{13}C] glucose has ^{13}C T_1 values of <1s. Obtaining a 2D spectrum of such a fast relaxing polarised sample *in one pulse* is therefore challenging. It is possible to increase the T_1 time by 30% using fully deuterated glucose by enabling *in vivo*

71

imaging [76]. However, deuteration removes the ability to acquire two-dimensional ^{13}C-^{1}H-HMBC/HMQC spectra.

Samples were prepared like the 1D experiments with two main differences: a higher concentration of glucose (2 M instead of 100 mM) and a smaller polarisation time (2 hours instead of 4) was used.

"The Two-Dimensional spectra were acquired using a small flip angle HMQC experiment [77] as described in chapter 4.1.3 with 8k data points in the direct dimension and 16 increments, a 15° flip angle (90° pulse length of 8.12 μsec) and a sweep width of 250 ppm."[21]

In Figure 4.5a it is shown that the spectrum obtained with the dissolution device (in red) has considerable lower line widths in the direct dimension resolving details of the peak shapes. Transfer is also faster, enabling the acquisition of more increments in the indirect dimension. The result is an enhanced resolution in the indirect dimension. Figure 4.5b shows the 72-80 ppm area, in which the comparison of the two spectra shows the advanced detail in the one acquired with the dissolution device.
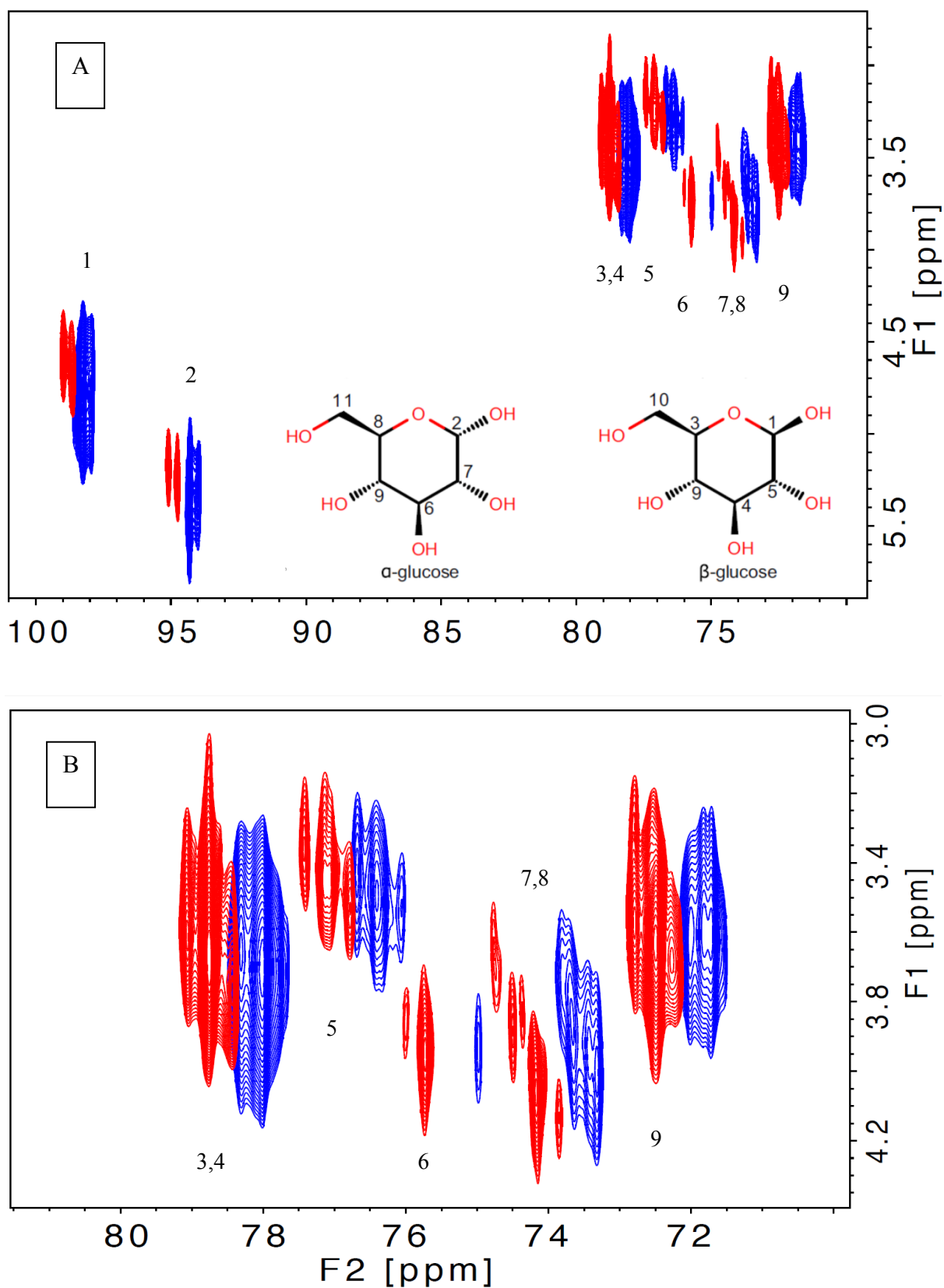
Figure 4.5 – *A) 2D ^{13}C-^{1}H-HMQC spectrum of [U-^{13}C]glucose. B) Zoom in of the 72-80 ppm area Taken from [21] Red is the specturm recorded with the new device, blue the spectrum without. They appear shifted for illustrative purposes only.*

Chapter 5 - Acetylated Compounds DNP

5.1 Introduction

Expanding the applicability of ex-situ Dissolution DNP has been the target of this chapter. The application of this method in samples for metabolomics analysis revealed the limiting factors, including fast relaxing nuclei, slow polarisation time, transfer sample instability and high running costs – liquid helium and trityl radical are on top of any instrumentation costs. The main benefit is the very intense signal that is produced from the polarised spin states. An equivalent signal in the ^{13}C channel usually needs very long acquisition times (hours to days) especially in slowly relaxing signals such as these from carbonyl groups. So the second benefit is quick acquisition that is usually less than a second for 1D experiments or less than 10 seconds in 2D. This also has to compare with an average quick HSQC experiment.

The fast relaxation times of polarised substances is one of the intrinsic disadvantages of ex-situ DNP. Although these times can vary from milliseconds to a couple of minutes, most of the nuclei species found in organic compounds, which are attached to protons relax fast. As ex-situ DNP is mainly used to polarise carbon (^{13}C), it is important to use carbons with long longitudinal relaxation times. In organic compounds one of the possible slow relaxing configurations is the carbonyl (C=O). An approach for having long lived tags could be to attach carbonyl groups with longer relaxation times in molecules of interest. This approach is been presented here.

5.2 Derivatisation of Aminoacids - Acetylation

An approach to enhance the sensitivity of ^{13}C spectra is to enrich natural abundance carbons with ^{13}C. Although this approach is easier for synthetic chemistry, for analytical chemistry derivatisation techniques have been applied. Raftery developed a

method to analyse aminoacids in human urine and human serum by reacting the protein free serum with labelled $(1,1)^{13}C_2$-acetic anhydrite[78]. Raftery's group already published a number of applications all based on the importance of aminoacid concentrations[79-84]. Acetylation is the chemical reaction of acetic anhydrite with a compound having a hydroxyl group (-OH) and the result is an ester. If acetic anhydrite is labelled with carbon-13 in the carbonyl position, the resulting ester will also be labelled in the carbonyl position. This enables to use the tag as a probe for small molecule compounds. Raftery showed that 13 aminoacids compounds can be detected in serum. The serum HSQC spectrum has worse quality than the standard aminoacid HSQC. The disadvantage of this approach is a relatively small chemical shift dispersion of the CO resonances and the need to utilise a long-range coupling to obtain an HMQC spectrum.

Here the goal was to explore whether it is also possible to obtain 2D HSQC type spectra to distinguish acetylated compounds in serum. For the DNP type experiments, the 2D correlation was inverted with carbon in the direct dimension and proton in the indirect. The result is the ability to record a 2D Proton-Carbon correlated spectrum with a mixture of aminoacids and apply this research for identifying aminoacids in samples derived from serum. In this work we used fetal bovine serum instead of human.

5.3 Materials and Methods

For the experiments of this chapter, three different samples types were prepared. The first sample type was a mixture of five amino acids, used to calibrate the pulse sequence, the sample transfer and the polarisation parameters. Five aminoacids on the edge of the HSQC spectra were selected, Glycine, Threonine, Valine, Alanine and Proline. The second sample was a mixture of 20 acetylated amino acids, to optimise

options used for a multiple peak HMQC. The third sample was an 'uknown' sample of acetylated FBS. The acetylated amino acids were prepared by diluting each aminoacid in water in a concentration of 100 mM and creating stock standards. For the mix of 5, 200 μl were taken to a total volume of 1 ml and 20 μl of labelled acetic anhydrite were reacted. Afterwards, sample was freeze dried and was reconstituted with 1 ml of D2O. So the concentration afterwards is 20mM for each. In the DNP cup, concentration is 10 mM (50uL of DMSO was added as a glassing agent). The concentration of 10 mM in the DNP cup results in a final concentration of 250 μM, as dissolution produces a 40-time dilution factor. A similar procedure was followed for the preparation of the 20 aminoacid mixture, 100 μl of each were taken to a volume of 200 μl and then reacted with 40 μl of labelled acetic anhydrite. Afterwards the same steps were followed to a final volume of 1 ml after the freeze drying reconstitution.

Table 5.1 – The 20 essential aminoacids with the 1 and 3 letter codes. One letter code is used in the peak assignment

G	Glycine	Gly	**P**	Proline	Pro
A	Alanine	Ala	**V**	Valine	Val
L	Leucine	Leu	**I**	Isoleucine	Ile
M	Methionine	Met	**C**	Cysteine	Cys
F	Phenylalanine	Phe	**Y**	Tyrosine	Tyr
W	Tryptophan	Trp	**H**	Histidine	His
K	Lysine	Lys	**R**	Arginine	Arg
Q	Glutamine	Gln	**N**	Asparagine	Asn
E	Glutamic Acid	Glu	**D**	Aspartic Acid	Asp
S	Serine	Ser	**T**	Threonine	Thr

The acetylated serum sample was prepared by taking 10 mL of FBS, adding 50 mL of methanol, spinning in a centrifuge for 15 min at 10,000 rpm. After removing the precipitate 50 mL of methanol was added, followed by an additional centrifugation step for 15 mins at 10.000 rpm. After removing the precipitated proteins again the solution was passed through a 10KDa cut-off filter to further remove proteins that

were not removed by the dual methanol precipitation. After this step the samples was

lyophilised, and then dissolved in D_2O. For DNP experiments 100 uL were pipetted

into the DNP cup along with an equal amount of DMSO-d_6. Table 5.1 shows the one

letter aminoacid code that is used in the assignment of the NMR spectra.

The pulse sequences used at these experiments were a simple 1D ^{13}C observe for 1-D

DNP and a ^{13}C-^{1}H HMQC for 2D DNP experiments [67]. To compare with thermal

samples, a ^{1}H-^{13}C HSQC pulse sequence was used.
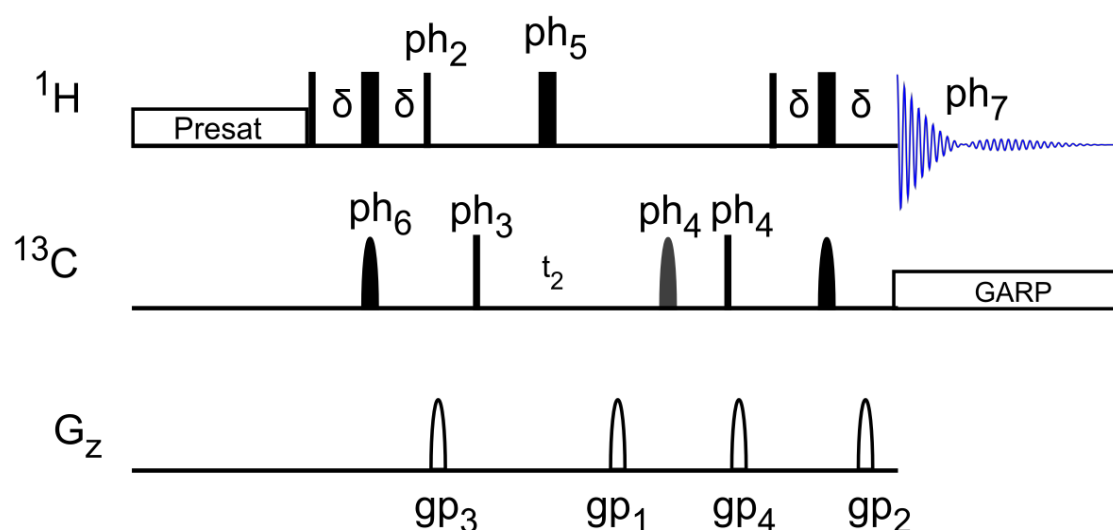
Figure 5.1 – The ^{1}H-^{13}C HSQC pulse sequence used for the Thermal acquired 2D expeirments. Phase cycling was as follows: ph_1: x, ph_2: y, ph_3: x-x, ph_4: x x x x −x −x −x −x ph_5: xx −x −x, ph_6: x, ph_7: x −x x −x −x x −x x
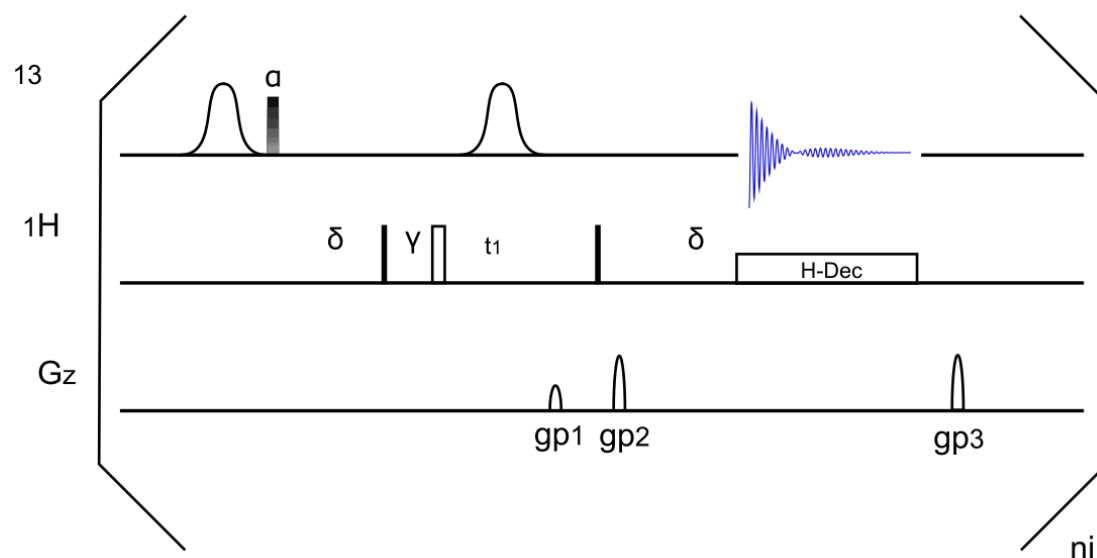
Figure 5.2 – The ^{13}C-^{1}H-FAST-HMQC used for the DNP 2D experiments. No phase cycling as it was a DNP run. n_i was 16. [67]

5.4 DNP Analysis

In order to evaluate the performance of the DNP experiment in analysing acetylated compounds, a simple standard sample of 5 aminoacids was prepared along with a more complex mixture of 20 aminoacids. The spectrum acquired thermally has considerably better resolution in the indirect dimension and all the aminoacids can be distinguished.
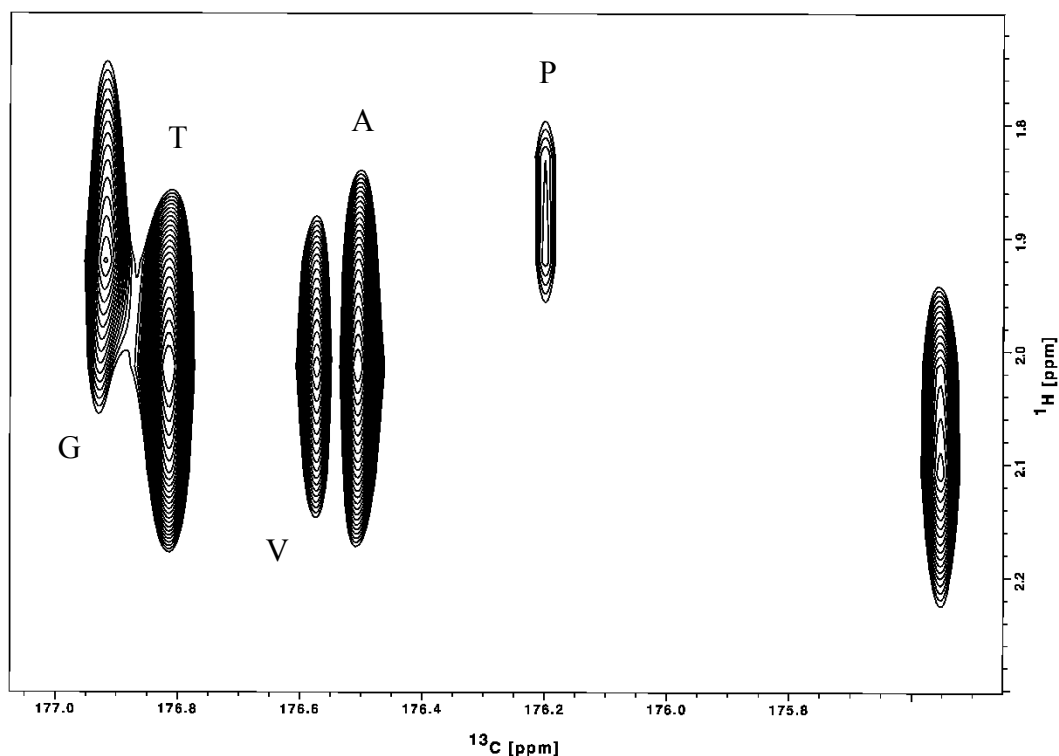
Figure 5.3 – ^{13}C-^{1}H HMQC of a mixture of 5 acetylated aminoacids.

Figure 5.3 is a polarised spectrum of the 5 aminoacids recorded with the 2D-Fast-HMQC. The polarised 2D spectrum shows considerably good resolution for a hyperpolarization experiment with an acquisition time of less than 10 seconds, but the indirect dimension has only 16 increments, in which only 9 had signal, so the resolution in the indirect dimension cannot be compared to the thermal HSQC. The benefit though is that with DNP and the inverse HMQC carbons are in the direct dimension and can have good resolution, thus the number of peaks is high. This is shown in figure 5.4.
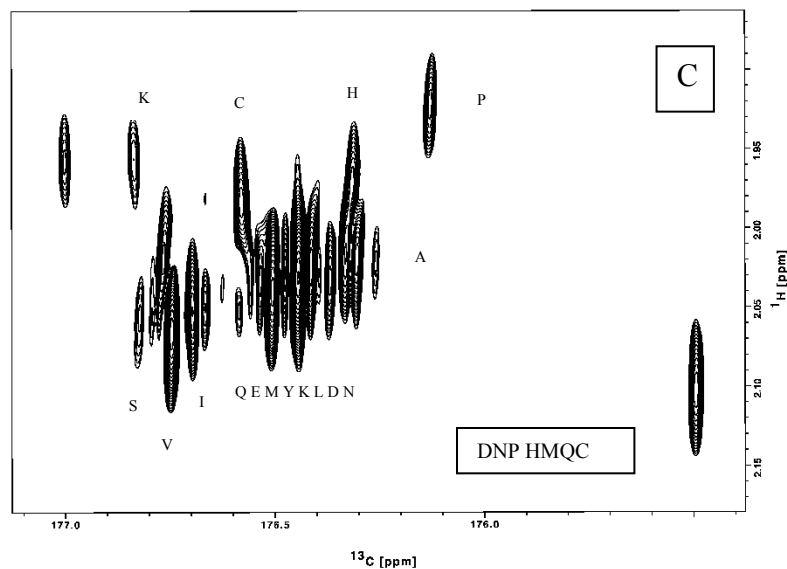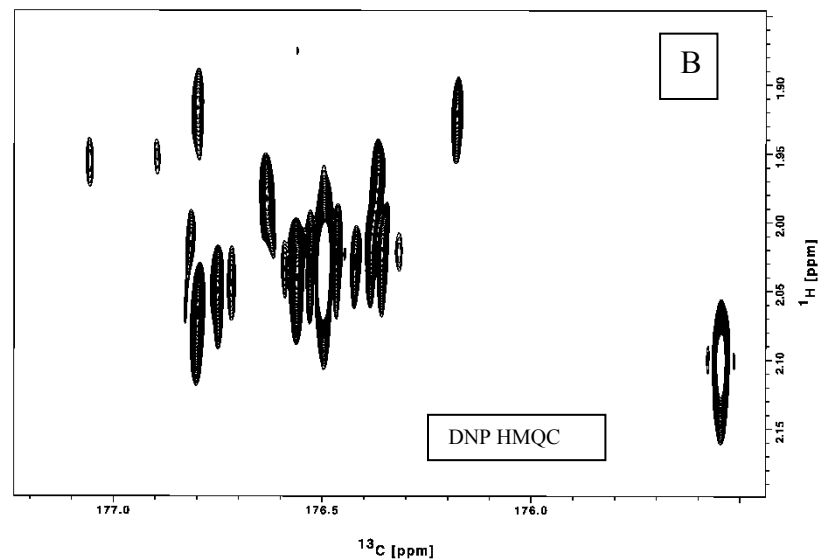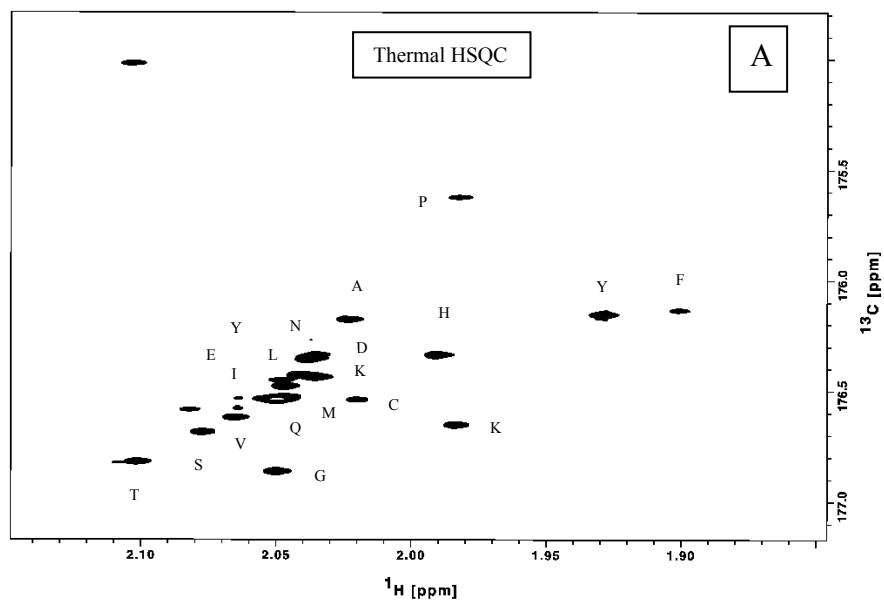
Figure 5.4 - A. ^{1}H-^{13}C HSQC of a mixture of 20 acetylated aminoacids. B. The same sample recorded with DNP and 13C-1H HMQC C. The same sample after optimising the 3J constant to 7 Hz – B-C spectral width is 4 in Direct and 1.5 in the Indirect dimension. Note that comparing A with B and C there is a 90° rotation, as Direct and Indirect observe channels are exchanged. Assignments from [78].

80

After determining the aminoacid standards and optimising the pulse sequences and the sample transfer for these experiments (increase the preacquisition delay) the acetylation technique was applied to derive the aminoacid content of Fetal Bovine Serum (FBS). The method can also applied to human blood serum that is a similar substrate. The experiments performed on Serum also were split into thermal and DNP to point out the difference.

In the determination of standard aminoacids the DNP method is not showing any advantage except for the faster acquisition time. This is different in the serum experiments, as the concentration of these cannot be artificially increased by building a high concentrated standard but the concentration ratios are rather different for different substrates. The signal enhancement that DNP brings can help identify peaks that were not visible without its use.

The main difficulty recording a DNP spectrum of acetylated serum is the purity of the sample, regarding the protein content. If protein content is high, acetic anhydrite is diverted in becoming a branch of a much larger protein instead of becoming a tag in a small molecule. For this reason a two stage methanol extraction was followed by filtering the sample through a 10 kDA filter. This combination produced considerably better samples that allowed for the polarised 2D spectrum to be recorded. The thermal HSQC and the polarised HMQC spectra are presented in figure 5.5.
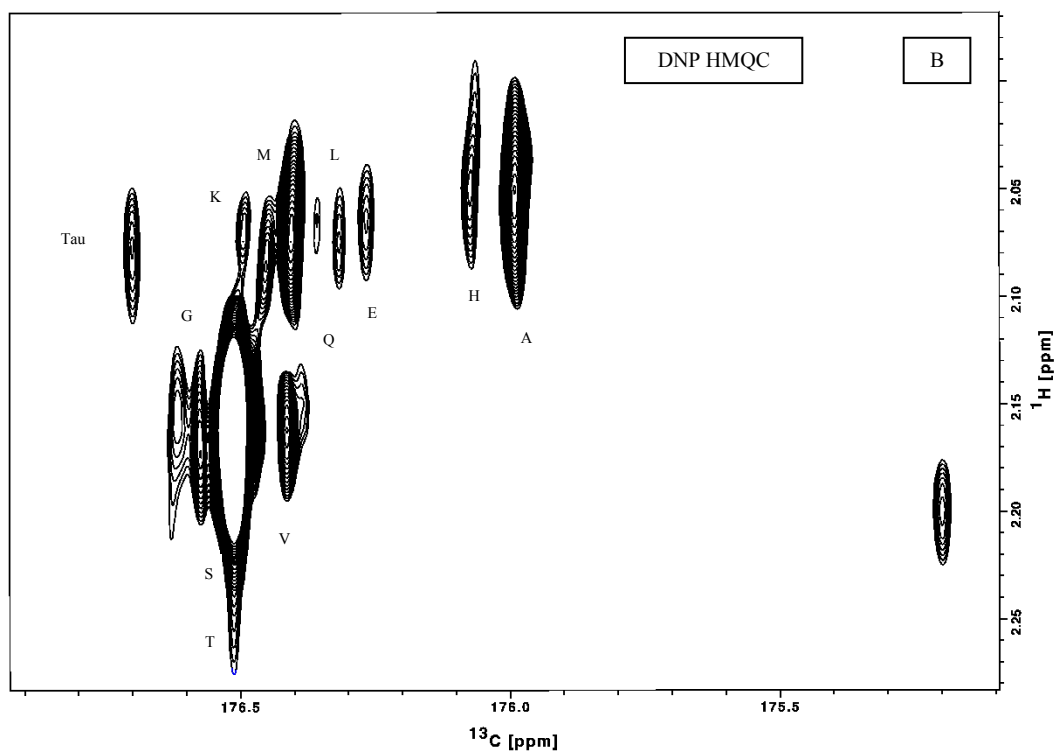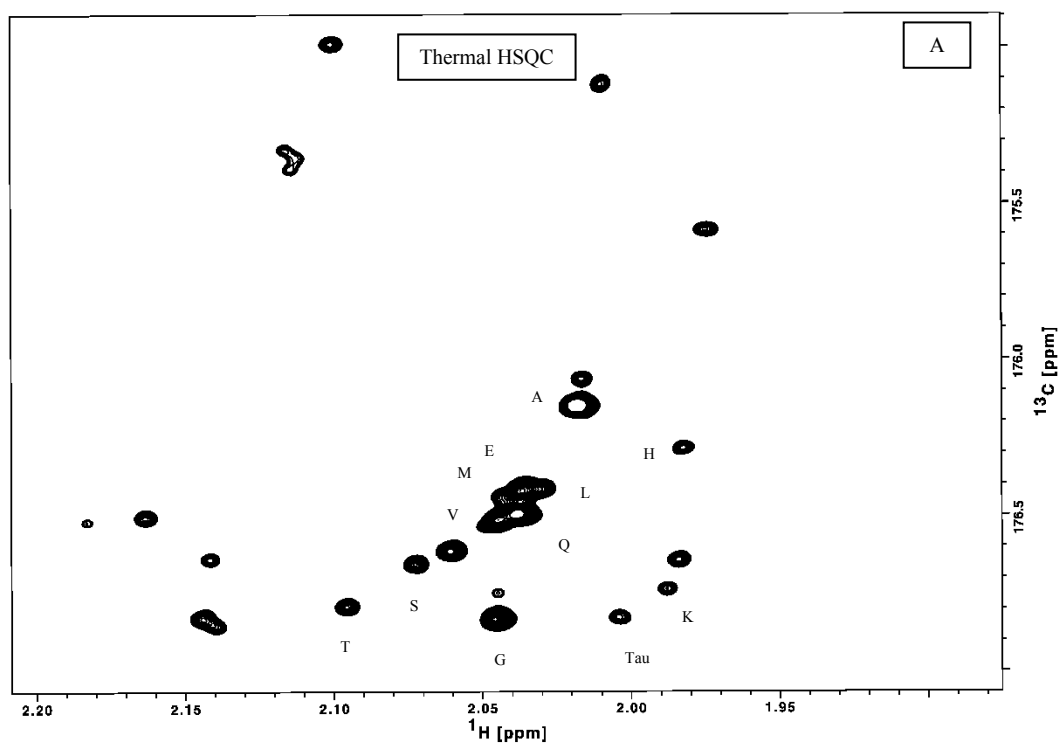
Figure 5.5 – A. ^{1}H-^{13}C HSQC of acetylated serum. B. The same sample recorded with DNP and ^{13}C-^{1}H HMQC – Note that comparing these spectra there is a 90° rotation, as Direct and Indirect observe channels are exchanged. Assignments from [78]

Possible future applications of this technique is expoitation of different sample matrices. Acetylation of aminoacids can be proven a powerful tool for 2D heteronuclear DNP correlated spectra, so application in biofluids that measuring of aminoacid distribution is important can be exploited further [79-84].

Combining the outcome of the previous chapter, a parallel receiver approach can be performed on ^{15}N and ^{13}C channels, if the necessary hardware (NMR probe having independent ^{15}N and ^{13}C channels) is available. Although the identification of ^{15}N is almost impossible due to low natural abudance these peaks could be possibly observed with DNP.

Chapter 6 - Parallel Receiver DNP

6.1 Introduction

Advancements in NMR instrumentation enables researchers to explore new avenues of science and perform new experiments. DNP would be a major step forward to overcome the massive limitations of NMR in sensitivity. Unfortunately there is no single design that meets the needs of common NMR applications. As was described in chapter 2, the *ex-situ* implementation affords by far the largest polarisations. However, the most significant disadvantage of *ex-situ* DNP is the limitation of one scan, limiting the acquisition time to the short longitudinal relaxation time of ^{13}C nuclei. Therefore the NMR signal decays in a short time, typically in a few seconds, depending on the molecule of interest. In molecules where multiple nuclei can be polarised the long relaxation times are usually not sufficient to obtain subsequent consecutive spectra.

A possible solution for this particular limitation is to use multiple receivers simultaneously along with NMR probes that have multiple radiofrequency coils. Erics Kupce presented several implementations of multiple receiver NMR experiments and applications termed PANSY (Parallel Acquisition NMR SpectroscopY) [85, 86]. Applications include proof of concept applications combining H-H COSY and H-C correlation spectra [85], protein NMR by incorporation of two multiple dimension experiments in a single pulse sequence [87], and single scan experiments [88].

For DNP experiments with multiple receivers the first problem is to polarise multiple nuclei with the same polarisation frequency. Reynolds et. al. [89] carried out a thorough study of this and showed that ^{13}C and ^{31}P have overlapping polarisation frequencies. In this study a new solid state probe was introduced that can be inserted

into the Hypersense polariser. This probe has a coil sufficiently close to the sample in the position where usually the dissolution wand is located to obtain ^{13}C spectra at 1.4 K in the polariser with reasonable sensitivity.

In order to study multiple nuclei it is necessary to tune and match this probe for each nucleus, e.g. ^{14}N, ^{13}C, ^{31}P etc. Reynolds described microwave sweeps and solid state build-ups for a range of nuclei. The microwave sweeps showed that although for ^{13}C and ^{31}P different polarisation mechanisms were expected, in practice the separation between the two maxima is small, suggesting that the polarisation mechanism is a mixture of the solid effect and thermal mixing in both cases. The aspect of polarising two nuclei is covered in the first session of this chapter, the Solid State DNP, in which this is applied to TetraMethylPhosphonium - TMP. The second problem explored in this chapter is the potential of observing multiple nuclei simultaneously after dissolution and transfer of the polarised sample. This is covered in the third part of this chapter, the Parallel Receiver dissolution DNP.

The advantage of performing this kind of experiment is to collect NMR data in half the time that would be required for sequential acquisitions. In case of dissolution DNP acquisition times are low compared to polarisation times, although still too long to acquire nuclei after each other. There are therefore considerable savings in NMR time if experiments are carried simultaneously for multiple nuclei. In the following chapters the methods used will be presented along with the data that was collected.

6.1.1 Sample Preparation

The spectrometer used for these experiments was equipped with two parallel receivers, which can operate on different nuclei. In order to carry out dual receiver measurements we used compounds containing ^{13}C and ^{31}P at the same time. One test

compound used was unlabelled ATP, which is useful as it shows singlet signals without couplings. TMP (tetra-methyl-phosphonium) was also used to demonstrate parallel acquisition of ^{13}C and ^{31}P. All the samples were diluted into 1:1 D$_2$O-Glycerol mixture to a final concentration of 1M, polarised with OX63 and dissolved using a 1:1 water-methanol mixture.

6.1.2 Tuning and matching circuit

We built several tune and match boxes for use with the Hypersense polariser housed in an aluminium box. At the beginning we tried building this with a breadboard but without insulation it acts as a receiver for environmental noise causing a peak in the middle of the spectrum that covered all the useful signals. We used two 1-30 pF trimmers (airtronics/johanson 5601) for tuning and matching and a selection of coils, some of them handmade by winding copper wire and some others, which were commercially available (with impedances in the range of mH). Changing the length of the cable connecting the probe changes the impedance matching, so with small adapters we were able to adjust the impedances. We used the fact that these RF circuits are multi-resonant, and we were able to bring two different resonant frequencies on top of the frequencies we required, at around 36 and 58 MHz for ^{13}C and ^{31}P respectively (always having in mind the 3.34 T polariser field).

6.1.3 NMR Spectrometer setup – Pulse sequences

In order to setup the system for DNP several experiments were performed with conventional NMR to optimise the operating parameters for the dual receiver system. For setting up the pulse sequence the system was set for acquisition of ^{31}P and ^{1}H. For DNP the system was converted to acquire carbon ^{13}C and phosphorus ^{31}P. The pulse program of Figure 6.2 was the one used to acquire carbon and phosphorus after dissolution.
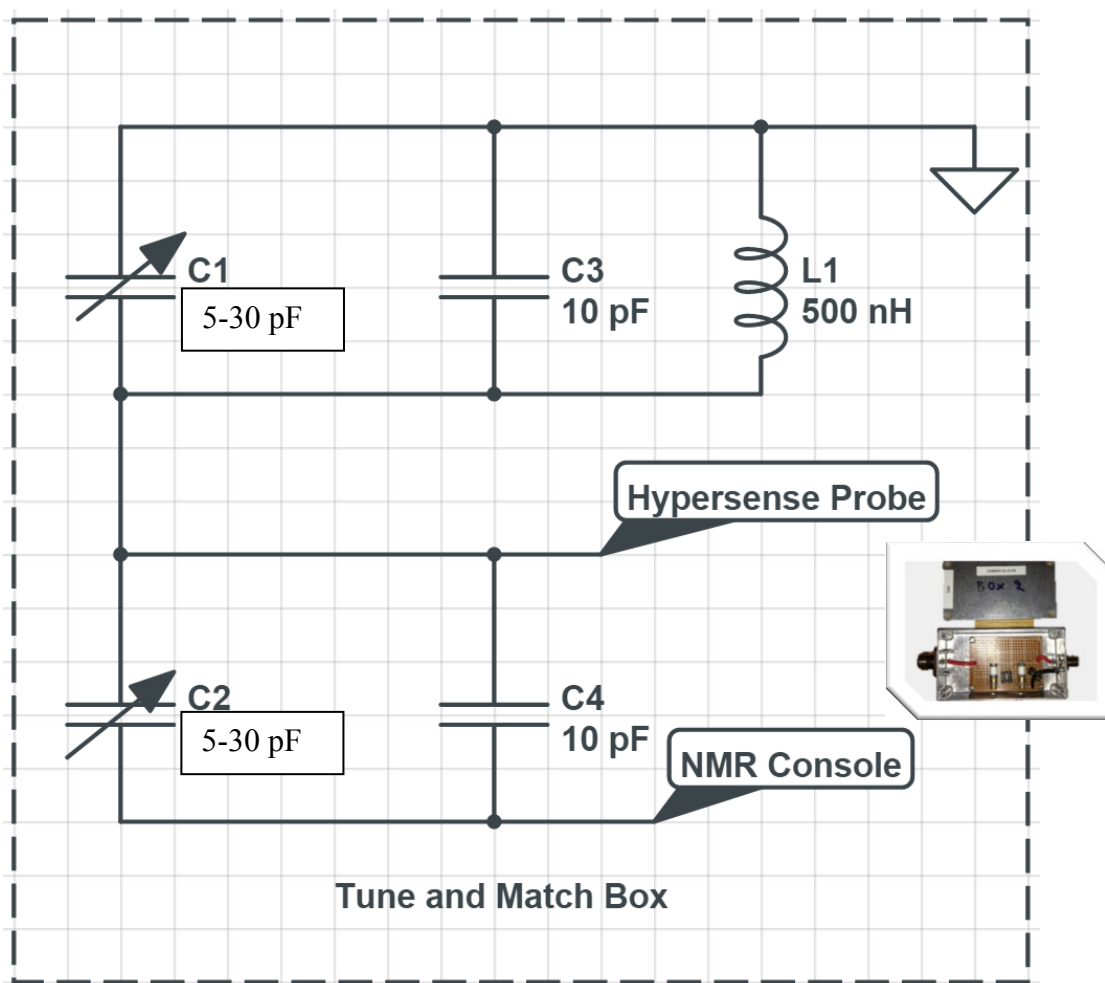
Figure 6.1 - *A tuning and matching circuit for $^{31}P/^{13}C$ solid state experiment built for the experiments described in this chapter. Solid state experiments for other than ^{13}C nuclei were conducted by connecting the Hypersense's internal probe with the 500 MHz Bruker console, which was set to the frequency of ^{13}C (35.7 MHz) and ^{31}P (57.8 MHz) for the acquisition of spectra.*
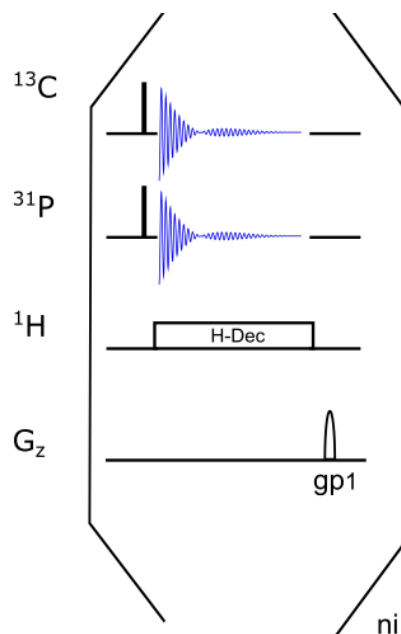
Figure 6.2 – Pulse program for Parallel Receiver DNP. Proton Decoupling is optional

6.2 Solid State DNP

The Hypersense includes a simple ^{13}C-tuned solid state probe that is commonly used to measure the level of ^{13}C-polarisation. This probe is needed to monitor the polarisation build-up and to carry out microwave sweeps in order to adjust the microwave frequency. Typically buildup curves are obtained by acquiring a signal with a small flip angle pulse, usually 5°, in regular intervals (varying between 1 to 10 minutes depending on the compound of interest).

Microwave sweeps are carried out by varying the microwave frequency in small steps (1-10 MHz) and recording a spectrum with a 5° angle every 30 minutes. In these ^{13}C intensity frequency versus frequency curves we show here the maximum polarisation intensity is reached. Initially this can be used to set the fixed microwave frequency for polarisations. However, from such microwave sweeps additional information can be extracted. From the separation of the positive and negative enhancement maxima the

polarisation mechanism can be determined. For the solid effect maxima separated by $2*\omega_N$ should be observed, whereas these maxima are not properly resolved for TM. The embedded probe has limited sensitivity because the coil is too far away from the sample and has a low filling factor.

For the calibration of simultaneous polarisations of multiple nuclei another probe was available, comparable to that used by Reynolds et al [89]. This external solid state probe can be inserted into the polarisation chamber without disassembling the system and has a coil directly surrounding the sample cup. This probe has a much better sensitivity and thus produces better quality frequency sweeps for ^{13}C and ^{31}P as shown in Figure 6.7 and 6.8.

For the experiments described here the overlap of polarisation frequencies was used. In theory a solid effect build-up mechanism was expected when using the OX63 radical. Microwave sweeps of ^{13}C and ^{31}P reveal that there is sufficient overlap between microwave frequencies for both nuclei that a compromise frequency can be used to polarise both nuclei simultaneously. In fact, when a nucleus is selected by setting a microwave frequency several nuclei with overlapping frequencies are inevitably polarised simultaneously.

In order to observe the build-up curves of the polarisation, a solid state probe tuned at both nuclear frequencies is needed, with a dual resonance tuning and matching circuit. In this work a dual resonance tune and match circuit was constructed (Figure 6.1) to enable tuning at both 37 MHz and 58 MHz (^{13}C and ^{31}P frequencies respectively at the 3.34 T magnet of the Hypersense).

In order to build and adjust the tuning circuit the wobbling function of the Bruker NMR Console Avance III was used. Using variable capacitors and coils in the circuit

shown in Figure 6.1, the resonance behaviour can be altered to match the needs of the various nuclei. Capacitors in parallel with the trimmers increase capacitance. The cable connecting the probe with the circuit also influences the resonance frequency of the circuit. It acts as a λ-l/2 cable where very small variations in length can give optimum frequency. The cable for this work was 1.5 m long.

The wobble curve obtained with the tuning circuit is shown in Figure 6.3. It shows that two resonating frequencies appear, and these frequencies can be tuned to match those of ^{13}C and ^{31}P. Both frequencies were tuned very well. The matching for the carbon frequency was slightly worse than for ^{31}P, although by far sufficient for the experiments needed.

Solid state experiments acquired in the polarizer produce broad signals as demonstrated in Figure 6.6 where the broad solid state signal of ^{31}P is displayed. The spectral width is 500 KHz and the linewidth is 30 KHz. These values are in accordance with Reynolds' [89] study.
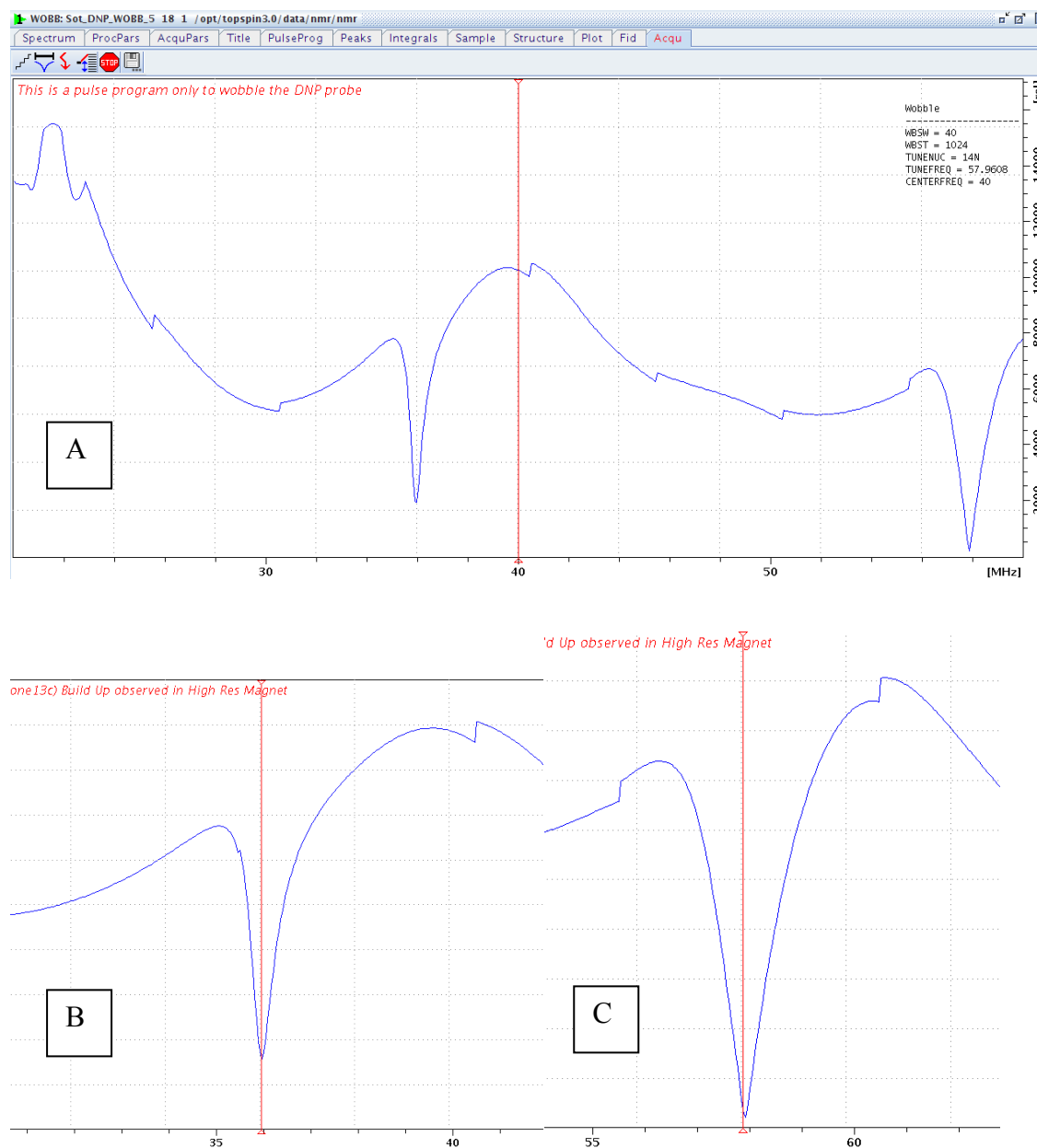
Figure 6.3 - Performance characteristics for the tuning and matching circuit built for the solid state probe, shown in Figure 6.1A. Wobble signal of the Hypersense Probe showing the two resonating frequencies for Carbon and Phosphorus B: Carbon Tune and Match C: Phosphorus tuning and matching.

Despite the double tuning arrangement common NMR instruments can only detect a signal of one nucleus each time. For the polarisation the decisive factor is the polarisation microfrequency that is chosen. While it is not always possible to polarise two remote frequencies in parallel without two microwave sources, some polarisation

frequencies are sufficiently close to obtain polarisation when a compromise frequency is chosen.

$$I(t) = 1.4996 * (1 - \exp(-0.0050*t))$$
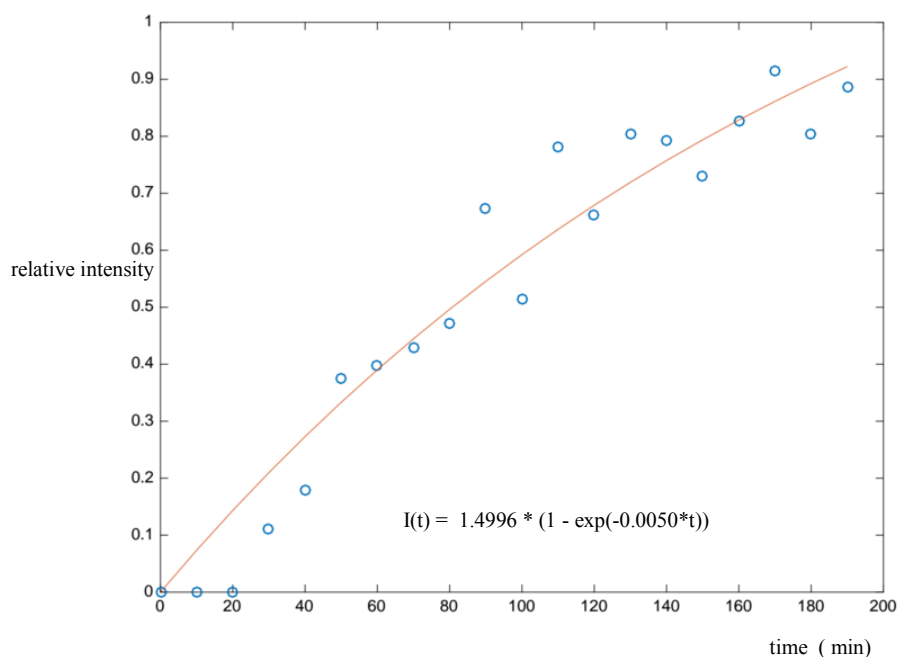
Figure 6.4 – Solid State build up of TMP with $^{13}C_2$-acetone in the sample matrix

$$I(t) = 0.9936 * (1 - \exp(-0.0144*t)) + 1.1195e\text{-}04 *t$$
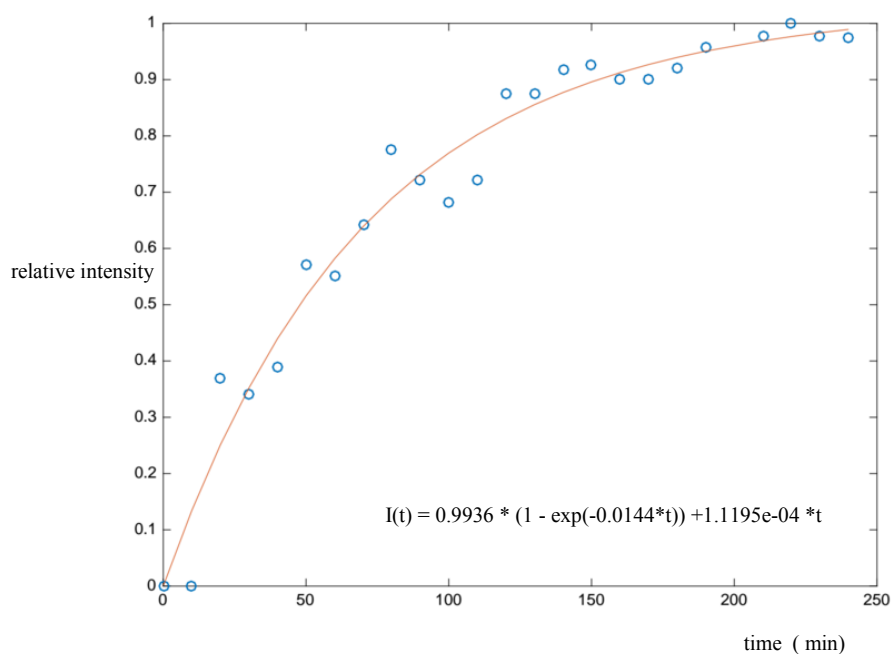
Figure 6.5 – 13C Solid State Build up of TetraMethylPhosphonium (1-^{13}C-TMP)

In order to measure polarisation curves experiments are carried out, where a single one-dimensional spectrum is acquired for each nucleus, depending on the microwave frequency. The maximum is taken to compose the build-up curve.

The way the solid-state DNP-NMR experiments were performed using the NMR console was to acquire a series of subsequent experiments, each using the same 1D pulse sequence, in conjunction with setting the Hypersense to trigger the NMR console every time it changes polarisation frequency. A small time difference between the two acquisitions (5 to 10 seconds) ensures that ringing or other artefacts are neither affecting nor producing signal.
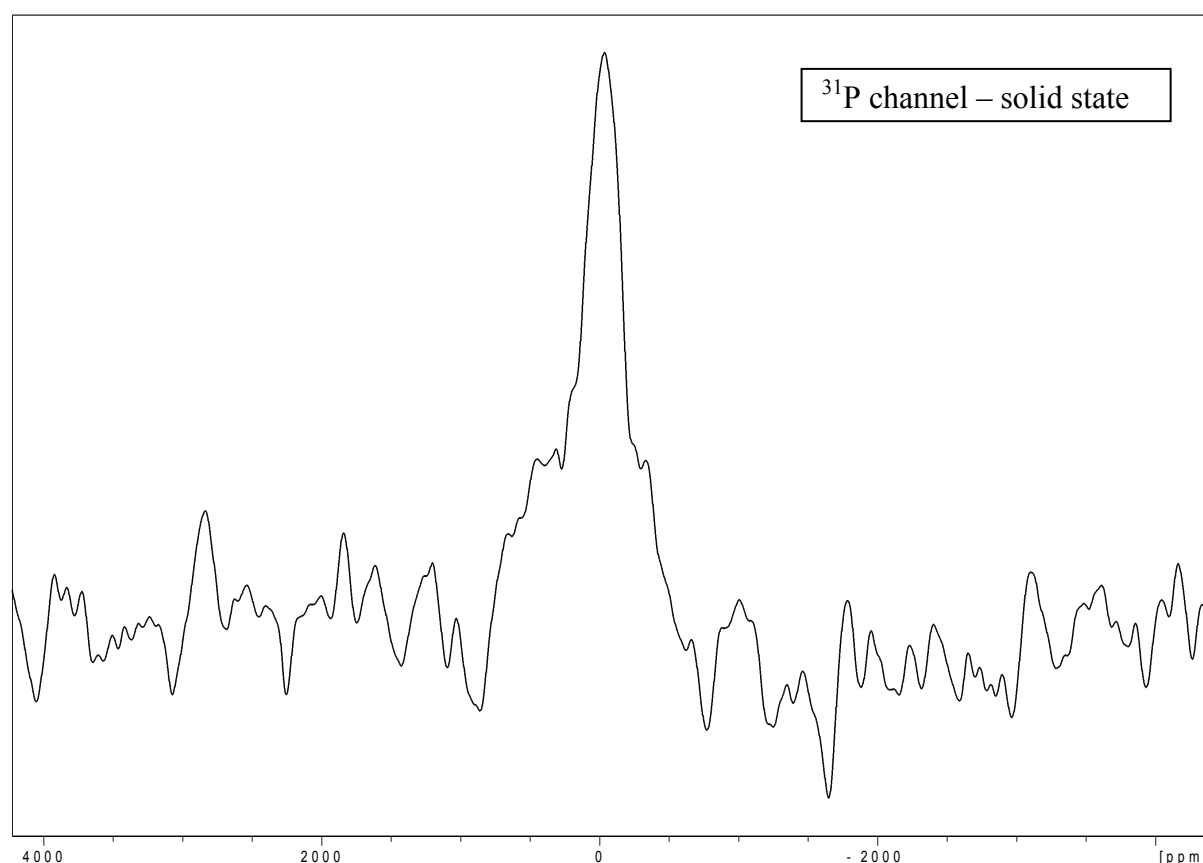
Figure 6.6 – A ^{31}P Solid State Spectrum of polarised ATP. Linewidth is 30 KHz and spectral width 500 KHz.

Although the Hypersense instruments incorporate a simple ^{13}C-spectrometer, the Bruker NMR console was used for the acquisition of all solid-state NMR spectra as it offers substantially more flexibility for the adjustment of spectral parameters. For microwave sweeps the microwave frequency was gradually incremented between 93.800 and 94.250 GHz while the NMR console was used to obtain NMR spectra of ^{13}C and ^{31}P with a small flip angle in small time intervals. In Figure 6.7 a comparison of microwave sweeps for ^{13}C and ^{31}P are shown. In theory, the maximum polarisation for a solid effect mechanism is at frequencies of $\omega_e \pm \omega_N$, this is 94.090 GHz $\pm$ 58 MHz for ^{31}P and ± 37 MHz for ^{13}C. The experiment confirms what was theoretically expected and the data observed from polarisation curves demonstrate the difference of the maxima frequencies (it is the difference between orange and blue line in Figure 6.7 on the horizontal –frequency- axis).
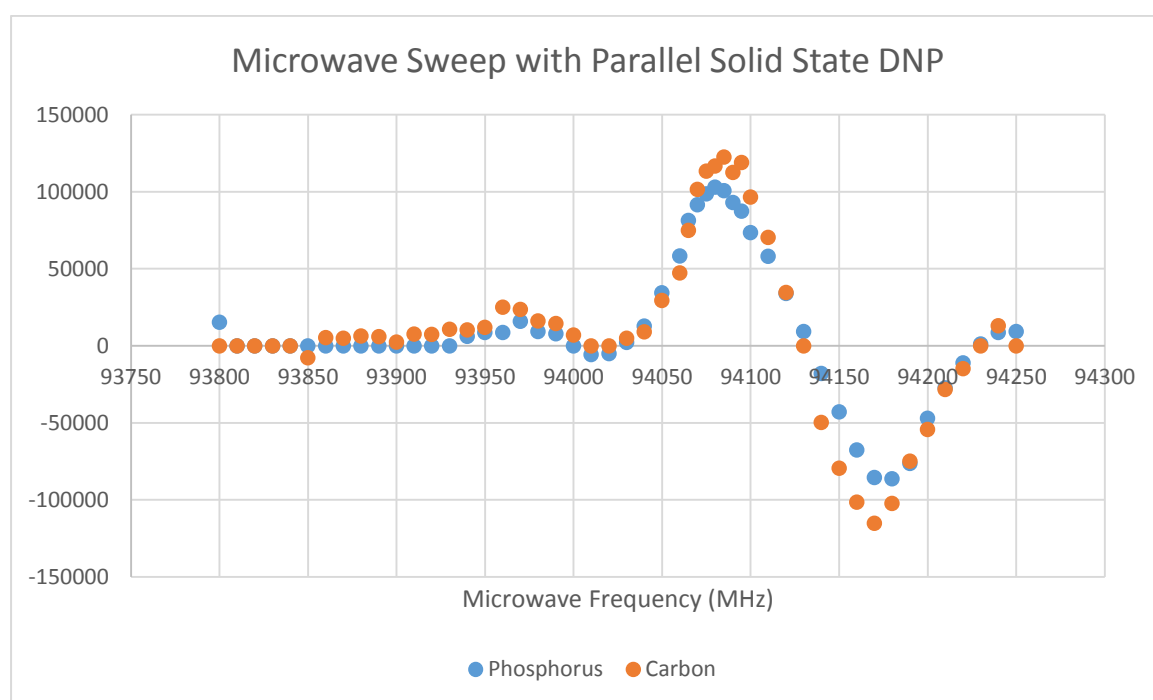
Figure 6.7 – Microwave Sweep of ^{13}C (red) and ^{31}P (blue) recorded in the same sample using the double resonance Tune and Match Box. Sample is ^{13}C$_2$-acetone and ATP
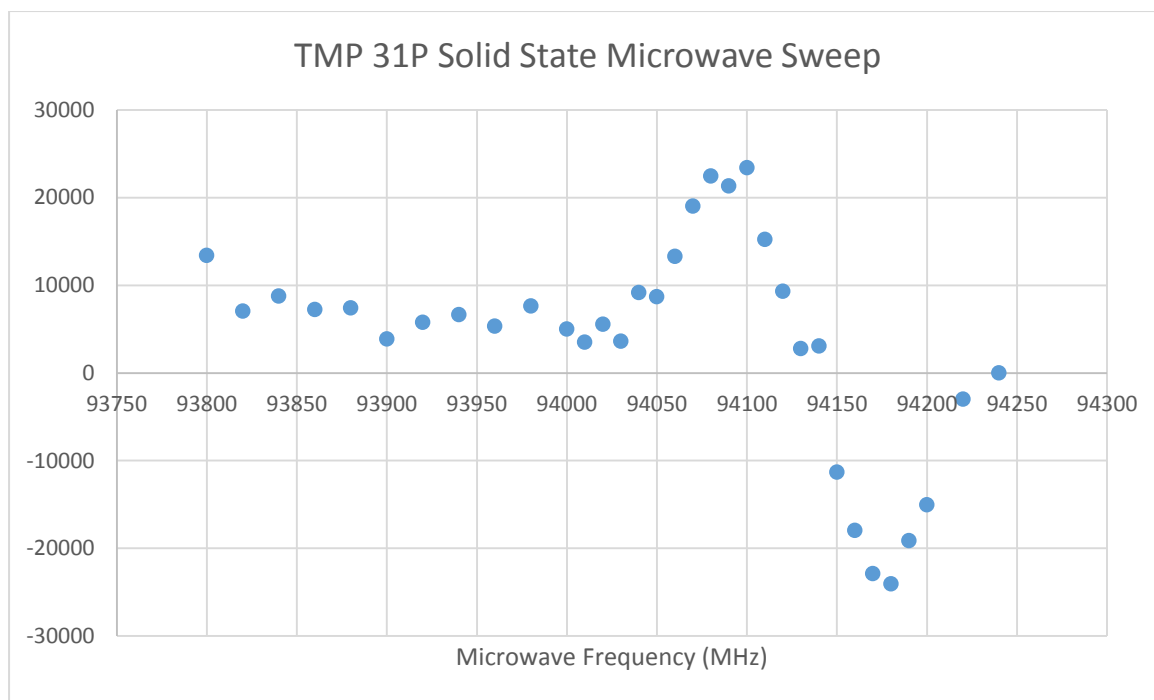
Figure 6.8. ^{31}P microwave sweep curve of Tetra-methyl-Phosphonium

The polarisation time for each data point is one hour, and as described earlier, a small delay is set between carbon and phosphorus acquisition (magnitude of 5-10 seconds).

6.3 Parallel Receiver Dissolution DNP

A series of experiments was performed using Parallel Receiver dissolution DNP. The main advantage of applying Parallel Receiver NMR in dissolution DNP is that more information can be gathered out of a single polarisation. This is potentially useful as polarisation takes typically 2 to 4 hours. As explained in the introduction polarisation of multiple nuclei is easily feasible.

The first compound that was selected for these series of experiments has been unlabelled ATP. Experiments were performed with and without polarisation. Using polarisation the sample's final concentration after dissolution was 0.1 mM. ATP was selected as a biologically relevant compound to show feasibility of such experiments in biological systems.

A spectrum of ATP was recorded after polarisation for 3 h. For ^{13}C/^{31}P parallel receiver experiments, the required instrumentation includes a dual resonance probe with carbon and phosphorus channels. We used a broadband probe with a separate phosphorus coil connected to a dual receiver console thus enabling to pulse and detect simultaneously in both frequencies. Utilising the overlap in polarisation frequencies that was explained earlier on chapter 6.2 we were able to acquire a spectrum for ATP for both ^{13}C and ^{31}P nuclei from the same sample (Figure 6.9). Experiments were also performed with a synthetic compound. In collaboration with Ildefonso Marin Montesinos from University of Barcelona, we were provided with TetraMethylPhosphonium, in which the phosphorus is attached to four methyl groups. In Figure 6.10 to 6.16 the analysis of the compound using Parallel Receiver DNP experiments on ^{13}C and ^{31}P channels is presented, along with the thermal spectrum of the compound.

The TMP sample was prepared by diluting 10.5 mg of TMP in 50 ml of D_2O and then adding 50 ml of glycerol as a glassing agent. Experimental conditions of the polarisation included 3 hours polarisation, 94.067 GHz polarisation frequency, 1.4 K temperature at the Helium bath and 55% Helium bath level. Dissolution was performed at 9 bar with 1:1 water – methanol mixture using the conventional dissolution system of the Hypersense polariser.

The non-decoupled ^{31}P spectrum of TMP in Figure 6.11b and the polarised equivalent in figure 6.12b show a complex J splitting. Phosphorus is bound to four methyl carbons that are equivalent, and these four carbons are bound each to 3 protons. Therefore the J_{HP} splitting that is expected is a 13 peak splitting, and as the J coupling to carbon creates an additional splitting, therefore 26 peaks are expected. From the Pascal triangle is possible to calculate the relative intensities of these peaks and see

how well the splittings are resolved compared to the theory. In practice, only peaks with sufficiently high intensity are observed in the spectrum. This means 9 signals instead of 13, so 18 peaks in total. In the DNP spectrum due to loss to linewidth, peak number is reduced to a total of 13 peaks. Table 6.1 shows that the theoretical approximation of the intensity of the peaks is in accordance with the experimental results. Small positive error increasing in the higher peaks comes from peaks showing as shoulders in other peaks due to the complicated nature of the spectrum.
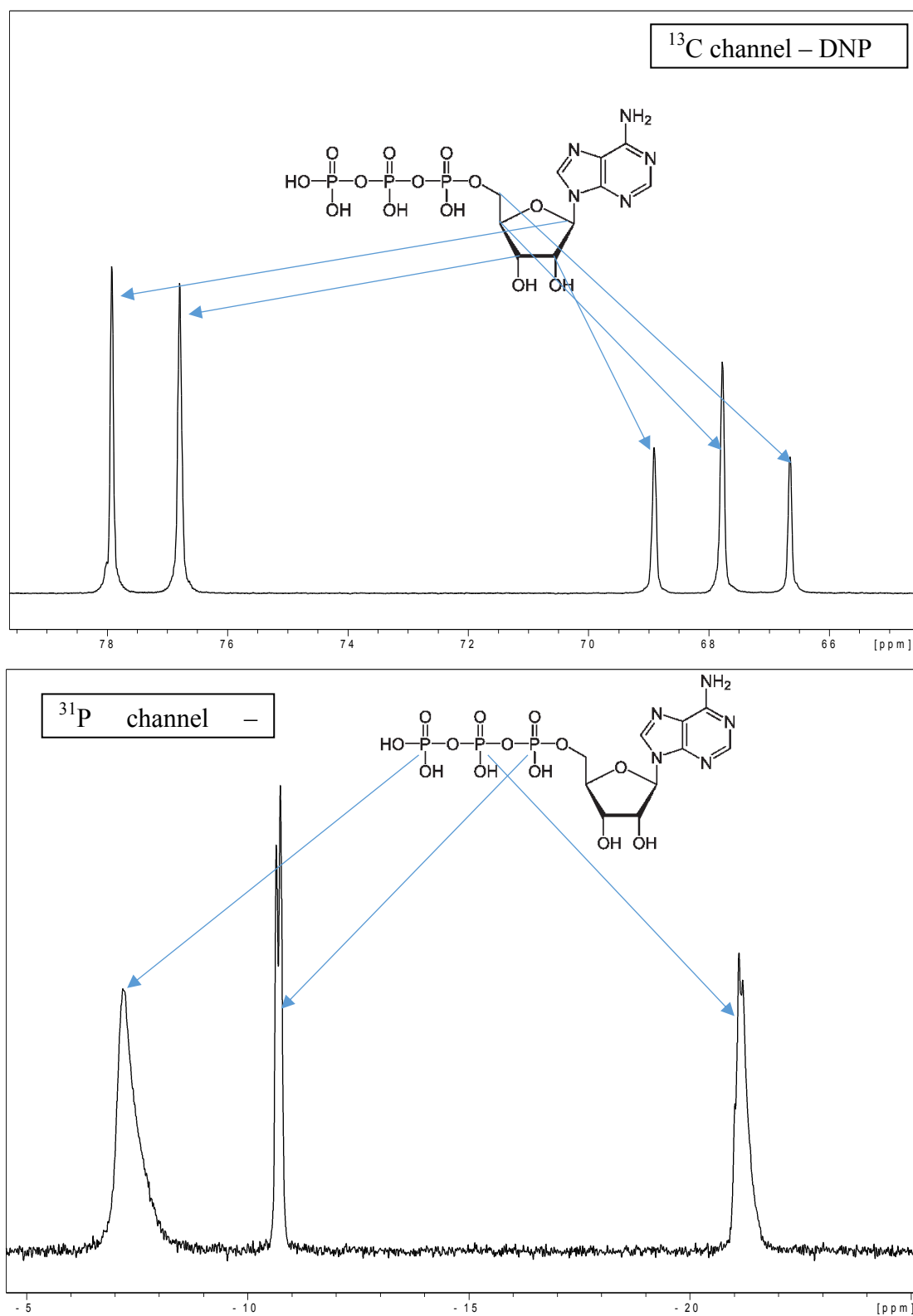
Figure 6.9 – ^{13}C and ^{31}P spectra acquired with parallel receiver Dissolution DNP. The two spectra were acquired simultaneously after 3h of polarisation with the Ox63 radical.
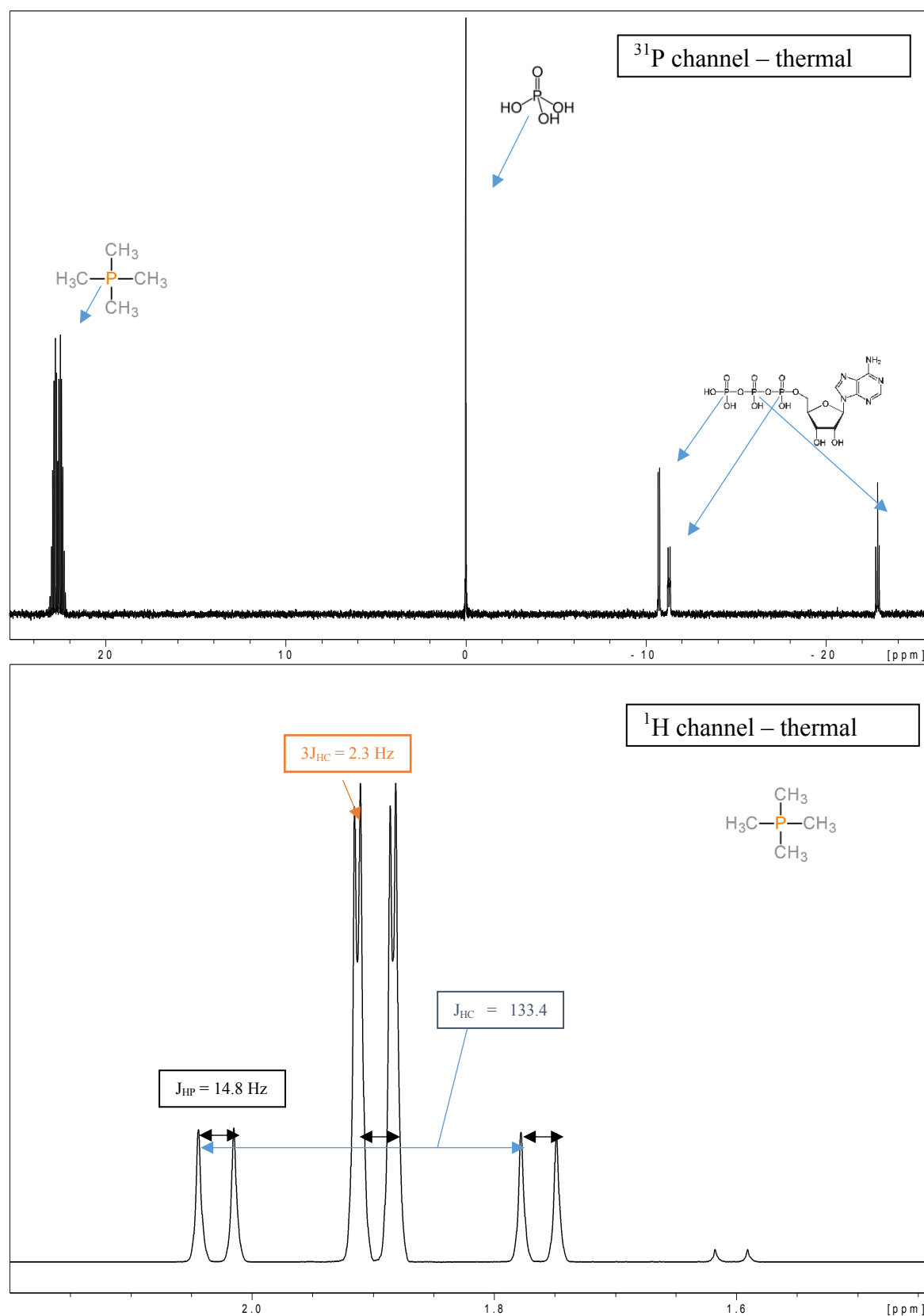
Figure 6.10 – A: ^{31}P channel thermal spectrum of a mixture of H_3PO_4, ATP and TMP B: ^{1}H channel thermal spectrum of TMP, zoomed in the methyl area.
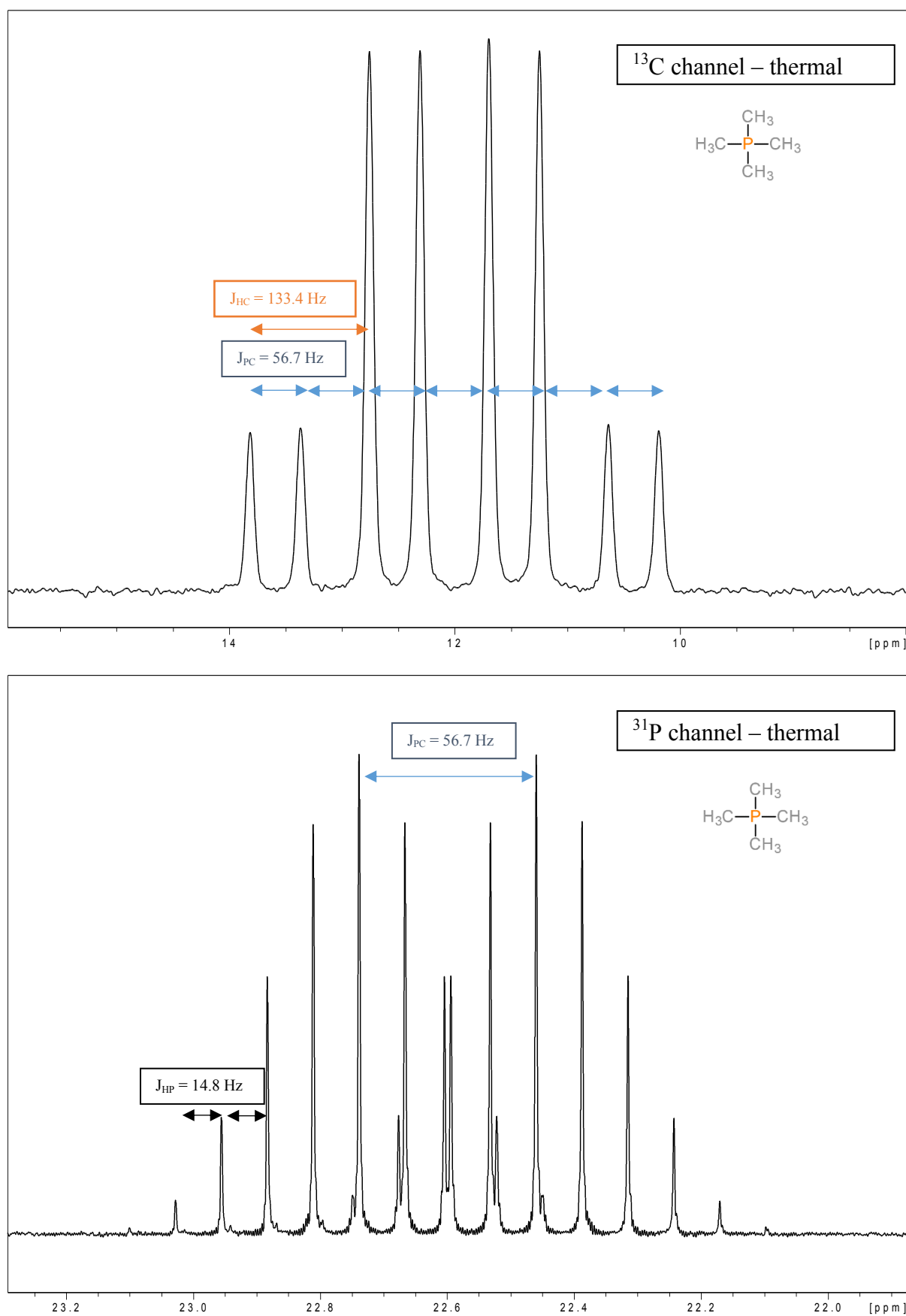
Figure 6.11 – A: ^{13}C thermal spectrum of TMP. B: ^{31}P thermal spectrum of TMP
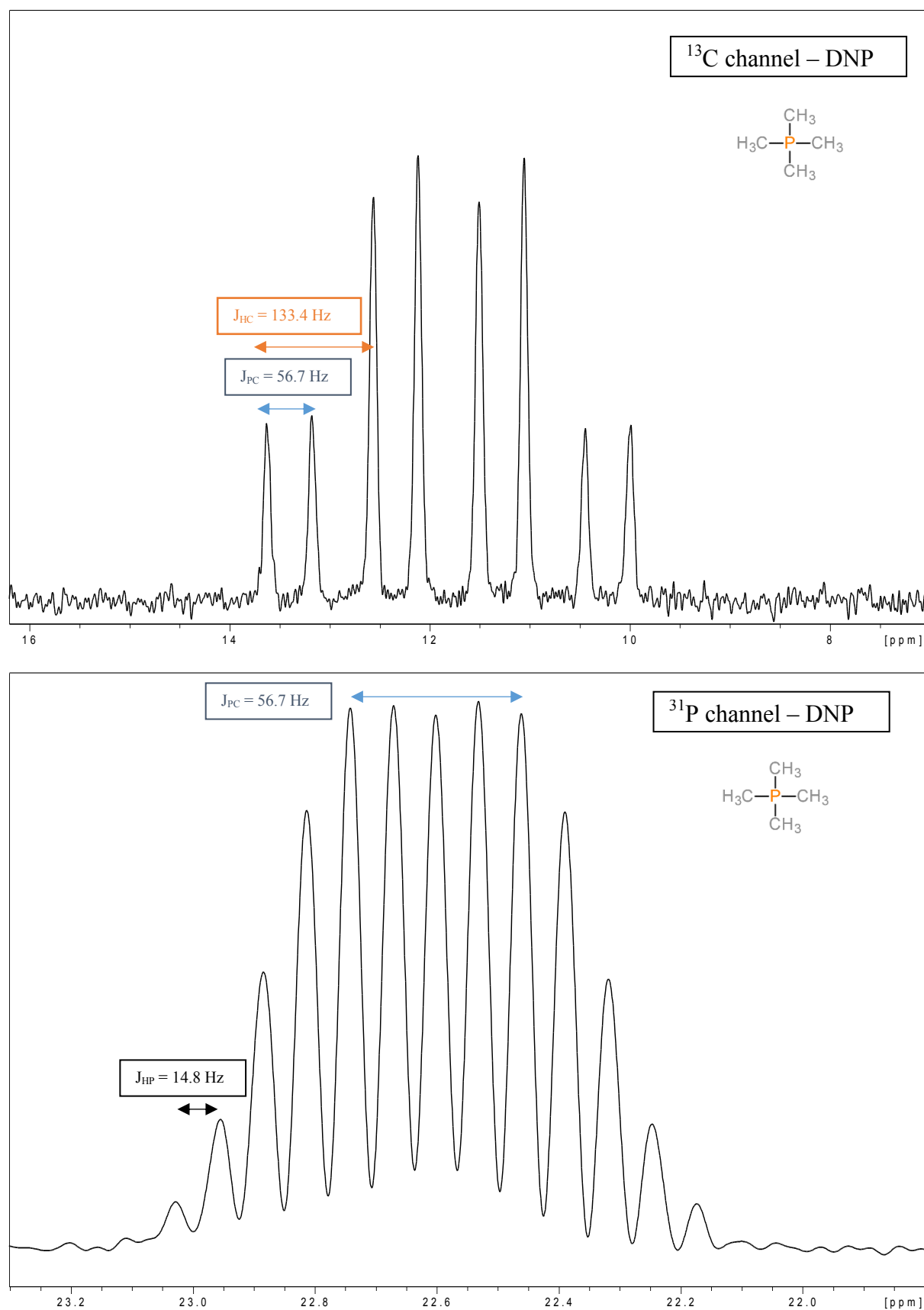
Figure 6.12 –a Parallel Receiver DNP experiment. The ^{13}C and ^{31}P spectra were acquired in parallel after polarisation. A: ^{13}C dissolution spectrum of TMP B: ^{31}P dissolution spectrum

```
                        1
                       1 1
                      1 2 1
                     1 3 3 1
                    1 4 6 4 1
                  1 5 10 10 5 1
                1 6 15 20 15 6 1
              1 7 21 35 35 32 7 1
            1 8 28 56 70 56 28 8 1
          1 9 36 84 126 126 84 36 9 1
        1 10 45 120 210 252 210 120 45 10 1
      1 11 55 165 330 462 462 330 165 55 11 1
    1 12 66 220 495 792 924 792 495 220 66 21 1
```

Figure 6.13 – The Pascal Triangle for 13 increments.
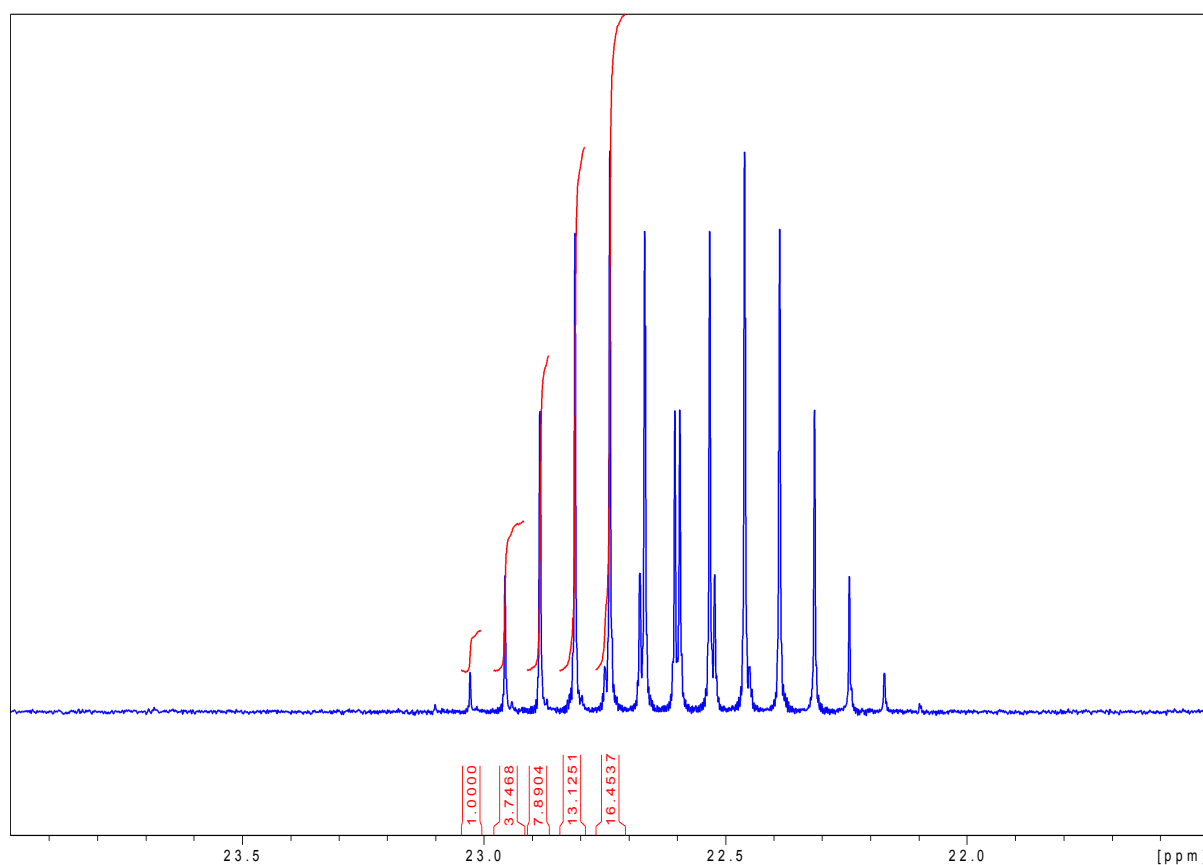
Figure 6.14 – Peak Integration for generating Table 6.1

Table 6.1 – Normalised integral for ^{31}P TMP peaks. Instead of 13 peaks, 9 can be observed with adequate signal producing a total of 18 peaks.

Theoretical Value from Pascal's triangle	Actual value based on peak integral and normalisation with the first peak
66	66
220	247.5
495	520.74
792	866.58
924	1085.7

6.4 Discussion

With the experiments performed in this chapter, it was shown that it is possible to utilise a Parallel Receiver DNP approach for dissolution DNP experiments.

One interesting aspect is the comparison of the linewidth between thermal and polarised experiments. Whilst with ^{13}C experiments the linewidth is comparable, experiments with ^{31}P always have bigger linewidth when comparing dissolution and non-dissolution DNP. This difference can not arise from the sample transfer because we would expect the same for both nuclei. It is most likely the chemical shift anisotropy of ^{31}P arising from the asymmetrical electronic structure of phosphorus that causes the observed broadening in the presence of the radical.
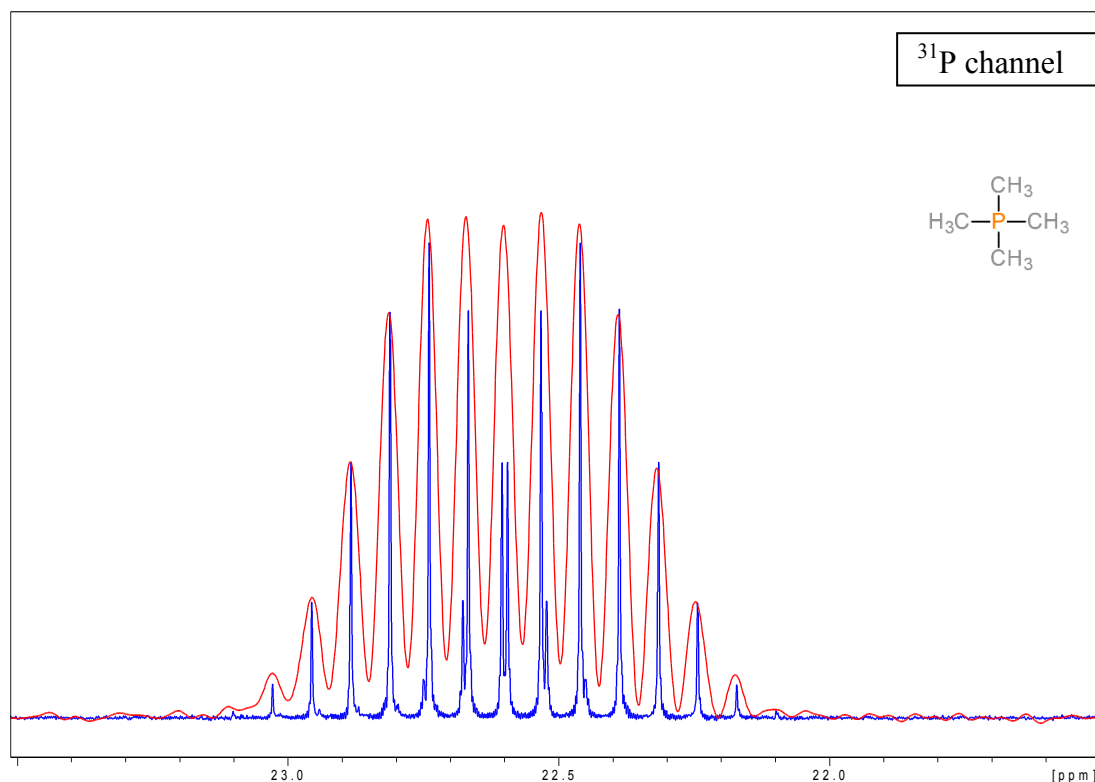
Figure 6.15 – Comparison of ^{31}P thermal (blue) and polarised (red) spectra

A second interesting aspect is the ability to carry out a quantitative analysis of the amount of phosphorus polarisation (Figure 6.16). As all the experiments were run without proton decoupling the splittings in the ^{13}C spectrum show that the polarisation of ^{31}P was less than that of ^{13}C. The polarisation frequency here was chosen to be optimal for ^{31}P (94.067 GHz). The methods described here offer a useful tool in order to take full advantage of the polarisation happened in each experiment, by recording a multi nuclei spectrum.
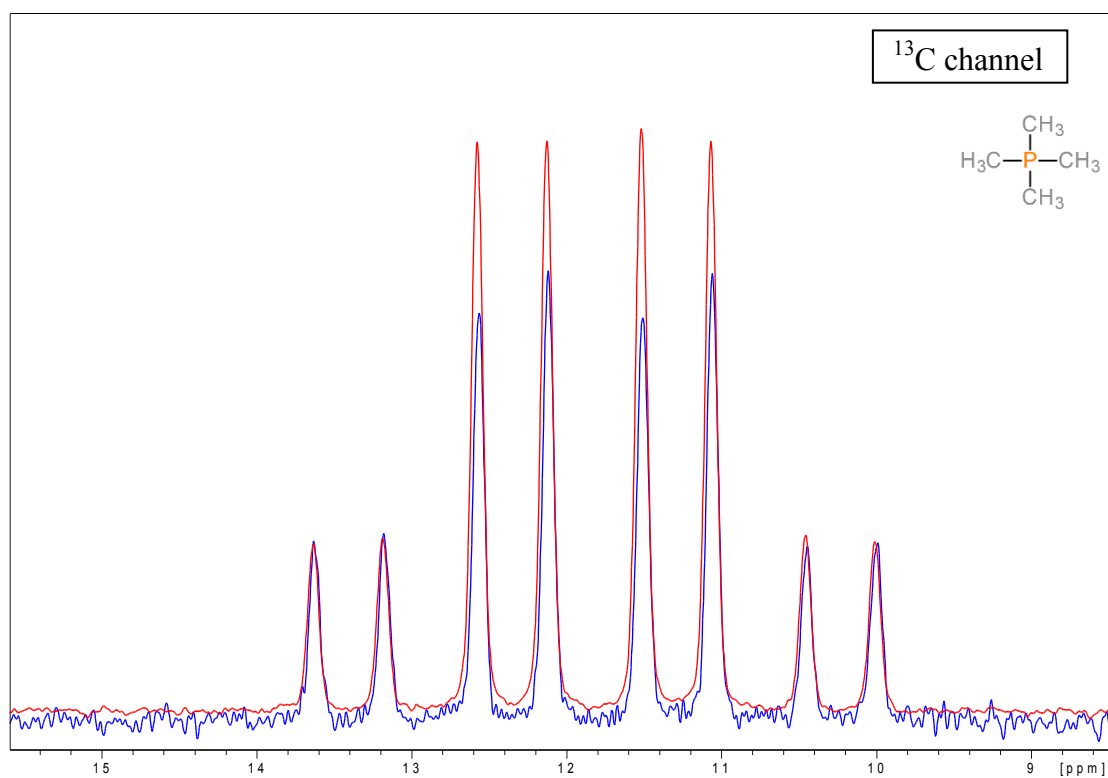
Figure 6.16 – Comparison of ^{13}C thermal (blue) and polarised (red) spectra of TMP. From the difference in the splitting intensity it is possible to estimate the level of polarisation of Phosphorus, in comparison to Carbon.

.

Chapter 7 - Discussion – Future aspects

The initial aim of this thesis was to build a pressure dissolution device for dissolution DNP that surpasses the gains of a previous published device [68]. The new dissolution device outperforms the previously published device in terms of spectral sensitivity, lineshape and reproducibility. The new device is based on a decentralized design of independent subsystems (e.g. liquid detector and touch screen interface) based on the open-source Arduino platform. The post-dissolution sample transfer device clearly extends the applicability of the D-DNP system. Owing to the enhanced NMR lineshapes it allows for experiments that otherwise were not possible. However there are further options that may become feasible based on this design.

A possible expansion is the addition of additional sensors to help perform a variety of different operations. Pressure sensors for example can help evaluate the performance of the sample transfer. Additional liquid detectors can help to determine the position of the liquid in the tubing which should enable a much more precise delivery of exact amounts of fluid into the NMR tube and thus lead to a possible reaction chamber where several liquids are combined for real-time reaction monitoring in the NMR tube. An additional pneumatic exhaust valve on the high pressure –transfer- line in combination with an increased transfer-line pressure can improve sample transfer speed.

Another approach is to use the I/O of the pressure system to supply a polarised precursor to a bioreactor within the NMR tube in order to measure the polarisation output in a similar way. But if the bioreactor is within an NMR tube already placed in the spectrometer, this limits the application to a low-pressure setting. An interesting point would be to have the bioreactor in the presence of the field (slow relaxation) and investigate pressure dependent metabolism.

A different approach is to change the pressure chamber in a way that mimics SIA (Sequential Injection Analysis) [90, 91], a common analytical chemistry technique. With this approach a sample can be injected along with the polarised liquid if it is pre-collected in a sample loop. This can enable the possibility of performing *in vivo* experiments to study a pressurised system. With the addition of a syringe pump and an extra multiposition valve, one can inject solutions in a loop connected to the pressure system. If the syringe pump is sufficiently powerful to withstand negative pressure, on the fly mixtures can also be prepared by injecting different amount of material with the syringe pump. If this is applied in a kinetic study it will obviously not be a real time feed but snapshots of the procedures happening *in vivo* and *in vitro*, with limiting factor for the resolution in the time domain being the polarisation time. Ideally this has to be combined with a polarising substance like pyruvic acid.

Possible future applications could be in reaction monitoring or kinetic studies using a bolus of polarised substrate mixed with a reactant in the NMR tube. A potential improvement of the current design would be the introduction of a flow element. In this way hyperpolarised material can periodically replenish the material that has lost its polarisation through relaxation inside the NMR probe.

Another aspect of this work was to create long-lived acetylated compounds. This theory is based on the fact that non-protonated carbons like the one of the carbonyl have long relaxation times [92]. There are more approaches published in literature. Deuteration of a compound can lead to prolonged relaxation times [76]. An example is glucose [70]. It is also shown that relaxation times are field dependent and this relation is not linear. For example $^{13}C_1$ nuclei in hyperpolarized pyruvate exposed to a magnetic field strength of 2T have twice the relaxation time compared to those in a 11.74 T magnetic field [93]. Thus molecular imaging of hyperpolarized pyruvate

benefits from a reduction of field strength. Malcolm Levitt pioneered the transfer of polarisation to singlet states[94]. This can be achieved using specialised pulse sequences [95, 96] and leads to prolonged relaxation times. Therefore using singlet states hyperpolarization can be stored for a longer time extending the applicability of D-DNP to slower time windows. It is also possible to use the formation of singlet states in *in vivo* experiments [97, 98]. The singlet states here either form by shaking the sample inside a magnetically shielded chamber, through which out of the possible states only the singlet state remains, or by relaxation using the fast relaxation times of the triplet state.

It was clearly possible to acquire simultaneous NMR spectra for both nuclei. A very interesting, yet unresolved observation was that while thermal spectra of ^{31}P show similar linewidths to the ^{13}C resonances, the ^{31}P lines are considerably broadened when the nuclei are hyperpolarized. Because the ^{13}C resonances acquired on the other channel showed narrow line widths, shimming or sample transfer or delivery problems can be excluded. Combined line-shape analysis of different nuclei in the same molecule could open up new ways to study relaxation phenomena in hyperpolarized ^{31}P samples with the ^{13}C acting as an internal reference.

The use of Dissolution DNP to perform experiments like an instrument for analytical chemistry has some limitations. For any sample, there is a large dilution factor arising from the dissolution step but also from adding a second solvent in the sample cup to ensure the glassy state. This brings a dilution factor of 80. The second limitation is that not all the nuclei species can be observed with DNP. This also alters the structural information, as even in the ideal case that narrow linewidth splittings can be observed, the structural information and the ratios will also embed the polarisation factor for

each nucleus. With specific settings and applications the research interest can be maintained.

The area that Dissolution DNP finds the most exciting applications is in conjunction with MRI to create a new diagnostic platform utilizing ^{13}C [99]. In this method the outcome is a combined DNP-MRI technique that can give real-time in-vivo information about metabolic pathways that can lead in interpretation of drug response in cancer treatment. This work is pioneered by Kevin Brindle and the applications are constantly growing [69]. The prospect for DNP-MRI at the moment of writing looks great as the one scan limitation of DNP becomes an advantage for the patient, who does not have to wait for a long scanning procedure.

Appendix 1 – Published Article 1

Title: Improved Stability and Spectral Quality in Ex Situ Dissolution DNP Using an Improved Transfer Device

Page 111

Improved Stability and Spectral Quality in Ex Situ Dissolution DNP Using an Improved Transfer Device

Sotirios Katsikis[1] · Ildefonso Marin-Montesinos[2] ·
Miquel Pons[2] · Christian Ludwig[1] · Ulrich L. Günther[1]

Abstract   Dissolution dynamic nuclear polarization (DNP) has become one of the predominant implementations for DNP. However, the technical implementation of transferring the sample from the polarizer to the nuclear magnetic resonance (NMR) system remains challenging. There is a need for additional technical optimizations in order to use dissolution DNP for biochemical and chemical applications. Here we show how a newly designed pressure dissolution kit considerably improves spectral quality and stability by enabling highly reliable and fast sample transfer to the NMR system.

1 Introduction

Dissolution dynamic nuclear polarization (DNP) has been quickly established as a research tool to study DNP, and has great potential as an add-on for a series of nuclear magnetic resonance (NMR) applications. The concept of polarizing at low temperatures (typically 1–3–1.4 K) [1] yields the highest possible polarizations by combing the actual polarization with a temperature factor (298 K/1.4 K ~ 200). However, the concept has serious inherent shortcomings, mostly arising from the necessity to melt the sample in a very short time, and to transfer it into an NMR tube in a different magnet for the NMR measurements. In the process the sample forms bubbles, and the transfer is suboptimal.

Electronic supplementary material   The online version of this article (doi:10.1007/s00723-015-0680-5) contains supplementary material, which is available to authorized users.

✉ Ulrich L. Günther
u.l.gunther@bham.ac.uk

[1]   School of Cancer Sciences, University of Birmingham, Edgbaston, Birmingham B15 2TT, UK

[2]   Biomolecular NMR Laboratory, Organic Chemistry Department, University of Barcelona, Martí i Franquès 1-11, 08028 Barcelona, Spain

Hilty and coworkers [2] introduced a system that keeps the dissolved sample under pressure after the dissolution, thus avoiding bubbles in the sample in the NMR magnet. A pressure gradient helps to speed up the transfer, and measurements can start immediately, as the sample does not need to settle and degas after the transfer. The implementation of this dissolution system has been challenging as sample tubes tend to break under the sudden pressure change, and the implementation using Labview is relatively expensive.

We have therefore redesigned this dissolution system for a simpler and mechanically more stable design. A robust and flexible microprocessor-based design has been developed that can readily be adapted to other polarizers. A new optical flow detector allows for reliable triggering of the transfer process. A graphical interface facilitates the use of this post-dissolution device. Here, we describe the newly designed concept along with applications that demonstrate a considerable improvement.

The setup employs the open-source Arduino architecture along with a customized sample holder. This architecture is sufficiently flexible to be adapted for other uses, including controlled release of a polarized sample onto cells for metabolic flux experiment. The system has been tested using a Hypersense polarizer, but should be applicable to any comparable system. Our data show considerably improved quality of one- and two-dimensional spectra and substantially improved data quality for longitudinal relaxation measurements.

2 Implementation

We used an Oxford Instruments Hypersense polarizer along a Bruker Avance500 III NMR spectrometer, equipped with a broadband 5 mm probe. The dissolution device was built to minimize the sample transfer time and to optimize sample stabilization in conjunction with this equipment. It triggers the spectrometer after a user-adjustable time period.

The overall arrangement of the dissolution device is shown in Fig. 1 (Fig. 1 S1 for the injection position). A high-pressure manifold (Fig. S3) splits the input pressure into two independent output pressures, one for pre-pressurizing the NMR tube (p_{LP}), the second to transfer the sample into the NMR tube and to keep it pressurized for the NMR measurement (p_{HP}). An electronic valve assembly consisting of 4 SMC VDW31 valves switched by 4 channel 5 V multi-relay module from Sainsmart opens the outputs of the manifold to the pressure lines.

Overall Operation Procedure After dissolution of the sample at 1.3–1.4 K by pressurized solvent in the Hypersense, it is transferred into the sample loop of a multi-way two-position valve (VICI C22 6180, 2 position 10 I/O valve with pneumatic actuator) with a pneumatic valve actuator (VIVI valco).

An optical detector triggers the switch of the multi-way valve to inject the sample under a pressure of p_{HP} into the NMR tube (Fig. S4). While line HP1 is constantly kept at the high pressure of p_{HP}, line HP2 is pressurized with a delay of typically 600 ms—the time of the sample transfer—to stabilize the sample in the NMR tube after transfer. The acquisition of the NMR spectrum is automatically triggered with
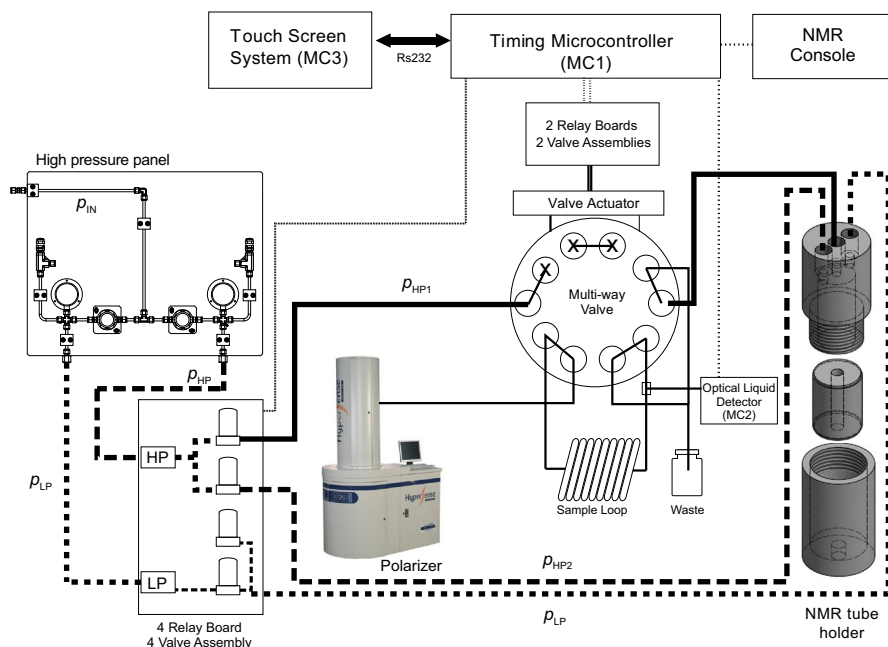
Fig. 1 Overall design of the pressure dissolution system showing the individual components and the connections in the system. The microcontrollers (MC) are used to control the pneumatic assembly. The high-pressure *panel* splits the input pressure into a low-output pressure p_{LP} for pre-pressurizing the device and a high-input pressure p_{HP} to transfer the sample to the NMR system and to keep it under pressure after the transfer

a delay of typically 1–2 s after switching the multi-way valve. With this the overall transfer until the measurement can start is 2–3.5 s after the start of the dissolution of the sample.

Microcontroller Assembly Figure 1 also provides an overview over the microcontrollers (MC) used for the overall device. As microcontroller platforms we employed Arduino microcontrollers. The main criteria for selecting the Arduino platform is that it offers a built-in programming board attached to the microcontroller at a very low price and the Open Source implementation of the hardware and software. A MC controller design is superior over computer-connected I/O interfaces.

We are using two Arduino Mega 2560 boards (based on the Atmel ATmega2560 microcontroller), clocked at 16 MHz frequency to control the valves and for the graphical display and an Arduino Nano V3 for the flow sensor. The first Arduino (MC1) is used to control the relay operations and timings of the valve assembly and the actuator of the multi-way valve. It receives a trigger from the optical liquid detector and triggers the spectrometer. MC2 is connected to a 3.2-in. touch screen to enable user level I/O, and to set the trigger delay (600 ms). The code for all 3 Arduino processors is provided as part of the supplementary material.

The Arduino Nano V3 (MC3) controls the liquid detector. For this we compared different concepts, starting from the implementation proposed by Bowen et al. who essentially used a capacitive conductivity detector. An altered design eliminated the need for an Operational Amplifier (OpAMp), thus also eliminating the need to Fourier transform the resulting signal (Fig. S5). The disadvantage of this design is that the actual detector consists of copper tubes placed around the PTFE sample tube connected to the output of the sample loop and this setup is highly sensitive towards mechanical rearrangements. Even the cable connecting this detector to its microcontroller platform had a severe influence on the signal detection.

We therefore tested optical detectors, starting with a home-built design using a Plexiglas cell attached to an LED light and a light-dependent resistor. Although this design worked more reliably it required the sample to pass through a transparent cell, which is not suitable for organic solvents. We finally selected a small commercially available detector (Optek Electronics OPB350) designed for 1/8 in. PTFE tubes. We programmed an Arduino (MC3) (Fig. S4) to control the Optek sensor, which detects liquid entering the sensor and triggers MC1 to inject the sample. This setup works reliably and is very insensitive to movements of the tube or the selection of the sample or solvent. It also works with transparent samples such as pure water, does not require the colored radical in the solution and can be placed adjacent to the multi-way valve to minimize the dead volume.

MC1 and MC3 are interconnected through a serial interface. When serial commands are sent from the touch screen interface (Fig. S2), a program processes the inputs and produces the relevant outputs for the valves. An automatic event loop controls the timing of the overall process during the actual dissolution.

The design of the sample holder appeared to be a crucial bottleneck as it bears a significant risk of breaking the NMR tubes under the high-pressure p_{HP}. Our design (Fig. S6) was modified from Senczenko and Köckenberger [3]. The published design fitted a PEEK barrel tightly around the NMR tube by heating the PEEK until it softened. The disadvantage of this design is the abrupt change of pressure to the outside of the NMR tube where PEEK barrel ends, causing regular breakage of NMR tubes at this position. To circumvent this, we lined a barrel with a slightly larger diameter than the NMR tube with a thin layer of silicon. The softness of the silicon prevented NMR tubes from breaking, but limits the maximum pressure to 15 bar. For safety reasons, we used a medium-walled NMR tube (Norell S-5-500-MW-7) with inner diameter of 3.43 mm.

3 Experimental

NMR Spectra One-dimensional (1D) ^{13}C spectra were recorded with one scan without proton decoupling, a flip angle of 15° (8.12 μs for 90° pulse) and 16 k data points, 250 ppm spectral width. Two-dimensional spectra were acquired using a small flip angle HMBC experiment as described earlier with 8 k data points in the direct dimension and 16 increments, a 15° flip angle (90° pulse length of 8.12 μs), a sweep width of 250 ppm.

Longitudinal relaxation measurements were carried out as described by Day et al. [4], using the single-scan FT (SSFT) method originally proposed by Kaptein [5]. A train of $30°$ pulses was employed, spaced 2 s apart with data acquisition during the first 500 ms of this period with a spectral width of 250 ppm. As described by Day a pulsed field gradient of 2 ms was employed to dephase remaining polarization.

DNP Polarizations were carried out using an Oxford Instruments Hypersense polarizer (Oxford Instruments Molecular Biotools Ltd, Eynsham, UK) with typical polarization times for ^{13}C of 2–4 h at 1.4 K, typically using a 2 mM concentration of the Ox63 radical [1]. For 1D experiments we polarized 100 mM [U-^{13}C]glucose in 100 μl of a D_2O:d-$_6$-DMSO mixture (1:1), which forms a glass state after freezing. For 2D experiments we used 2 M [U-^{13}C]glucose in the same solvent. For the dissolution we used 4 ml of a water:methanol (80:20) mixture. Samples were polarized for 2 h for 2D spectra, including SSFT spectra, and 4 h for 1D.

The pressures and timings of the dissolution device were optimized for transfer speed and sample stability. Considering that the pressure difference drives the sample transfer a larger difference between p_{HP} and p_{LP} is preferable, although p_{LP} must be sufficiently large to minimize forces on the NMR tube arising from the pressure jump. Additionally, the final pressure should be >10 bar, the pressure used for the dissolution in the Hypersense. An optimal setup for our system was found for pressures of $p_{HP} = 12$ and $p_{LP} = 3$ bars, and a time delay of 600 ms. Pressures and delay will depend on the individual implementation, in particular the distance from the polarizer to the magnet (in our case les than 1.5 m).

4 Results and Discussion

The optimized dissolution device was tested for sample stability. For this a series of pictures taken of the NMR tube as sample is transferred shows steady filling within 1.3 s without forming bubbles arising from the gas in the sample (Fig. S7). This can be achieved reproducibly and without any sample breakage.

To test the device we polarized ^{13}C-labeled glucose for which it has been challenging to obtain NMR spectra owing to the fast relaxation of the glucose ^{13}C. Although the relaxation time of glucose can be increased by 30 % using deuteration, which has enabled in vivo chemical shift imaging, deuteration removes the option to acquire ^{13}C-^1H-HMQC or spectra. Here we show that [6] we can obtain one-dimensional spectra reproducibly with a significantly improved quality. In dissolution DNP the sample suffers from a large load of gas dissolved in the sample owing to the high-pressure dissolution, which is typically carried out at 9–10 bar. After this pressure is reduced the gas dissolved in the solvent is released causing bubbles. This results in low-quality spectra owing to loss of homogeneity. For glucose with ^{13}C T_1 values of <1 s a short transfer time is also essential. Figure 2 shows the improvement achieved from the pressure dissolution device for a 1D spectrum of [U-^{13}C]glucose with a transfer time of ∼2 s. While the spectrum shown in Fig. 1a suffers from bad resolution and low intensity (owing to a transfer time of ca 5 s), the spectrum in panel B obtained with the dissolution device has
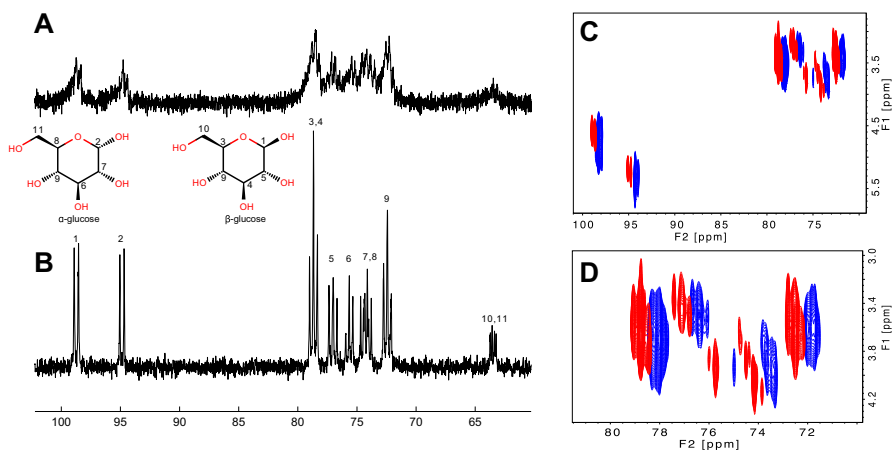
Fig. 2 1D-^{13}C-spectrum of [U-^{13}C]glucose after 4 h of polarization recorded **a** without, **b** with the pressure dissolution system. **c**, **d** 2D small flip angle HMQC acquired after 2 h of polarization without (*blue*) and with (*red*) the pressure dissolution system (the spectrum without the dissolution system has been slightly shifted for better visibility of the changes) (color figure online)
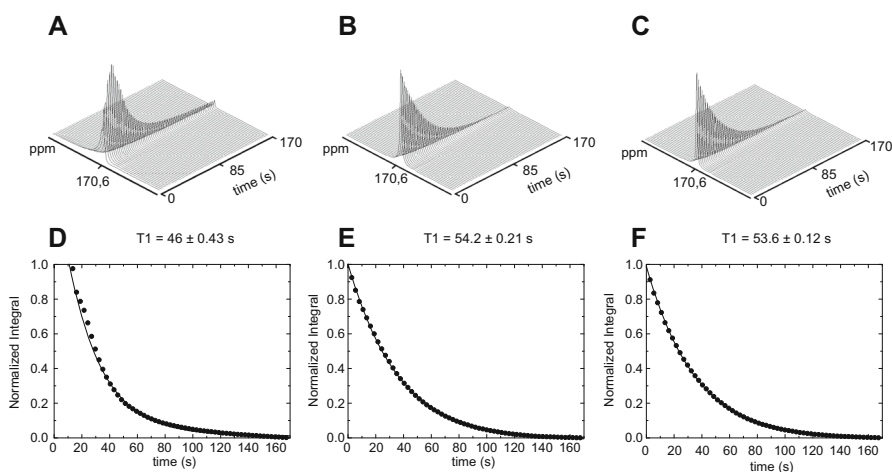
Fig. 3 **a** Repeated sequential small flip angle spectra of hyperpolarized 1-^{13}C-pyruvate collected every 2 s, acquired after a flip angle of 30° using the Hypersense transfer mechanism. **b**, **c**, Same train of spectra using the pressure dissolution kit. **d–f** SSFT data from **a–c** fitted using Eq. 8 from [4] to calculate a T_1 relaxation time

excellent intensity and shows sharp lines, revealing the proton–carbon and carbon–carbon couplings.

The pressure dissolution system has similar advantages for two-dimensional small flip angle HMQC spectra [7] as shown in Fig. 2c, d. Spectra obtained with the dissolution device shown in red have considerably lower line widths in the direct

dimension and thus resolve details of the peak shapes. Considering the faster transfer it was also possible to acquire additional increments, thus improving the resolution in the indirect dimension.

In order to demonstrate the increased stability achieved, we carried out SSTF longitudinal relaxation time measurements using Day's method [4] (Fig. 3). Figure 3a shows the expected instability arising from sample stabilization. For the simulation in Fig. 3e the first 4 data points had to be omitted, as they show a build-up of signal arising from a slow sample stabilization over 8–10 s. Figure 3b, c, f, g demonstrate the advantage obtained with the pressure dissolution kit. The T_1 obtained was the same for two consecutive polarizations within small error limits. Data points could be used from time zero which is 600 ms after the sample transfer was started.

In conclusion, we present a new design for a high-pressure dissolution device for dissolution DNP, which can be used along the Hypersense or any other implementations of this form of DNP. As part of our supplementary material, we provide sufficient detail of the design to enable its implementation in other laboratories.

References

1. J.H. Ardenkjaer-Larsen, B. Fridlund, A. Gram, G. Hansson, L. Hansson, M.H. Lerche, R. Servin, M. Thaning, K. Golman, Proc. Natl. Acad. Sci. USA **100**, 10158 (2003)
2. S. Bowen, C. Hilty, Phys. Chem. Chem. Phys. **12**, 5766 (2010)
3. W. Senczenko, Ph. D. Thesis, University of Nottingham, Dissolution Dynamic Nuclear Polarisation NMR Spectroscopy In Conjunction With Fast Sample Injection, Nottingham, 2012
4. I.J. Day, J.C. Mitchell, M.J. Snowden, A.L. Davis, J. Magn. Reson. **187**, 216 (2007)
5. R. Kaptein, K. Dijkstra, C.E. Tarr, J. Magn. Reson. **24**, 295 (1976)
6. T.B. Rodrigues, E.M. Serrao, B.W. Kennedy, D.E. Hu, M.I. Kettunen, K.M. Brindle, Nat. Med. **20**, 93 (2014)
7. C. Ludwig, I. Marin-Montesinos, M.G. Saunders, U.L. Günther, J. Am. Chem. Soc. **132**, 2508 (2010)

Appendix 2 – Arduino Development Code

APPENDIX 2

Arduino Programs for controlling the dissolution device

Software for MC1 – For Arduino Compiler version 1.03

```
/*
 Switch statement  with serial input
 http://www.arduino.cc/en/Tutorial/SwitchCase2
 */
//SOTIRIS DESCRIPTION
//UPDATE ON 26/11/2013 - I change all the switch commands to letters and keep numbers only for
timings, so I can read with parseint without the need of character identifier.
/*
 STRING ON SCREEN   :12345608
 SERIAL IN RECEIVED :78341209
 PORTS DIGITAL CTRL :674723--
 */



// Definition of interrupt names
#include < avr/io.h >
// ISR interrupt service routine

// constants won't change. They're used here to
// set pin numbers:
const int sensePin = 20;     // the number of the pushbutton pin
const int triggerpin =  52;     // the number of the LED pin


//SETTINGS FOR THE DELAY ENGAGEMENT
int delays[]={100,200,250,300,350,400,450,500,550,600,650,700,750,800,850,900,950,999};
int indexdel=9;
int uclost = 300;
int konter;
char inByte[4];



//PNEUMATIC VALVE CONTROLS
```

```
void setup()

{

  // initialize serial communication:

  Serial3.begin(9600);


  pinMode(triggerpin,OUTPUT);

  //  Serial.begin(9600);


  // initialize the LED pins:

  for (int thisPin = 2; thisPin <= 7; thisPin++)

  {

    pinMode(thisPin, OUTPUT);

  }

  pinMode(sensePin, INPUT);


  digitalWrite(sensePin,HIGH);

//  digitalWrite(triggerpin,LOW);

  // pinMode(ledPin, OUTPUT);

  //  attachInterrupt(3, blink, CHANGE);

}


void resetbyte()

{

  inByte[1]=0;

  inByte[2]=0;

  inByte[3]=0;

  inByte[4]=0;

}


void empty()

{

    for (int lala = 1; lala <=2; lala++)

    {

    Serial3.read();

    }

}


void loop()
```

```
{

  if (Serial3.available() > 0)

    {

    inByte[1] = Serial3.read();

    }

    // do something different depending on the character received.

    // The switch statement expects single number values for each case;

    // in this exmaple, though, you're using single quotes to tell

    // the controller to get the ASCII value for the character.  For

    // example 'a' = 97, 'b' = 98, and so forth:

  {

    switch (inByte[1])


    {


      case 'A':

        {

                  resetbyte();

          empty();

          digitalWrite(triggerpin, LOW);

          delay(100);

          digitalWrite(triggerpin, HIGH);


        }

      break;


      case 'X':

        {

          Serial3.print('D');

          Serial3.println(delays[indexdel]);

          delay(5);

          resetbyte();

          empty();

        }

      break;


      case 'F' :

        {

          digitalWrite(2, LOW);
```

```
        resetbyte();

        empty();

      }

  break;


  case 'G':

    {

      digitalWrite(3, LOW);

      resetbyte();

      empty();

    }

  break;


  case 'D':

    {

      digitalWrite(4, LOW);

      resetbyte();

      empty();

    }

  break;


  case 'E':

      {

       digitalWrite(5, LOW);

       resetbyte();

       empty();

      }

  break;


  case 'B':

      {

      digitalWrite(6, LOW);

      delay(2000);

      digitalWrite(6, HIGH);

      resetbyte();

      empty();

      }

  break;
```

```
case 'C':
  {
    digitalWrite(7, LOW);

    delay(2000);

    digitalWrite(7, HIGH);

    resetbyte();

    empty();
  }
break;


case 'I':
  {
  resetbyte();

  empty();

  // DISSOLUTION START POINT

  digitalWrite(7, LOW); //

  delay(2000);

  digitalWrite(7, HIGH);

  delay(100);

  digitalWrite(6, LOW); // main valve put in position

  delay(2000);

  digitalWrite(6, HIGH); ///main valve put in position

  digitalWrite(3, LOW); // open low pressure valve

  digitalWrite(4, LOW);

  delay(500);

  digitalWrite(4, HIGH);// open and close vent valve for low    pressure

  delay(1000);

  digitalWrite(2,LOW); // high pressure

  delay(2000);

  // if sensePin=LOW;


  while(digitalRead(sensePin) != HIGH) {
  } // do nothing - WARNING - THIS HANGS THE ARDUINO UNTIL DIGITAL TRIGGER SIGNAL
RECEIVED.

  digitalWrite(7,LOW); //valve position air pulse on

  delay(delays[indexdel]);

  digitalWrite(5,LOW); //Stabilising Pressure

  delay(50);

  //digitalWrite(2,HIGH);
```

```
      digitalWrite(triggerpin,LOW); //trigger pulse for NMR

      delay(100);

      digitalWrite(triggerpin,HIGH);

      delay(1250); //to add up for two seconds for the Valve

      digitalWrite(7,HIGH); //valve position air pulse off

      //this is where it is supposed to end, next is only for debugging

      //I can use multiple delays and having a pin in unchanged state.

      //With this trich I can use 2 delays of total time 2 second (time needed for the
Pneumatic Valve Switch)

      //and alter the injection time delay (can vary between 0 - 2000ms).

      //The 2 delays can be preprogrammed values after optimisation and preselected in a new
menu called "dissolution options").

      //
       }

      break;


      case 'H':
      {
      for (int thisPin = 2; thisPin <= 7; thisPin++)
      {
        digitalWrite(thisPin, HIGH);
      }
      resetbyte();
      empty();
      }
      break;


      case 'S':
      {
        int sot = Serial3.parseInt();
        empty();
        resetbyte();
        for (konter=0; konter<=17; konter++)
          {
            if (sot == delays[konter])
              {
                indexdel = konter;
              }
          }
```

```
        }
      break;


      default:
        {
    // turn all the LEDs off:
    //    for (int thisPin = 2; thisPin <= 7; thisPin++)
    //      {
    //        digitalWrite(thisPin, HIGH);
    //      }
        }
    }
  }
}
```

Touch Screen Arduino (MC3):

```
// UTouch_ButtonTest (C)2010-2012 Henning Karlsen

// web: http://www.henningkarlsen.com/electronics

// Sotiris Description - This is the software version with delay // changing added.
v11.13.zita


#include <UTFT.h>

#include <UTouch.h>

#include <avr/pgmspace.h>


// Declare which fonts we will be using

extern uint8_t BigFont[];

extern uint8_t SmallFont[];


// Uncomment the next two lines for the Arduino 2009/UNO

//UTFT        myGLCD(ITDB24D,19,18,17,16);   // Remember to change the model parameter to suit
your display module!

//UTouch      myTouch(15,10,14,9,8);


// Uncomment the next two lines for the Arduino Mega

UTFT         myGLCD(ITDB32S, 38,39,40,41);   // Remember to change the model parameter to suit
your display module!

UTouch       myTouch(6,5,4,3,2);


int x, y, counter, konter;

int uclost = 300;

char stCurrent[20]="";

char timings[9]="";

char delaysot[4]="600";

char trigsot[4]="120";

char ucset[4];

int stCurrentLen=0;

int delays[]={

  100, 200, 250, 300, 350, 400, 450, 500, 550, 600, 650, 700, 750, 800, 850, 900, 950, 999};

int indexdel=9;

//char stLast[20]="";

extern unsigned int

BHAMMUNI[0xD24],
```

```
SOT[0xD24],

EU[0xD25],

PIC121[0x1F68],

PICMC[0xD24],

PIC111[0xD25];


/*************************
 **   Custom functions   **
 *************************/
void sotosmenu()

{

  myGLCD.setBackColor(0, 0, 0);

  myGLCD.print("UoB Dissolution KIT", 2, 1);

  //myGLCD.drawBitmap(20, 0, 58, 58, Full_Moon);

  //   myGLCD.drawBitmap(205, 40, 100, 32, OILOG);

  myGLCD.drawBitmap(10, 30, 50, 60, BRUMUNI);

  //myGLCD.drawBitmap(80, 40, 100, 33, EU);

  //   myGLCD.drawBitmap(90, 40, 84, 35, META);

  myGLCD.drawBitmap(90, 28, 134, 60, PIC121);

  myGLCD.drawBitmap(250, 35, 52, 50, PICMC);

  myGLCD.drawBitmap(180, 210, 140, 24, SOT);

  myGLCD.setFont(SmallFont);

  myGLCD.print("University of Birmingham", CENTER, 115);

  myGLCD.print("2012-2013", CENTER, 130);

  myGLCD.print("v11.13.zita", LEFT, 225);

  myGLCD.setFont(BigFont);

  myGLCD.print("TOUCH TO CONTINUE", CENTER, 170);

  myGLCD.setFont(BigFont);


}

void debugRelays()

{

  Serial3.write('H');

  myGLCD.print("-", LEFT, 200);

  delay(500);

  Serial3.write('F');

  myGLCD.print("--", LEFT, 200);

  delay(500);

  Serial3.write('H');
```

```
myGLCD.print("---", LEFT, 200);

delay(500);

Serial3.write('G');

myGLCD.print("----", LEFT, 200);

delay(500);

Serial3.write('H');

myGLCD.print("-----", LEFT, 200);

delay(500);

Serial3.write('D');

myGLCD.print("------", LEFT, 200);

delay(500);

Serial3.write('H');

myGLCD.print("-------", LEFT, 200);

delay(500);

Serial3.write('E');

myGLCD.print("--------", LEFT, 200);

delay(500);

Serial3.write('H');

myGLCD.print("---------", LEFT, 200);

delay(500);

Serial3.write('B');

myGLCD.print("----------", LEFT, 200);

delay(500);

Serial3.write('H');

myGLCD.print("-----------", LEFT, 200);

delay(500);

Serial3.write('C');

myGLCD.print("------------", LEFT, 200);

delay(500);

Serial3.write('H');

myGLCD.print("------------>", LEFT, 200);

delay(500);

myGLCD.print("             ", LEFT, 200);

}


void touchIN()

{

  if (myTouch.dataAvailable());

  myTouch.read();
```

```
  x=myTouch.getX();

  y=myTouch.getY();

}


void settingsmenu()

{

  //drawButtons();


  myGLCD.setColor(0,0,50);

  myGLCD.setBackColor(0,0,255);

  myGLCD.fillRoundRect (10,10,310,230); //frame

  myGLCD.setColor(0,0,255);              //button ok

  myGLCD.fillRoundRect (250,180,300,220);

  myGLCD.setColor(255,255,255);

  myGLCD.print("DEF", 250, 192);

  myGLCD.setColor(0,0,255);              //button upload

  myGLCD.fillRoundRect (120,180,220,220);

  myGLCD.setColor(255,255,255);

  myGLCD.print("UPLOAD", 122, 192);

  myGLCD.setColor(0,0,255);              //button cancel

  myGLCD.fillRoundRect (30,180,90,220);

  myGLCD.setColor(255,255,255);

  myGLCD.print("GET", 35, 192);

  myGLCD.setBackColor(0,0,255);

  myGLCD.setColor(0,0,255);

  myGLCD.fillRoundRect (90,60,120,90);

  myGLCD.fillRoundRect (180,60,210,90);

  myGLCD.setColor(255,255,255);

  myGLCD.print("-",98,67);

  myGLCD.print("+",188,67);

  myGLCD.setBackColor(0,0,50);

  myGLCD.printNumI(delays[indexdel],127,67);

  myGLCD.print("DELAY",110,40);

  myGLCD.setColor(255,255,255);

  myGLCD.drawRect(80,35,220,95);

  myGLCD.setBackColor(0,0,50);


  myGLCD.setBackColor(0,0,255);

  myGLCD.setColor(0,0,255);
```

```
myGLCD.fillRoundRect (90,125,120,155);

myGLCD.fillRoundRect (180,125,210,155);

myGLCD.setColor(255,255,255);

myGLCD.print("-",98,133);

myGLCD.print("+",188,133);

myGLCD.setBackColor(0,0,50);

myGLCD.print(trigsot,127,133);

myGLCD.print("TRIGGER",90,105);

myGLCD.setColor(255,255,255);

myGLCD.drawRect(80,100,220,158);

myGLCD.setBackColor(0,0,50);




//Try to draw the arrows with the array of values




//End

do
{
  touchIN();
  myGLCD.print("Timing Settings",40,15);
  myGLCD.print("                ",80,160);


  while ((y>=60) && (y<=90) && (x>=90) && (x<=120))
  {
    touchIN();
    myGLCD.print("minus",80,160);
    delay(100);
    if (indexdel>=1)
    {
      indexdel=indexdel-1;
    }


    myGLCD.printNumI(delays[indexdel],127,67);
  }


  while ((y>=60) && (y<=90) && (x>=180) && (x<=210))
  {
```

```
          touchIN();

          myGLCD.print("plus",80,160);

          delay(100);

          if (indexdel<=16)

          {

            indexdel=indexdel+1;

          }


          myGLCD.printNumI(delays[indexdel],127,67);

       }



     while ((y>=180) && (y<=220) && (x>=30) && (x<=90))

     {

        touchIN();

        delay(100);

        //          myGLCD.print("DOWNLOADING",80,160);
//THIS IS THE ROUTINE FOR THE SERIAL I/O  - START
//***********************************************

        Serial3.write('X');

        if (Serial3.available() > 0)

         {
//         myGLCD.print("DOWNLOADING",80,160);

          ucset[1]=0;

          ucset[2]=0;

          ucset[3]=0;

          ucset[4]=0;

          ucset[1] = Serial3.read();

          ucset[2] = Serial3.read();

          ucset[3] = Serial3.read();

          ucset[4] = Serial3.read();


          if (ucset[1]=='D')

           {

           int sot = (((100*(ucset[2]-'0')) + (10*(ucset[3]-'0'))) + (ucset[4]-'0'));

            myGLCD.printNumI(sot,80,160);

            for (konter=0; konter<= 17; konter++)

              {

              if  (sot == delays[konter])
```

```
                      {
                       indexdel = konter ;
                       myGLCD.print("                    ",80,160);
                       myGLCD.printNumI(konter,80,160);
                       delay(20);
                       myGLCD.print("                   ",80,160);
                       myGLCD.printNumI(delays[indexdel],80,160);
                       delay(20);
                       }
                      }


               myGLCD.printNumI(delays[indexdel],127,67);
                delay(100);
              }
          }
        }


       while ((y>=180) && (y<=220) && (x>=120) && (x<=220))
       {
         touchIN();
         delay(300);
         myGLCD.print("UPLOADING",80,160);
         delay(200);
         Serial3.print('S');
         Serial3.println(delays[indexdel]);
       }
//***********************************************************
//This is where the serial routine ends.
       while ((y>=180) && (y<=220) && (x>=250) && (x<=300))
       {
         touchIN();
         myGLCD.print("DEFAULTS",80,160);
         indexdel=9;
         myGLCD.printNumI(delays[indexdel],127,67);
       }
     }
   while (((y>=1) && (y<=239) && (x>=1) && (x<=319)));


   myGLCD.setBackColor(0,0,0);
```

```
    myGLCD.clrScr();

    drawButtons();


    //      while ((y>=180) && (y<=220) && (x>=250) && (x<=300));

    //      if ((y>=25) && (y<=65))  // Upper row


    //          waitForIt(5, 25, 50, 65);
}



void drawButtons()
{
  // Draw the upper row of buttons
  //SOTIRIS BUTTON 1
  myGLCD.print("UoB Dissolution KIT", 2, 1);
  myGLCD.setColor(0, 0, 255);
  myGLCD.setBackColor(0, 0, 255);
  myGLCD.fillRoundRect (5, 25, 50, 65);
  myGLCD.setColor(255, 255, 255);
  //    myGLCD.drawRoundRect (5, 25, 50, 65);
  myGLCD.print("V1", 10, 35);
  //SOTIRIS BUTTON 2
  myGLCD.setColor(0, 0, 255);
  myGLCD.fillRoundRect (55, 25, 100, 65);
  myGLCD.setColor(255, 255, 255);
  //    myGLCD.drawRoundRect (55, 25, 100, 65);
  myGLCD.print("V2", 60, 35);
  //SOTIRIS BUTTON 3
  myGLCD.setColor(0, 255, 0);
  myGLCD.setBackColor(0, 255, 0);
  myGLCD.fillRoundRect (105, 25, 150, 65);
  myGLCD.setColor(255, 255, 255);
  //    myGLCD.drawRoundRect (105, 25, 150, 65);
  myGLCD.print("V3", 110, 35);
  //SOTIRIS BUTTON 4
  myGLCD.setColor(0, 0, 255);
  myGLCD.setBackColor(0, 0, 255);
  myGLCD.fillRoundRect (155, 25, 200, 65);
  myGLCD.setColor(255, 255, 255);
```

```
//     myGLCD.drawRoundRect (155, 25, 200, 65);

myGLCD.print("V4", 160, 35);

//SOTIRIS BUTTON 5

myGLCD.setColor(0, 0, 255);

myGLCD.fillRoundRect (205, 25, 250, 65);

myGLCD.setColor(255, 255, 255);

//     myGLCD.drawRoundRect (205, 25, 250, 65);

myGLCD.print("V5", 210, 35);

//SOTIRIS BUTTON 6 (NEW)

myGLCD.setColor(0, 0, 255);

myGLCD.fillRoundRect (255, 25, 300, 65);

myGLCD.setColor(255, 255, 255);

//     myGLCD.drawRoundRect (255, 25, 300, 65);

myGLCD.print("V6", 260, 35);


// Draw the center row of buttons

// BUTTON 6 Sotiris

//  myGLCD.setColor(0, 0, 255);

//  myGLCD.fillRoundRect (10, 70, 60, 120);

//  myGLCD.setColor(255, 255, 255);

//  myGLCD.drawRoundRect (10, 70, 60, 120);

//  myGLCD.print("V6", 20, 87);

// OFF BUTTON

myGLCD.setColor(0, 0, 255);

myGLCD.fillRoundRect (5, 70, 100, 120);

myGLCD.setColor(255, 255, 255);

//  myGLCD.drawRoundRect (5, 70, 100, 120);

myGLCD.print("OFF", 30, 87);

// Draw the lower row of buttons

myGLCD.setColor(255, 0, 0);

myGLCD.setBackColor(255, 0, 0);

myGLCD.fillRoundRect (105, 70, 200, 120);

myGLCD.setColor(255, 255, 255);

//  myGLCD.drawRoundRect (105, 70, 200, 120);

myGLCD.print("CLR", 130, 87);

myGLCD.setColor(0, 0, 255);

myGLCD.setBackColor(0, 0, 255);

myGLCD.fillRoundRect (205, 70, 300, 120);

myGLCD.setColor(255, 255, 255);
```

```
  // myGLCD.drawRoundRect (205, 70, 300, 120);

  myGLCD.print("DEBUG", 215, 87);

  myGLCD.setColor(0, 255, 0);

  myGLCD.setBackColor(0, 255, 0);

  myGLCD.fillRoundRect (105, 125, 200, 180);

  myGLCD.setColor(255, 255, 255);

  // myGLCD.drawRoundRect (105, 125, 200, 180);

  myGLCD.print("START", 115, 143);

  myGLCD.setColor(0, 0, 255);

  myGLCD.setBackColor(0, 0, 255);

  myGLCD.fillRoundRect (205, 125, 300, 180);

  myGLCD.setColor(255, 255, 255);

  // myGLCD.drawRoundRect (205, 125, 300, 180);

  myGLCD.print("TRIG", 220, 143);


  myGLCD.setColor(0, 0, 0);

  myGLCD.setBackColor(0, 0, 0);

  myGLCD.fillRoundRect (40, 125, 90, 180);

  myGLCD.setColor(255, 255, 255);

  myGLCD.drawRoundRect (40, 125, 90, 180);

  myGLCD.print("SET", 42, 143);

  myGLCD.setBackColor (0, 0, 0);

}


void updateStr(int val)

{

  if (stCurrentLen<20)

  {

    stCurrent[stCurrentLen]=val;

    stCurrent[stCurrentLen+1]='\0';

    stCurrentLen++;

    myGLCD.setColor(0, 255, 0);

    myGLCD.print(stCurrent, LEFT, 224);

    myGLCD.setColor(255, 255, 255);

  }

  else

  {

    myGLCD.print("                    ",LEFT,224);

    stCurrentLen=0;
```

```
    stCurrent[stCurrentLen]=val;

    stCurrent[stCurrentLen+1]='\0';

    stCurrentLen++;

    myGLCD.setColor(0, 255, 0);

    myGLCD.print(stCurrent, LEFT, 224);

    myGLCD.setColor(255, 255, 255);

  }

}


// Draw a red frame while a button is touched

//void waitForIt(int x1, int y1, int x2, int y2)

//{

//  myGLCD.setColor(255, 0, 0);

//  myGLCD.drawRoundRect (x1, y1, x2, y2);

//  while (myTouch.dataAvailable())

//    myTouch.read();

//  myGLCD.setColor(255, 255, 255);

//  myGLCD.drawRoundRect (x1, y1, x2, y2);

//}


/*************************

 **  Required functions  **

 *************************/


void setup()

{

  // Initial setup

  myGLCD.InitLCD();

  myGLCD.clrScr();

  counter=0;

  myTouch.InitTouch();

  myTouch.setPrecision(PREC_MEDIUM);


  myGLCD.setFont(BigFont);

  myGLCD.setBackColor(0, 0, 0);

  sotosmenu();

  Serial3.begin(9600);

}
```

```
void loop()

{

  counter=counter+1;

  while (true)

  {


    if (myTouch.dataAvailable())

    {

      myTouch.read();

      x=myTouch.getX();

      y=myTouch.getY();


      if ((y>=1) && (y<=239) && (x>=1) && (x<=319) && (counter<=1))

      {

        myGLCD.clrScr();

        drawButtons();

        counter=counter+1;

        myGLCD.printNumI(counter, LEFT, 160);

      }


      else if ((y>=25) && (y<=65))  // Upper row

      {

        if ((x>=5) && (x<=50))  // Button: 1

        {

          //         waitForIt(5, 25, 50, 65);

          Serial3.write('B');

          myGLCD.print("Valve 1-10 (CW)", CENTER, 192);

          updateStr('1');

          counter=counter+1;

          myGLCD.printNumI(counter, LEFT, 160);

          delay(500);

          myGLCD.print("                   ", CENTER, 192);

        }

        if ((x>=55) && (x<=100))  // Button: 2

        {

          //         waitForIt(55, 25, 100, 65);

          Serial3.write('C');

          myGLCD.print("Valve 1-2 (CCW)", CENTER, 192);

          updateStr('2');
```

```
    delay(500);

    myGLCD.print("                    ", CENTER, 192);

  }

  if ((x>=105) && (x<=150))  // Button: 3

  {

    //          waitForIt(105, 25, 150, 65);

    Serial3.write('D');

    myGLCD.print("Pressure Relieved", CENTER, 192);

    updateStr('3');

    delay(500);

    myGLCD.print("                    ", CENTER, 192);

  }

  if ((x>=155) && (x<=200))  // Button: 4

  {

    //          waitForIt(155, 25, 200, 65);

    Serial3.write('E');

    myGLCD.print("Stable Pressure HI", CENTER, 192);

    updateStr('4');

    delay(500);

    myGLCD.print("                    ", CENTER, 192);


  }

  if ((x>=205) && (x<=250))  // Button: 5

  {

    //          waitForIt(205, 25, 250, 65);

    Serial3.write('F');

    updateStr('5');

    myGLCD.print("Chase Pressure HI", CENTER, 192);

    delay(500);

    myGLCD.print("                    ", CENTER, 192);

  }

  if ((x>=255) && (x<=300))  // Button: 6

  {

    //          waitForIt(255, 25, 300, 65);

    Serial3.write('G');

    updateStr('6');

    myGLCD.print("Back Pressure LO", CENTER, 192);

    delay(500);

    myGLCD.print("                    ", CENTER, 192);
```

```
    }
  }
  else if ((y>=70) && (y<=120))  // Center row
  {
    if ((x>=5) && (x<=100))  // Button: 0
    {
      //          waitForIt(5, 70, 100, 120);
      Serial3.write('H');
      myGLCD.print("!!VALVES DEACTIVATED!!", CENTER, 192);
      updateStr('0');
      delay(500);
      myGLCD.print("                      ", CENTER, 192);
    }
    {
      if ((x>=105) && (x<=200))  // Button: Clear
      {
        //          waitForIt(105, 70, 200, 120);
        stCurrent[0]='\0';
        stCurrentLen=0;
        myGLCD.clrScr();
        indexdel=9;
        konter=1;
        counter=1;
        sotosmenu();
      }
      if ((x>=205) && (x<=300))  // Button: Debug


      {
        debugRelays();
      }



    }



  }
  else if ((y>=125) && (y<=180))  // Bottom row
  {
    if ((x>=40) && (x<=90))//Button: Settings
```

```
          {
            settingsmenu();
          }
          if ((x>=105) && (x<=200))  // Button: Start
          {
            //          waitForIt(55, 25, 100, 65);
            Serial3.write('I');
            myGLCD.print("DISSOLUTION STARTED", CENTER, 192);
            updateStr('8');
            delay(1000);
            myGLCD.print("                   ", CENTER, 192);
          }
          if ((x>=205) && (x<=300))  // Button: Trigger
          {
            //          waitForIt(55, 25, 100, 65);
            Serial3.write('A');
            myGLCD.print("NMR TRIGGERED", CENTER, 192);
            updateStr('a');
            delay(1000);
            myGLCD.print("                   ", CENTER, 192);
          }
        }
      }
    }
  }
```

Liquid detecting Arduino (MC2):

```
int sense =2;
int led = 13;
int trigger = 12;

int senselevel;

void setup()
{
//  analogReference(DEFAULT); //isn't necessary
  pinMode(led, OUTPUT);
  pinMode(trigger, OUTPUT);
  pinMode(sense, INPUT);
  Serial.begin(9600);
}


void loop()
{
 senselevel=0;
 senselevel = analogRead(sense);

  if (senselevel>600)
   { digitalWrite(led,HIGH);
     digitalWrite(trigger,HIGH);
   }
  else
   { digitalWrite(led,LOW);
     digitalWrite(trigger,LOW);
   }
 Serial.println(senselevel);
```

List of References

1. Atkins, P.W. and R. Friedman, *Molecular quantum mechanics*. 4th ed. 2005, New York: Oxford University Press. xiv, 573 p.
2. Pauli, W., *On the connection of the arrangement of electron groups in atoms with the complex structure of spectra*. Zeitschrift Fur Physik, 1925. **31**: p. 765-783.
3. Pauli, W., *The connection between spin and statistics*. Physical Review, 1940. **58**(8): p. 716-722.
4. Bloch, F., W.W. Hansen, and M. Packard, *Nuclear Induction*. Physical Review, 1946. **69**(3-4): p. 127-127.
5. Purcell, E.M. and R.V. Pound, *A Nuclear Spin System at Negative Temperature*. Physical Review, 1951. **81**(2): p. 279-280.
6. Purcell, E.M., *Research in Nuclear Magnetism*. Science, 1953. **118**(3068): p. 431-436.
7. Ernst, R.R. and W.A. Anderson, *Application of Fourier Transform Spectroscopy to Magnetic Resonance*. Review of Scientific Instruments, 1966. **37**(1): p. 93-+.
8. Ernst, R.R., *Fourier Difference Spectroscopy*. Journal of Magnetic Resonance, 1971. **4**(2): p. 280-&.
9. Jeffries, C.D., *Dynamic Orientation of Nuclei*. Ann Rev Nucl Sci, 1964. **14**.
10. Levitt, M.H., *Spin dynamics: basics of nuclear magnetic resonance*. 2nd ed. 2008: John Wiley & Sons Ltd.
11. Overhauser, A.W., *Polarization of nuclei in metals*. Physical Review, 1953. **92**(2): p. 411-415.
12. Carver, T.R. and C.P. Slichter, *Experimental verification of the overhauser nuclear polarization effect*. Physical Review, 1956. **102**(4): p. 975-980.
13. Ardenkjaer-Larsen, J.H., et al., *Increase in signal-to-noise ratio of > 10,000 times in liquid-state NMR*. Proc Natl Acad Sci U S A, 2003. **100**(18): p. 10158-63.
14. Frydman, L. and D. Blazina, *Ultrafast two-dimensional nuclear magnetic resonance spectroscopy of hyperpolarized solutions*. Nature Physics, 2007. **3**(6): p. 415-419.
15. Kuprov, I., *http://spindynamics.org/Spin-Dynamics---Part-I---Lecture-01.php*. 2015.
16. Abragam, A., *Principles of nuclear magnetism*. 1961, Oxford University Press.
17. Claridge, T., *High-Resolution NMR Techniques in Organic Chemistry*. 2nd ed. 2009: Elsevier.
18. Gunther, U.L., *Dynamic Nuclear Hyperpolarization in Liquids*. Top Curr Chem, 2011.
19. Skoog, D.A., F.J. Holler, and T.A. Nieman, *Principles of instrumental analysis*. 5th ed. Saunders golden sunburst series. 1998, Philadelphia
Orlando, Fla.: Saunders College Pub. ;
Harcourt Brace College Publishers.
20. Ernst, R. and H. Primas, *Nuclear Magnetic Resonance in Diamagnetic Materials - High Resolution Nmr-Instrumentation - Recent Advances and Prospects*. Discussions of the Faraday Society, 1962(34): p. 43-&.

21. Katsikis, S., et al., *Improved Stability and Spectral Quality in Ex Situ Dissolution DNP Using an Improved Transfer Device.* Applied Magnetic Resonance, 2015. **46**(7): p. 723-729.

22. Carver, T.R. and C.P. Slichter, *Polarization of nuclear spins in metals [15].* Physical Review, 1953. **92**(1): p. 212-213.

23. Becerra, L.R., et al., *Dynamic nuclear polarization with a cyclotron resonance maser at 5 T.* Physical Review Letters, 1993. **71**(21): p. 3561-3564.

24. Eisenschmid, T.C., et al., *Para hydrogen induced polarization in hydrogenation reactions.* Journal of the American Chemical Society, 1987. **109**(26): p. 8089-8091.

25. Messerle, B.A., et al., *Structure and dynamics in metal phosphine complexes using advanced NMR studies with para-hydrogen induced polarisation.* Journal of the Chemical Society-Dalton Transactions, 1999(9): p. 1429-1435.

26. Kaptein, R., K. Dijkstra, and K. Nicolay, *Laser photo-CIDNP as a surface probe for proteins in solution.* Nature, 1978. **274**(5668): p. 293-294.

27. Grosse, S., et al., *Field cycling by fast NMR probe transfer: Design and application in field-dependent CIDNP experiments.* Applied Magnetic Resonance, 1999. **17**(2-3): p. 211-225.

28. Ludwig, C., et al., *Quantum rotor induced hyperpolarization.* Proceedings of the National Academy of Sciences of the United States of America, 2010. **107**(24): p. 10799-10803.

29. Haupt, J., *A new effect of dynamic polarization in a solid obtained by rapid change of temperature.* Physics Letters A, 1972. **38**(6): p. 389-390.

30. Bifone, A., et al., *NMR of laser-polarized xenon in human blood.* Proceedings of the National Academy of Sciences of the United States of America, 1996. **93**(23): p. 12932-12936.

31. Navon, G., et al., *Enhancement of solution NMR and MRI with laser-polarized xenon.* Science, 1996. **271**(5257): p. 1848-1851.

32. Albert, M.S., et al., *Biological magnetic resonance imaging using laser-polarized 129Xe.* Nature, 1994. **370**(6486): p. 199-201.

33. Levitt, M.H., *Spin dynamics : basics of nuclear magnetic resonance.* 2001, Chichester ; New York: John Wiley & Sons. xxiv, 686 p.

34. Hausser, K.H. and D. Stehlik, *Dynamic nuclear polarization in liquids.* Adv. Magn. Reson., 1968. **3**: p. 79-139.

35. Hovav, Y., A. Feintuch, and S. Vega, *Theoretical aspects of dynamic nuclear polarization in the solid state - The solid effect.* Journal of Magnetic Resonance, 2010. **207**(2): p. 176-189.

36. Hovav, Y., A. Feintuch, and S. Vega, *Theoretical aspects of dynamic nuclear polarization in the solid state - The cross effect.* Journal of Magnetic Resonance, 2012. **214**: p. 29-41.

37. Bajaj, V.S., et al., *Dynamic nuclear polarization at 9T using a novel 250 GHz gyrotron microwave source.* Journal of Magnetic Resonance, 2003. **160**(2): p. 85-90.

38. Ysacco, C., et al., *Properties of dinitroxides for use in dynamic nuclear polarization (DNP).* Phys Chem Chem Phys, 2010. **12**(22): p. 5841-5.

39. McMurry, J., *Organic chemistry.* 4th ed. 1996, Pacific Grove: Brooks/Cole Pub. Co.

40. Macholl, S., H. Johannesson, and J.H. Ardenkjaer-Larsen, *Trityl biradicals and 13C dynamic nuclear polarization.* Phys Chem Chem Phys, 2010. **12**(22): p. 5804-17.

41.   Liu, Y., et al., *Trityl-nitroxide biradicals as unique molecular probes for the simultaneous measurement of redox status and oxygenation.* Chemical Communications, 2010. **46**(4): p. 628-630.

42.   MacHoll, S., H. Jóhannesson, and J.H. Ardenkjaer-Larsen, *Trityl biradicals and 13C dynamic nuclear polarization.* Physical Chemistry Chemical Physics, 2010. **12**(22): p. 5804-5817.

43.   Gabellieri, C., et al., *Dynamic nuclear polarization with polychlorotriphenylmethyl radicals: Supramolecular polarization-transfer effects.* Angewandte Chemie - International Edition, 2010. **49**(19): p. 3360-3362.

44.   Paniagua, J.C., et al., *Polychlorinated trityl radicals for dynamic nuclear polarization: The role of chlorine nuclei.* Physical Chemistry Chemical Physics, 2010. **12**(22): p. 5824-5829.

45.   Tseitlin, M., et al., *Use of the Frank sequence in pulsed EPR.* J Magn Reson, 2011. **209**(2): p. 306-9.

46.   Türke, M.T. and M. Bennati, *Saturation factor of nitroxide radicals in liquid DNP by pulsed ELDOR experiments.* Physical Chemistry Chemical Physics, 2011. **13**(9): p. 3630-3633.

47.   Kuzma, N.N., et al., *Cluster formation restricts dynamic nuclear polarization of xenon in solid mixtures.* J Chem Phys, 2012. **137**(10): p. 104508.

48.   Lumata, L., et al., *The effect of 13C enrichment in the glassing matrix on dynamic nuclear polarization of [1-13C]pyruvate.* Physics in Medicine and Biology, 2011. **56**(5): p. N85-N92.

49.   Dorn, H.C., et al., *Flow dynamic nuclear polarization, a novel method for enhancing NMR signals in flowing fluids.* Journal of Magnetic Resonance (1969), 1988. **79**(3): p. 404-412.

50.   Stevenson, S., T. Glass, and H.C. Dorn, *13C Dynamic Nuclear Polarization: An Alternative Detector for Recycled-Flow NMR Experiments.* Analytical Chemistry, 1998. **70**(13): p. 2623-2628.

51.   Stevenson, S. and H.C. Dorn, *13C dynamic nuclear polarization: A detector for continuous-flow, on-line chromatography.* Analytical Chemistry, 1994. **66**(19): p. 2993-2999.

52.   Dorn, H.C., et al., *The flow transfer of a bolus with 1H dynamic nuclear polarization from low to high magnetic fields.* Chemical Physics Letters, 1989. **155**(2): p. 227-232.

53.   Wind, R.A., et al., *Dynamic nuclear polarization in the nuclear rotating frame.* Journal of Magnetic Resonance (1969), 1988. **79**(3): p. 577-582.

54.   Wind, R.A., H. Lock, and M. Mehring, *13C knight shift saturation and 1H dynamic nuclear polarization in a polycrystalline sample of the organic conductor (fluoranthenyl)2PF6.* Chemical Physics Letters, 1987. **141**(4): p. 283-288.

55.   Wind, R.A., et al., *Applications of dynamic nuclear polarization in 13C NMR in solids.* Progress in Nuclear Magnetic Resonance Spectroscopy, 1985. **17**(C): p. 33-67.

56.   Wind, R.A., et al., *Experimental setup for enhanced 13C NMR spectroscopy in solids using dynamic nuclear polarization.* Journal of Magnetic Resonance (1969), 1983. **52**(3): p. 424-434.

57.   Krahn, A., et al., *Shuttle DNP spectrometer with a two-center magnet.* Physical Chemistry Chemical Physics, 2010. **12**(22): p. 5830-5840.

58.   Reese, M., et al., *1H and13C dynamic nuclear polarization in aqueous solution with a two-field (0.35 T/14 T) shuttle DNP spectrometer.* Journal of the American Chemical Society, 2009. **131**(42): p. 15086-15087.

59.   Reese, M., et al., *Construction of NMR DNP shuttle spectrometer: First experimental results and evaluation of optimal performance characteristics.* Applied Magnetic Resonance, 2008. **34**(3-4): p. 301-311.

60.   Prandolini, M.J., et al., *High-field dynamic nuclear polarization in aqueous solutions.* Journal of the American Chemical Society, 2009. **131**(17): p. 6090-6092.

61.   Morley, G.W., et al., *Efficient dynamic nuclear polarization at high magnetic fields.* Physical Review Letters, 2007. **98**(22).

62.   Carravetta, M. and M.H. Levitt, *Long-lived nuclear spin states in high-field solution NMR.* Journal of the American Chemical Society, 2004. **126**(20): p. 6228-6229.

63.   Feintuch, A., et al., *A Dynamic Nuclear Polarization spectrometer at 95 GHz/144 MHz with EPR and NMR excitation and detection capabilities.* Journal of Magnetic Resonance, 2011. **209**(2): p. 136-141.

64.   Becerra, L.R., et al., *A Spectrometer for Dynamic Nuclear Polarization and Electron Paramagnetic Resonance at High Frequencies.* Journal of Magnetic Resonance, Series A, 1995. **117**(1): p. 28-40.

65.   Ardenkjær-Larsen, J.H., et al., *Increase in signal-to-noise ratio of >10,000 times in liquid-state NMR.* Proceedings of the National Academy of Sciences of the United States of America, 2003. **100**(18): p. 10158-10163.

66.   Sowerby, A., *Molecules in minute detail.* Chemistry and Industry (London), 2005(17): p. 21-23.

67.   Ludwig, C., et al., *Application of ex situ dynamic nuclear polarization in studying small molecules.* Physical Chemistry Chemical Physics, 2010. **12**(22): p. 5868-5871.

68.   Bowen, S. and C. Hilty, *Rapid sample injection for hyperpolarized NMR spectroscopy.* Phys Chem Chem Phys, 2010. **12**(22): p. 5766-70.

69.   Serrao, E.M., et al., *MRI with hyperpolarised [1-13C]pyruvate detects advanced pancreatic preneoplasia prior to invasive disease in a mouse model.* Gut, 2015.

70.   Rodrigues, T.B., et al., *Magnetic resonance imaging of tumor glycolysis using hyperpolarized 13C-labeled glucose.* Nat Med, 2014. **20**(1): p. 93-7.

71.   Arduino, *https://www.arduino.cc/.* 2015.

72.   Bowen, S. and C. Hilty, *Rapid sample injection for hyperpolarized NMR spectroscopy.* Physical Chemistry Chemical Physics, 2010. **12**(22): p. 5766-5770.

73.   Bowen, S. and C. Hilty, *Time-resolved dynamic nuclear polarization enhanced NMR spectroscopy.* Angewandte Chemie - International Edition, 2008. **47**(28): p. 5235-5237.

74.   Chen, H.Y. and C. Hilty, *Implementation and Characterization of Flow Injection in Dissolution Dynamic Nuclear Polarization NMR Spectroscopy.* Chemphyschem, 2015. **16**(12): p. 2646-52.

75.   Day, I.J., et al., *Applications of DNP-NMR for the measurement of heteronuclear T-1 relaxation times.* Journal of Magnetic Resonance, 2007. **187**(2): p. 216-224.

76. Allouche-Arnon, H., et al., *Deuteration of a molecular probe for DNP hyperpolarization--a new approach and validation for choline chloride.* Contrast Media Mol Imaging, 2011. **6**(6): p. 499-506.

77. Ludwig, C., et al., *Optimizing the polarization matrix for ex situ dynamic nuclear polarization.* Journal of the American Chemical Society, 2010. **132**(8): p. 2508-2509.

78. Shanaiah, N., et al., *Class selection of amino acid metabolites in body Fluids using chemical derivatization and their enhanced C-13 NMR.* Proceedings of the National Academy of Sciences of the United States of America, 2007. **104**(28): p. 11540-11544.

79. Ye, T., et al., *C-13-Formylation for Improved Nuclear Magnetic Resonance Profiling of Amino Metabolites in Biofluids.* Analytical Chemistry, 2010. **82**(6): p. 2303-2309.

80. Gowda, G.A.N., Y.N. Gowda, and D. Raftery, *Expanding the Limits of Human Blood Metabolite Quantitation Using NMR Spectroscopy.* Analytical Chemistry, 2015. **87**(1): p. 706-715.

81. Gowda, G.A.N., Y.N. Gowda, and D. Raftery, *Massive Glutamine Cyclization to Pyroglutamic Acid in Human Serum Discovered Using NMR Spectroscopy.* Analytical Chemistry, 2015. **87**(7): p. 3800-3805.

82. Gowda, G.A.N. and D. Raftery, *Quantitating Metabolites in Protein Precipitated Serum Using NMR Spectroscopy.* Analytical Chemistry, 2014. **86**(11): p. 5433-5440.

83. Gowda, G.A.N., et al., *Quantitative Analysis of Blood Plasma Metabolites Using Isotope Enhanced NMR Methods.* Analytical Chemistry, 2010. **82**(21): p. 8983-8990.

84. Wei, S.W., et al., *Ratio Analysis Nuclear Magnetic Resonance Spectroscopy for Selective Metabolite Identification in Complex Samples.* Analytical Chemistry, 2011. **83**(20): p. 7616-7623.

85. Kupce, E., R. Freeman, and B.K. John, *Parallel acquisition of two-dimensional NMR spectra of several nuclear species.* Journal of the American Chemical Society, 2006. **128**(30): p. 9606-9607.

86. Kupce, E. and R. Freeman, *Parallel receivers and sparse sampling in multidimensional NMR.* Journal of Magnetic Resonance, 2011. **213**(1): p. 1-13.

87. Kupce, E., L.E. Kay, and R. Freeman, *Detecting the "Afterglow" of C-13 NMR in Proteins Using Multiple Receivers.* Journal of the American Chemical Society, 2010. **132**(51): p. 18008-18011.

88. Donovan, K.J., E. Kupce, and L. Frydman, *Multiple Parallel 2DNMR Acquisitions in a Single Scan.* Angewandte Chemie-International Edition, 2013. **52**(15): p. 4152-4155.

89. Reynolds, S. and H. Patel, *Monitoring the solid-state polarization of 13C, 15N, 2H, 29Si and 31P.* Applied Magnetic Resonance, 2008. **34**(3-4): p. 495-508.

90. Economou, A., *Sequential-injection analysis (SIA): A useful tool for on-line sample-handling and pre-treatment.* Trac-Trends in Analytical Chemistry, 2005. **24**(5): p. 416-425.

91. Economou, A., P.D. Tzanavaras, and D.G. Themelis, *Sequential-injection analysis: A useful tool for clinical and biochemical analysis.* Current Pharmaceutical Analysis, 2007. **3**(4): p. 249-261.

92.   Wilson, D.M., et al., *Generation of hyperpolarized substrates by secondary labeling with [1,1- 13C] acetic anhydride.* Proceedings of the National Academy of Sciences of the United States of America, 2009. **106**(14): p. 5503-5507.

93.   Chattergoon, N., et al., *Field dependence of T1 for hyperpolarized [1-13C]pyruvate.* Contrast Media Mol Imaging, 2013. **8**(1): p. 57-62.

94.   Carravetta, M., O.G. Johannessen, and M.H. Levitt, *Beyond the T1 limit: Singlet nuclear spin states in low magnetic fields.* Physical Review Letters, 2004. **92**(15): p. 153003-1.

95.   Pileio, G., M. Carravetta, and M.H. Levitt, *Storage of nuclear magnetization as long-lived singlet order in low magnetic field.* Proceedings of the National Academy of Sciences of the United States of America, 2010. **107**(40): p. 17135-17139.

96.   Tayler, M.C., et al., *Direct enhancement of nuclear singlet order by dynamic nuclear polarization.* J Am Chem Soc, 2012. **134**(18): p. 7668-71.

97.   Laustsen, C., et al., *Hyperpolarized singlet NMR on a small animal imaging system.* Magn Reson Med, 2012. **68**(4): p. 1262-5.

98.   Marco-Rius, I., et al., *Hyperpolarized singlet lifetimes of pyruvate in human blood and in the mouse.* NMR Biomed, 2013. **26**(12): p. 1696-704.

99.   Mansson, S., et al., *13C imaging-a new diagnostic platform.* Eur Radiol, 2006. **16**(1): p. 57-67.